DEVELOPMENT OF AN ACTIVE PITCH CONTROL SYSTEM FOR WIND TURBINES

F.M. den Heijer

12253456

Dissertation submitted in partial fulfilment of the requirement for the degree

Master of Engineering

at the Potchefstroom campus of the North-West University

Supervisor: Mr. A.S. Jonker

November 2008

ACKNOWLEDGMENTS

Ek dra hierdie studie op aan my Verlosser Jesus Christus en gee alle eer aan Hom. Ek dank Hom vir alles en sy ontelbare seëninge. Aan my vrou Olga wil ek baie dankie sê vir haar liefde en onophoudelike ondersteuning.

Die volgende persone dank ook ek graag:

Attie Jonker vir sy leiding deur die studie.

Wally Thöle vir die vervaardiging van die prototipe.

Attie en Uys Jonker vir Jonker Sailplanes se hulpbronne wat aan my beskikbaar gestel is.

Danie Dahms en Nico van Meurs van Aero Energy vir die skenking van die AE1kW lemme.

My pa vir sy hulp met die verf en toetsing van die prototipe.

Gideon Coetzee vir al sy praktiese wenke.

Corné Oosthuizen vir sy hulp met die eDAQ lite data opnemer.

Willem den Heijer en Morné Coetzee vir hulle hulp met die proeflesing.

ABSTRACT

A wind turbine needs to be controlled to ensure its safe and optimal operation, especially during high wind speeds. The most common control objectives are to limit the power and rotational speed of the wind turbine by using pitch control.

Aero Energy is a company based in Potchefstroom, South Africa, that has been developing and manufacturing wind turbine blades since 2000. Their most popular product is the AE1kW blades. The blades have a tendency to over-speed in high wind speeds and the cut-in wind speed must be improved.

The objective of this study was to develop an active pitch control system for wind turbines. A prototype active pitch control system had to be developed for the AE1kW blades. The objectives of the control system are to protect the wind turbine from over-speeding and to improve start-up performance.

An accurate model was firstly developed to predict a wind turbine's performance with active pitch control. The active pitch control was implemented by means of a two-stage centrifugal governor. The governor uses negative or stalling pitch control. The first linear stage uses a soft spring to provide improved start-up performance. The second non-linear stage uses a hard spring to provide over-speed protection.

The governor was manufactured and then tested with the AE1kW blades. The governor achieved both the control objectives of over-speed protection and improved start-up performance. The models were validated by the results.

It was established that the two-stage centrifugal governor concept can be implemented on any wind turbine, provided the blades and tower are strong enough to handle the thrust forces associated with negative pitch control.

It was recommended that an active pitch control system be developed that uses positive pitching for the over-speed protection, which will eliminate the large thrust forces.

Keywords: pitch control, wind turbine, centrifugal governor, over-speed protection, cut-in wind speed, blade element-momentum theory, rotor, generator, stall, feathering.

OPSOMMING

’n Windturbine se werking moet beheer word om te sorg dat dit veilig en optimaal werk, veral gedurende hoë wind snelhede. Die mees algemene beheerdoelwit is om die wind turbine se drywing en rotasie snelheid te beperk deur die steek te beheer.

Aero Energy is ’n maakskappy wat in Potchefstroom, Suid-Afrika gevestig is. Hulle ontwikkel windturbinelemme al sedert 2000. Hulle gewildste produk is die AE1kW lemme. Die lemme is geneig om in hoë wind kondisies hulle maksimum rotasiesnelheid te oorsky. Hulle aanvangswerking moet ook verbeter word.

Die doelwit van hierdie studie was om ’n aktiewe steekbeheerstelsel te ontwikkel vir windturbines. ’n Prototipe steekbeheerstelsel moes ontwikkel word vir die AE1kW lemme. Die doelwitte van die beheerstelsel is om die windturbine te beskerm teen spoedoorskryding en om die aanvangswerking te verbeter.

’n Akkurate model was eerstens ontwikkel om ’n windturbine met aktiewe steekbeheer se werking te voorspel. ’n Twee-stadia sentrifugale reëllaar was gebruik om die aktiewe steekbeheer te toe te pas. Die reëllaar gebruik negatiewe of stol steekbeheer. Die eerste lineêre stadium gebruik ’n sagte veer vir verbeterde aanvangswerking. Die tweede nie-lineêre stadium gebruik ’n harde veer vir beskerming teen spoedoorskryding.

Die reëllaar was vervaardig en getoets met die AE1kW lemme. Die reëllaar het voldoen aan die beheerdoelwitte van beskerming teen spoedoorskryding en verbeterde aanvangswerking. Die modelle is geverifieer met die toets resultate.

Daar is bevind dat indien die lemme en toring sterk genoeg is om die stukragte van negatiewe steekbeheer te hanteer, die twee-stadia sentrifugale reëllaar konsep op enige windturbine toegepas kan word.

Dit was aanbeveel dat ’n aktiewe steekbeheerstel ontwikkel word wat van positiewe steekbeheer gebruik maak vir die beskerming teen spoedoorskryding, wat sal wegdoen met die groot stukragte.

Sleutelwoorde: steekbeheer, windturbine, sentrifugale reëllaar, spoedoorskrydingsbeskerming, aanvangswindspoed, lem-element-momentum-teorie, rotor, opwekker, staak, positiewe steekbeheer.

CONTENTS

Page

LIST OF FIGURES

NOMENCLATURE

a	Axial flow induction factor	
a'	Tangential flow induction factor	
c	Chord	m
c_T	Annular thrust coefficient	
C_L	Airfoil lift coefficient	
C_D	Airfoil drag coefficient	
C_M	Airfoil pitching moment coefficient	
C_P	Rotor power coefficient	
C_T	Rotor thrust coefficient	
C_Q	Rotor torque coefficient	
D	Diameter	m
D	Drag	N
f	Probability distribution	
F	Force	N
F	Flapping moment	Nm
F	Loss factor	
I	Second moment of area	m^4
J	Mass moment of inertia	$kg.m^2$
k	Spring stiffness	N/m
k	Wind shape factor	
L	Lift	N
L	Length	m
m	Mass	kg
M	Moment	Nm
N	Number of blades	
p	Pitch	°
P	Power	kW
Q	Torque	Nm
r	Radius	m
R	Blade radius	m
T	Thrust	N
U	Driving force	N
V_∞	Free stream wind speed	m/s
V	Wind speed	m/s
$\bar{V}_\infty$	Mean wind speed	m/s
W	Resultant velocity	m/s
x	normalized blade radius	
x	Displacement	m

RPM	Rotational speed	rpm
TSR	Tip speed ratio	
α	Angle of attack	°
β	Blade angle	°
ϕ	Air flow angle	°
λ	Tip speed ratio	
θ	Angle	°
ρ	Density	kg/m^3
σ	Stress	MPa
Γ	Gamma function	
Ω	Rotational speed	rad/s
$\dot{\Omega}$	Rotational acceleration	rad/s^2
Subscript properties		
cent	Centrifugal	
gen	Generator	
load	Generator load, external load	
m	mass	
mom	momentum	
off	offset	
rotor	Rotor blades	
R	Root	
T	Tip	
0.25	Pitching moment	
Governor Subscript properties		
c1	Governor connector c1	
c2	Governor connector c2	
axle	Length	
undef	Undeflected	
comp	Compressed solid	
springs	Spring	
s1	Governor soft spring	
s2	Governor hard spring	

Chapter 1 Introduction

1.1 Background

The primary cause for the development of modern wind turbine technology has been the oil crisis and extreme rise in oil prices in the seventies. Due to the enormous increase in electricity demand over the last 100 years, it has become very important to consider the environmental impact of power generation. Using a wind turbine for electricity generation results in a very low CO_2 emission over the wind turbine's entire life cycle. Wind turbine technology has reached the point where it is now feasible and reliable to use as a major supplement to fossil fuels. On a good site, the energy recovery period can be less than 1 year (Burton et al. 2001, pp.1-7). Small wind turbine technology offers major advantages for rural or remote communities (Corbus et al. 1999).

A wind turbine extracts energy from the wind by slowing down the mass of air that moves through the rotor, thus changing its momentum (Gasch & Twele 2005, p.30). The shaft of the rotor is connected to a gearbox (to increase the shaft speed if necessary) and the gearbox then to the generator. The generator then converts this shaft power into electricity. Depending on the size of the wind turbine, it is either connected to the country's electric grid or used as a battery charging station (Gasch & Twele 2005, pp. 43-44).

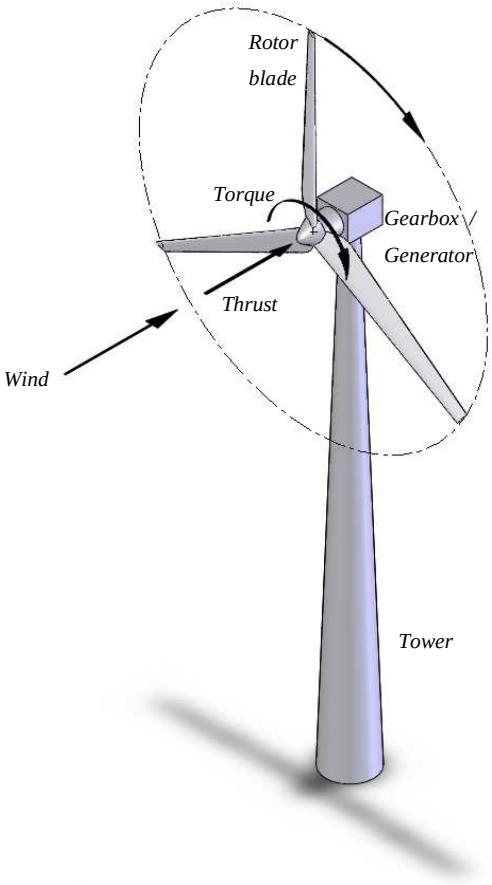

Figure 1.1 *A 3-bladed horizontal-axis wind turbine*

A wind turbine's performance is characterized by the amount of power, torque and thrust it generates at a specific wind speed and rotational speed (Burton et al. 2001, p.173). The performance characteristics and the rotational speed need to be controlled to ensure safe and optimal operation, especially during high wind speeds. The most common control objectives are to limit the power and rotational speed (Gasch & Twele 2005, pp. 319-328). The start-up torque can also be controlled to provide better start-up of the wind turbine (Gasch & Twele 2005, p.89).

Aero Energy is a company based in Potchefstroom, South Africa, that has been developing and manufacturing wind turbine blades since 2000. Their most popular product is the AE1kW blades. The blades are used on small 3-bladed horizontal axis wind turbine systems that are used for charging batteries for small homes and remote rural areas (Bosman 2003).

1.2 Problem statement

The AE1kW wind turbines blades developed by Aero Energy have a tendency to over-speed in high wind speeds and the cut-in wind speed must be improved.

1.3 Objectives of this study

- The objective of this study is to develop an active pitch control system for wind turbines. A prototype active pitch control system must be developed for the AE1kW blades. The control objectives of the control system are to protect the wind turbine from over-speeding and to improve the start-up performance.

- To develop the control system, an accurate model must be developed to predict the system's behaviour.

- A prototype pitch-control system must be designed, manufactured and tested with the AE1kW blades.

1.4 Scope of the study

- Chapter 2 provides a background on wind turbine performance. A detailed discussion is given of pitch control and its performance impact. The different types of control and implementation methods are discussed. A decision is made on which type of control will be best suited to achieve the objectives of this study.

- Chapter 3 provides the theoretical background necessary to model a wind turbine with active pitch control. The blade element-momentum theory is discussed in detail. The centrifugal control theory and the governor kinematics are developed and discussed in detail.

- Chapter 4 gives a discussion of the application of the theory to model the performance of a wind turbine with a centrifugal governor. The preliminary modelling results and the results necessary for the conceptual design are discussed.

- Chapter 5 gives a discussion of the conceptual design of the governor and the development of the final concept which will be best suited to achieve the control objectives.

- Chapter 6 gives a discussion of the detail design of the governor, which include the minimization of the external influence on the governor, the strength design of the most critical part and the design of the control system.

- Chapter 7 gives a discussion of the testing procedures and the test setups of the governor prototype. The initial test, its results, the necessary design modifications, the final tests and findings are discussed.

- Chapter 8 gives the conclusions and recommendations of the study.

Chapter 2 Literature study

2.1 Introduction

This chapter provides a background on wind turbine performance. A detailed discussion is given of pitch control and its performance impact. The different types of control and implementation methods are discussed. A decision is made on which type of control will be best suited to achieve the objectives of this study.

2.2 Performance

The prospective application of a wind turbine determines its rated power. The wind speed where the rated power is reached is known as the rated wind speed and is chosen to minimize the cost of the wind turbine and maximize the energy yield (Gasch & Twele 2005, p.6).

To predict the performance, the blade element-momentum theory (BEM) is used. For a given wind speed, rotational speed, blade geometry and aerodynamic design the BEM theory yields a specific torque, power and thrust (Burton et al. 2001, pp. 59-65). For a range of wind speeds and rotational speeds a power curve is obtained like the one in Figure 2.1(a).

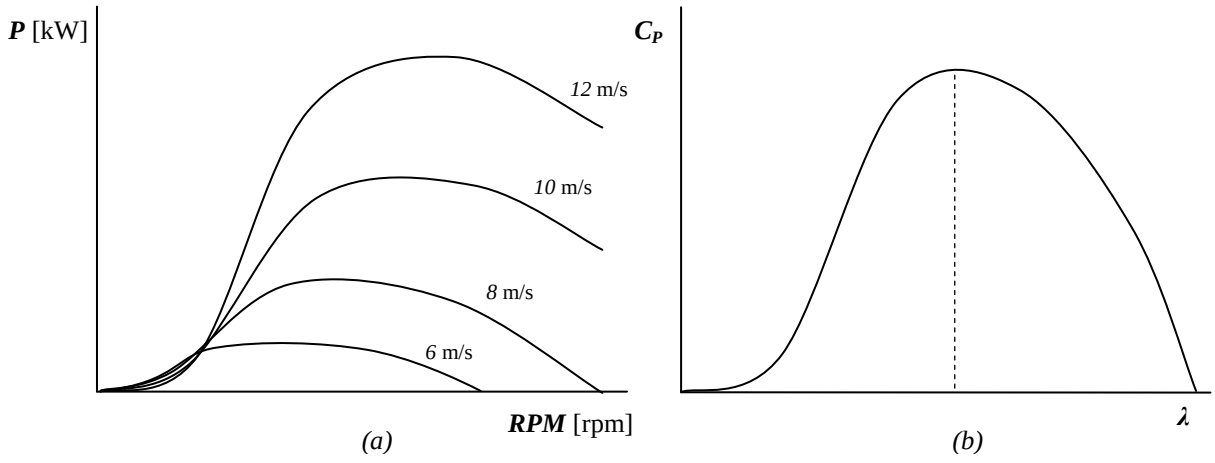

Figure 2.1 *(a) Power relative to rotational speed and (b) power coefficient relative to tip speed ratio (Gasch & Twele 2005, pp. 181-190)*

Assuming that the aerodynamic performance of the blades does not deteriorate, the performance characteristics of the blades are represented by non-dimensional curves relative to the tip speed ratio λ, which is the ratio of the tip speed to the wind speed. The main performance indicator of a wind turbine is its C_P-*TSR* curve, which gives the power coefficient relative to the tip speed ratio (Burton et al. 2001, p. 173). The same performance data shown in Figure 2.1(a) is shown in dimensionless form in Figure 2.1(b). Wind turbine rotors develop their peak efficiency only at a specific tip speed ratio (Burton et al. 2001, pp.64-65).

The power characteristics of the wind turbine system are determined by the power of the gearbox and generator matching the power of the blades. Depending on the type of generator used, the wind turbine will either be fixed speed or variable speed. A fixed speed wind turbine will only operate optimally at the wind speed corresponding to its optimal tip speed ratio. With a variable speed wind turbine the rotational speed is controlled as the wind speed changes. This ensures that the wind turbine operates close to its optimal tip speed ratio (Burton et al. 2001, pp.360-362). Figure 2.2 shows an example of a variable speed wind turbine, with the generator curve intersecting the wind turbine's power curve at its operating points. For a specific wind speed, the wind turbine will rotate at a specific rotational speed and generate a specific amount of power, assuming steady-state operation.

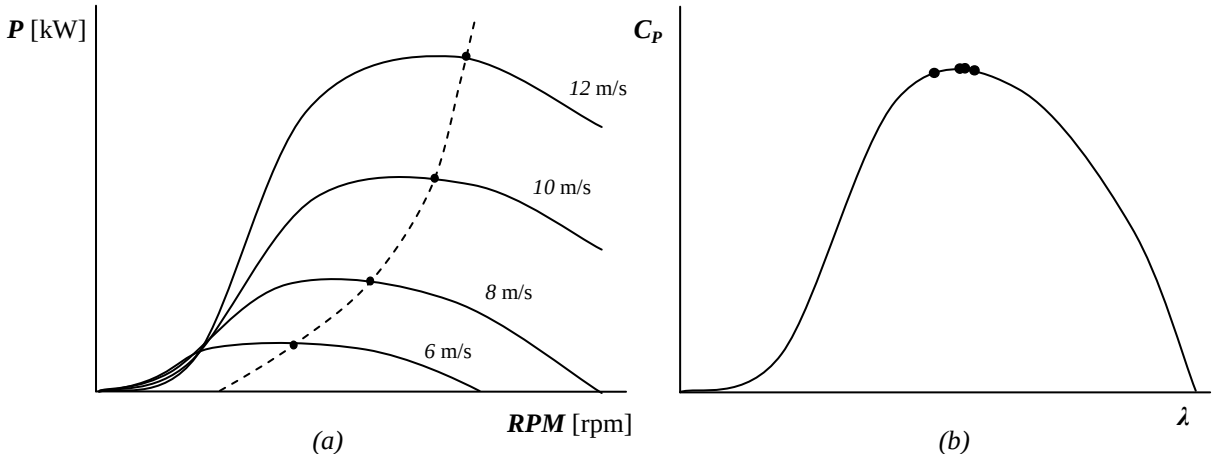

Figure 2.2 *(a) Generator intersecting the power curves and (b) operating points on the C_P-TSR curve*

A small stand-alone wind turbine used for battery charging mainly uses a permanent magnet alternator connected to a battery bank with a rectifier. This type of wind turbine is also a variable speed turbine, but the speed is not actively controlled. The power is dictated solely by the rotational speed and the interaction of the battery bank with the alternator (Muljadi et al. 1995).

Cogging torque is an inherent characteristic of permanent magnet alternators. For the wind turbine to start, the wind speed must increase to where the torque produced by the rotor overcomes the generator's cogging torque (Muljadi & Green 2002).

2.3 Control

A wind turbine needs to be controlled to ensure safe and optimal operation, especially during high wind speeds. This is done by the control system which continually regulates the rotor speed, torque, power or thrust (Gasch & Twele 2005, p. 319).

The two most common control objectives are to regulate the rotor speed or to regulate the power output. Common control methods are passive stall, pitch control and generator load control (Burton et al. 2001, pp.472-478). Pitch control is the most common means of controlling a wind turbine's performance. Either increasing or decreasing the blade's pitch has a major impact on its performance (Burton et al. 2001, p.475). When the blades' pitch is increased, the blades are turned more into the wind or into a feathering position. This is called pitching towards feather or positive pitching. Decreasing the pitch turns the blades out of the wind to a position more perpendicular to the wind. This is called pitching towards stall or negative pitching (Figure 2.3) (Gasch & Twele 2005, pp. 322-323).

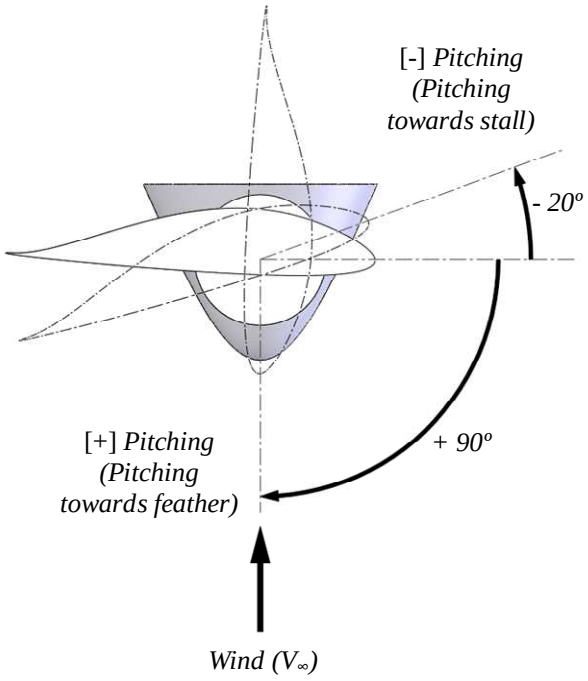

Figure 2.3 *Pitching directions and possible ranges required*

At above rated wind speeds positive pitch control provides a very effective means of regulating the power output. Increasing the pitch results in a decrease of the angle of attack and the lift coefficient, which in turn limits the power output (Figure 2.4) (Burton et al. 2001, p.475).

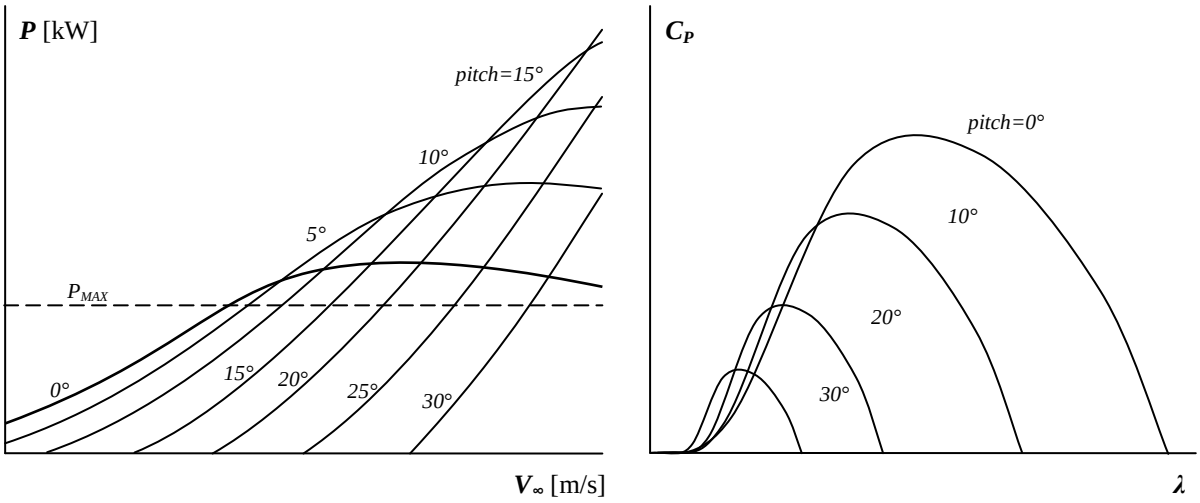

Figure 2.4 *Example curves showing the effect of positive pitch change (Burton et al. 2001, pp.352-357)*

For a positive pitch control system to provide effective power regulation the pitch has to be changed very rapidly to react to wind gusts. Also, a pitch range of $p = 0^\circ$ to 35° may be required to regulate the power and a pitch of up to $p = 90^\circ$ or full feather to provide effective aerodynamic braking (Figure 2.3). Fast closed-loop control using hydraulic actuators and electronics are best suited for positive pitch control (Burton et al. 2001, pp.351-355).

At above rated wind speeds a negative pitch control system regulates the power by decreasing the pitch. This results in an increased angle of attack and increased stall, lower lift and higher drag and thus decreased power (Figure 2.5) (Burton et al. 2001, p.475). A negative effect of decreasing the pitch is that it leads to large thrust loads on the blades and the tower (Gasch & Twele 2005, p.323).

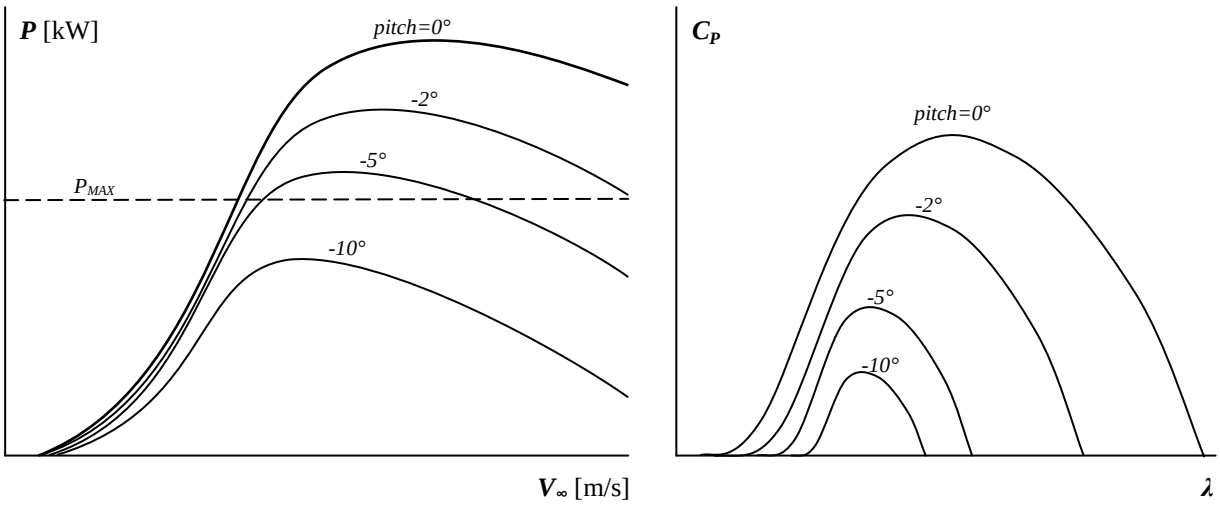

Figure 2.5 *Example curves showing the effect of negative pitch change (Burton et al. 2001, pp.352-357)*

Once a large part of the blade is stalled, only small pitch movements are required to regulate the power and much less dynamic pitch activity. To regulate the power, a pitch range as small as $p = 0^\circ$ to -5° may be required and for full aerodynamic breaking only $p = -20^\circ$ (Figure 2.3) (Burton et al. 2001, pp.355-356). Because of the shorter regulating distance and lesser dynamic pitch activity, negative pitch control can easily be implemented using a simple mechanical control unit (Gasch & Twele 2005, p.89).

With a variable speed wind turbine that uses a permanent magnet alternator connected to a battery bank, an increasing rotor speed corresponds to an increasing power (Muljadi et al. 1995). Using either positive or negative pitch control to limit the power will also limit the rotor speed.

The start-up torque can be controlled to provide better start-up of a wind turbine. With an increasing pitch angle, the torque coefficient C_Q at $\lambda = 0$ increases (Figure 2.6). If the blades have a positive pitch at start-up, it will result in an increased torque at start-up. If a permanent magnet alternator is used, an increased start-up torque will overcome the generator's cogging torque at a lower wind speed, thus decreasing the cut-in wind speed (Muljadi & Green 2002).

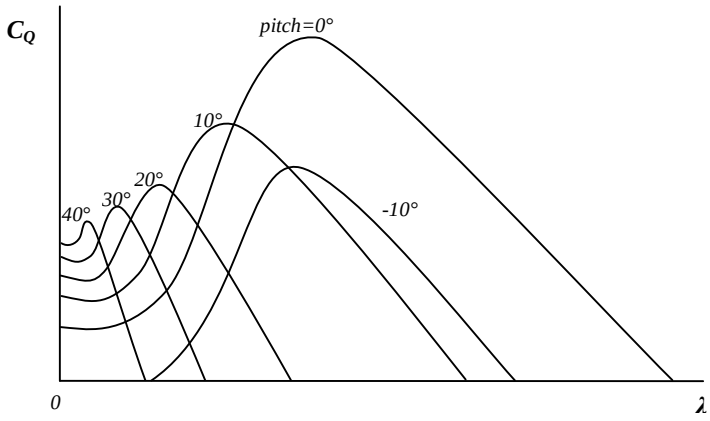

Figure 2.6 *The effect of pitch change on the torque coefficient (Gasch & Twele 2005, pp.190-191)*

Pitching from a positive pitch angle suitable for start-up, towards stall to limit the rotor speed, provides the possibility to achieve both control objectives without changing the pitching direction (Figure 2.7) (Gasch & Twele 2005, p.89).

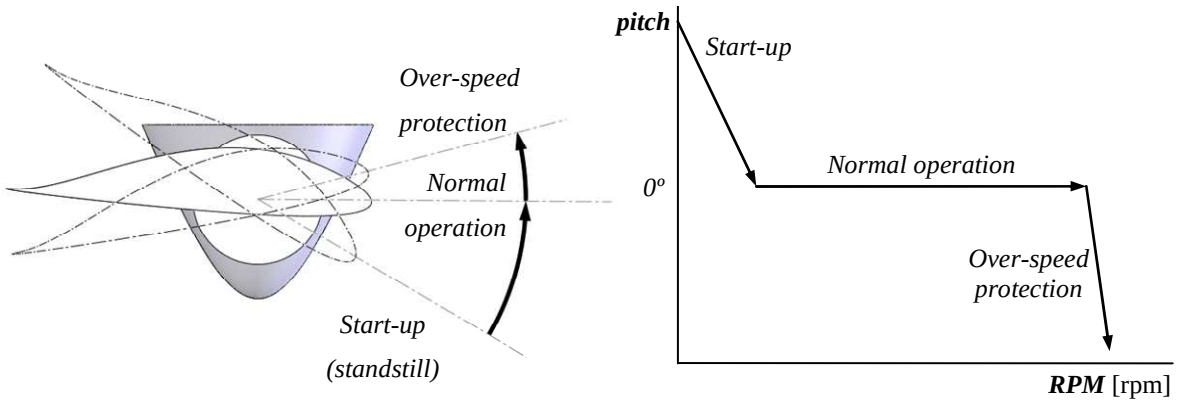

Figure 2.7 *One-directional transition from standstill to operation to over-speed using pitch towards stall*

2.4 Control implementation

Wind turbine controls can be classified into three groups, which depends on how the control is implemented, the method of actuation and its complexity (Gasch & Twele 2005, p. 320):

- Secondary or over-speed protection, like a mechanical brake.
- Simple control systems, which are mainly used on stand-alone wind turbines not connected to a grid. These systems use proportional control regulated by centrifugal force or wind pressure. Simple control is used on small wind turbine systems, because it is more affordable and feasible. It provides over-speed protection and continuous control during normal operation.
- Fast closed-loop control systems, which continually monitor the wind turbine's performance and make immediate adjustments. These systems require fast electric or hydraulic actuators, electronics and are used on large grid-connected wind turbines, where it would be feasible to implement. It provides over-speed protection and continuous control during normal operation.

A centrifugal governor is a simple proportional controller. With a linear increase in rotational speed, the displacement increases linearly. The equilibrium of the forces and moments caused by the mass and spring determines the angular displacement (Figure 2.8) (Dorf & Bishop 2001, p.4).

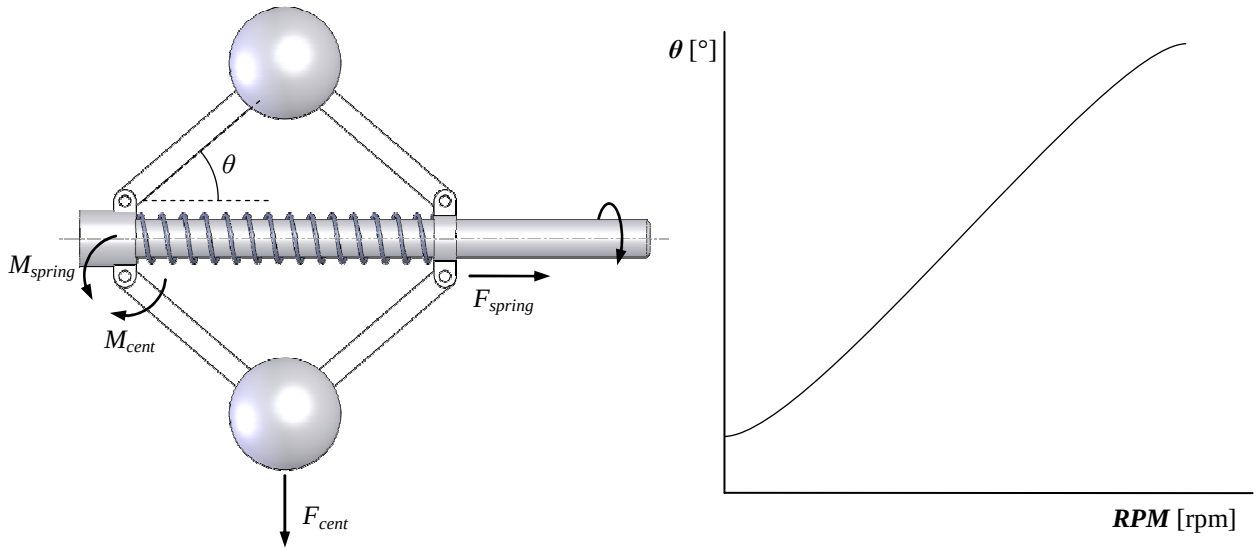

Figure 2.8 *A simple centrifugal controller and its angular displacement*

Gasch & Twele (2005, pp.89-90) proposes that with using pitching towards stall, the same centrifugal governor can be used, where it initially works against a soft spring to provide better start-up and then against a harder spring to provide power and speed regulation (Figure 2.9).

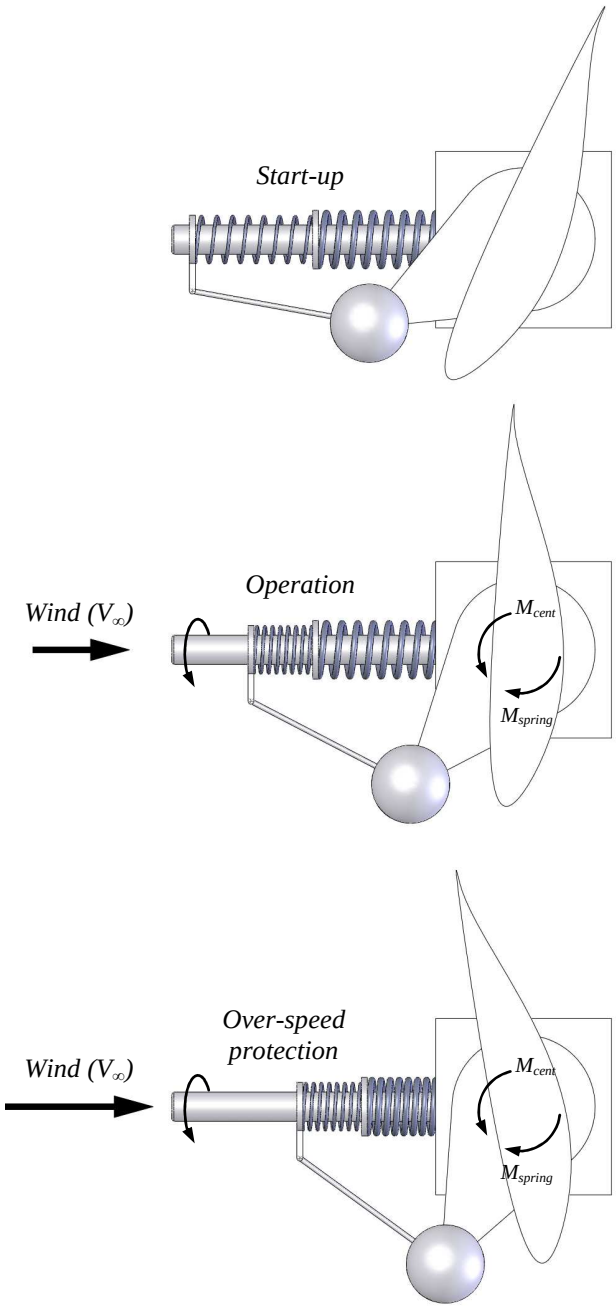

Figure 2.9 *Proposed centrifugal governor concept for improved start-up and over-speed protection (Gasch & Twele 2005, pp.89-90)*

2.5 Summary

In this chapter it was established that negative pitch control is best suited to achieve both control objectives of improved start-up and over-speed protection and that it can be implemented using a centrifugal governor with two springs, each with a different stiffness.

Chapter 3 Theory

3.1 Introduction

This chapter provides the theoretical background necessary to model a wind turbine with active pitch control. The blade element-momentum theory is discussed in detail. Wind speed frequency distributions are discussed. The centrifugal control theory and the governor kinematics are developed and described in detail.

3.2 Wind turbine system

Figure 3.1 shows the flow diagram of a complete wind turbine system, with the generator connected directly to the rotor blades. If there is a sudden gust of wind, the rotor torque will exceed the generator torque. Depending on the inertia of the system, the rotor will accelerate until the rotor torque equals the generator torque and the system is in a steady-state. Depending on the wind speed, the rotor will rotate at a specific speed and generate a specific amount of power (Gasch & Twele 2005, p.321). In this study only the steady-state of the system will be considered. To model the rotor blades the blade element-momentum theory is used.

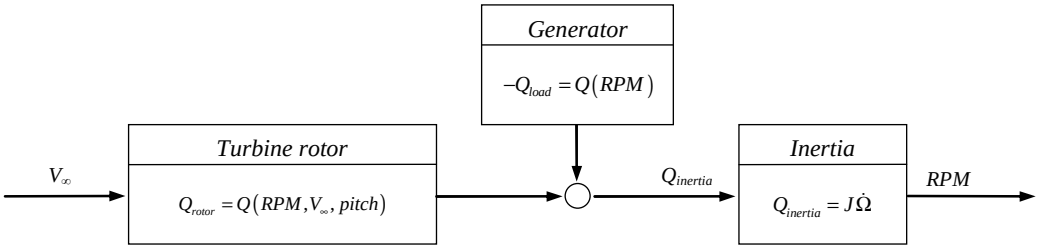

Figure 3.1 *Wind turbine system block diagram*

3.3 Blade element-momentum theory

For a given wind speed V_∞, rotational speed Ω, blade geometry and aerodynamic design the blade element-momentum theory yields a specific thrust T, torque Q and power P. The assumption of the BEM theory is that the aerodynamic lift and drag forces on the blade element at radius r, with infinitesimal length δr, are solely responsible for the change of momentum of the air which passes through the annulus swept by the element (Figure 3.2) (Burton et al. 2001, pp. 59-65).

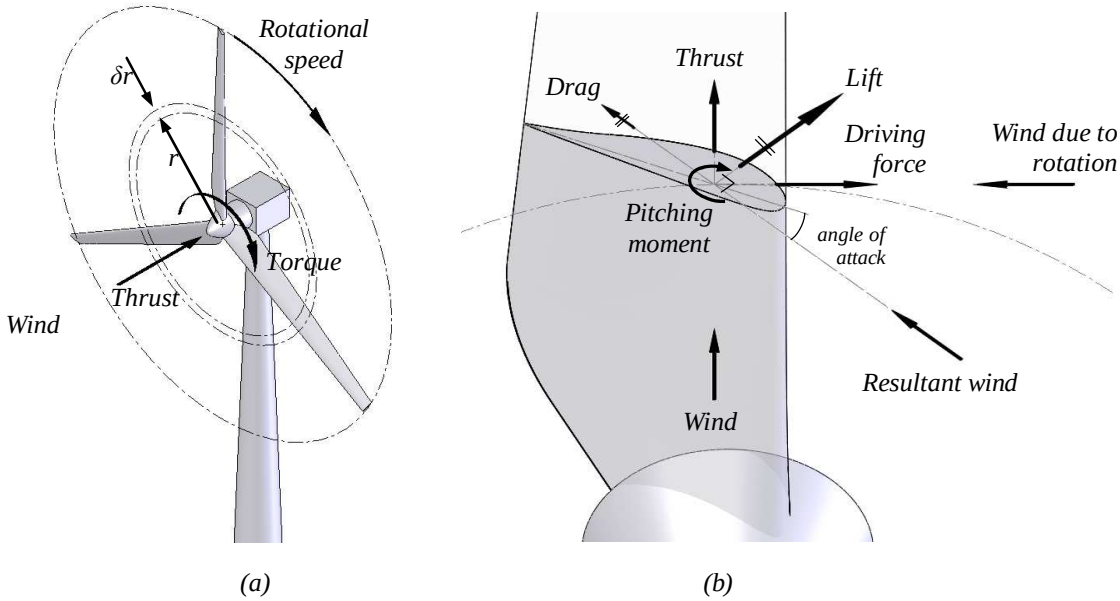

Figure 3.2 *(a) Annulus swept out by the blade element at r and (b) blade element velocities and forces*

The forces on a blade element can be calculated using its two-dimensional airfoil characteristics, namely its lift coefficient C_L and drag coefficient C_D. They are a function of the angle of attack α. The angle of attack α is determined by the incident resultant velocity W in the plane of the blade element. The incident velocity W is determined by the wind speed or free-stream velocity V_∞, rotational speed Ω and the flow induction factors a and a' (Figure 3.2(b) and Figure 3.3) (Burton et al. 2001, p.60).

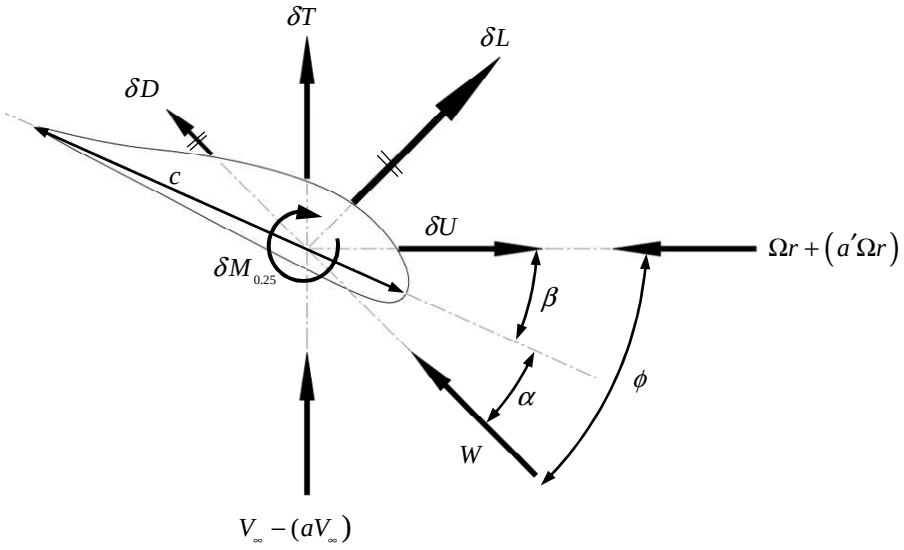

Figure 3.3 *Blade element velocities and forces at radius r*

The free-stream velocity V_∞ is decreased by $(a \cdot V_\infty)$ because the rotor decelerates the wind. The factor a is called the axial flow induction factor.

The flow that just enters the rotor has no rotational movement. Because the air exerts a torque on the rotor, the rotor exerts an equal and opposite torque on the air. This reaction torque causes the air to rotate in a direction opposite to that of the rotor. This is the induced rotational or tangential velocity $(a' \cdot \Omega \cdot r)$, with a' the tangential induction factor. This component is added to the wind due to the rotation $(\Omega \cdot r)$ (Figure 3.3) (Burton et al. 2001, p.60).

For a specific V_∞, Ω and r, the resultant velocity W is given by

$$W = \sqrt{V_\infty^2 (1-a)^2 + (\Omega r)^2 (1+a')^2} \tag{3.1}$$

which acts at an angle ϕ relative to the plane of rotation, with

$$\sin(\phi) = \frac{V_\infty (1-a)}{W}, \cos(\phi) = \frac{\Omega r (1+a')}{W} \tag{3.2}$$

The angle of attack α is

$$\alpha = \phi - \beta \tag{3.3}$$

The lift force on a span-wise infinitesimal length δr, normal to the direction of W is

$$\delta L = \frac{1}{2} \rho W^2 c C_L \cdot \delta r \tag{3.4}$$

and the drag force, in line with W is

$$\delta D = \frac{1}{2} \rho W^2 c C_D \cdot \delta r \tag{3.5}$$

The resolved axial component of the forces or the thrust force δT is

$$\begin{aligned} \delta T &= (\delta L \cos(\phi) + \delta D \sin(\phi)) \cdot \delta r \\ &= \frac{1}{2} \rho W^2 c (C_L \cos(\phi) + C_D \sin(\phi)) \end{aligned} \tag{3.6}$$

The resolved tangential component of the forces or the driving force δU is

$$\delta U = \left(\delta L \sin(\phi) - \delta D \cos(\phi)\right) \cdot \delta r \tag{3.7}$$

and the torque δQ is

$$\begin{aligned} \delta Q = \delta U \cdot r &= \left(\delta L \sin(\phi) - \delta D \cos(\phi)\right) \cdot r \cdot \delta r \\ &= \frac{1}{2} \rho W^2 c \left(C_L \sin(\phi) - C_D \cos(\phi)\right) \cdot r \cdot \delta r \end{aligned} \tag{3.8}$$

To evaluate equations (3.1) to (3.8), the induction factors a and a' still need to be calculated. As stated earlier, the assumption of the BEM theory is that the forces of a blade element are solely responsible for the change of momentum of the air which passes through the annulus swept by the element. The assumption must be applied to calculate the induction factors (Burton et al. 2001, pp.61-62). Equating the resolved axial force from equation (3.6) for *N* blades with the change in axial momentum in the annulus, one gets

$$\begin{aligned} &\left(\frac{1}{2} \rho W^2 c \left(C_L \cos(\phi) + C_D \sin(\phi)\right)\right) N \cdot \delta r \\ &= \left(4a(1-a) \cdot \rho V_\infty^2 r + \frac{1}{2} \rho \left(2a' \Omega r\right)^2 2\pi r\right) \cdot \delta r \end{aligned}$$

with

$$c_T = 4a(1-a) \tag{3.9}$$

being called the annular thrust coefficient (Burton et al. 2001, p.66). Simplifying leads to

$$\frac{1}{2} \rho W^2 N c \left(C_L \cos(\phi) + C_D \sin(\phi)\right) \cdot \delta r = \pi \rho r \left(C_T V_\infty^2 + \left(2a' \Omega r\right)^2\right) \cdot \delta r \tag{3.10}$$

Equating the torque produced by the blade elements from equation (3.8) for *N* blades with the change in the angular momentum in the annulus one gets

$$\frac{1}{2} \rho W^2 N c \left(C_L \sin(\phi) - C_D \cos(\phi)\right) \cdot r \cdot \delta r = \left(4\pi \rho V_\infty \left(\Omega r\right) a' \left(1-a\right) r^2\right) \cdot \delta r \tag{3.11}$$

The induction factors a and a' are solved iteratively until equations (3.10) and (3.11) are satisfied and equations (3.1) to (3.8) can be evaluated for a specific V_∞, Ω and r.

To obtain the rotor's performance for a specific V_∞ and Ω, equations (3.1) to (3.11) must be evaluated for each blade element at chosen radius r intervals and integrated to obtain the rotor's thrust, torque and power (Gasch & Twele 2005, p.174):

$$T = N\int_0^R (\delta T)\,\delta r \tag{3.12}$$

$$Q = N\int_0^R (\delta U \cdot r)\,\delta r = N\int_0^R (\delta Q)\,\delta r \tag{3.13}$$

$$P = \Omega Q \tag{3.14}$$

To obtain a complete performance characteristic of the rotor, equations (3.1) to (3.14) must be evaluated for a range of wind speeds and rotational speeds.

To obtain the non-dimensional performance characteristics, the power coefficients C_P, torque coefficients C_Q and thrust coefficients C_T must be determined as a function of the tip speed ratio λ (Gasch & Twele 2005, p.175):

$$C_P = \frac{P}{\frac{1}{2}\rho V_\infty^3 \pi R^2} \tag{3.15}$$

$$C_T = \frac{T}{\frac{1}{2}\rho V_\infty^{\,2} \pi R^2} \tag{3.16}$$

$$C_Q = \frac{Q}{\frac{1}{2}\rho V_\infty^{\,2} \pi R^3} \tag{3.17}$$

$$\lambda = \frac{\Omega R}{V_\infty} \tag{3.18}$$

A permanent magnet alternator's torque is a function of its rotational speed (Muljadi et al. 1995). At a steady-state the torque generated by the rotor blades will be equal to the torque of the generator. The power of the rotor blades will also be equal to the power of the generator:

$$\begin{aligned} Q(V_\infty, \Omega) &= Q_{load}(\Omega) \\ P(V_\infty, \Omega) &= P_{load}(\Omega) \end{aligned} \tag{3.19}$$

3.3.1 Turbulent windmill state

A wind turbine running at a high tip speed ratio is heavily loaded with a high axial induction factor (a) distribution. The annular thrust coefficient c_T from equation (3.9) of the BEM theory becomes invalid for high induction factors and will yield inaccurate results. For a>0.4, an empirical relationship between c_T and a is used (Buhl 2005):

$$\begin{aligned} c_T &= 4a(1-a) \quad \text{for } a < 0.4 \\ c_T &= \frac{8}{9} + \left(4 - \frac{40}{9}\right)a + \left(\frac{50}{9} - 4\right)a^2 \quad \text{for } a \geq 0.4 \end{aligned} \tag{3.20}$$

Figure 3.4 shows the comparison between the theoretical c_T and empirical c_T. Note that the loss factor F was excluded from equation (3.20), because it is already included in (3.23) and (3.24).

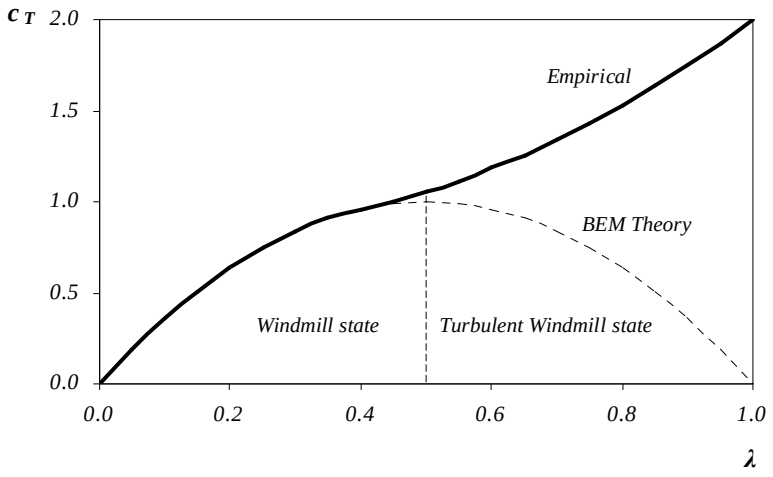

Figure 3.4 *Comparison between theoretical c_T and empirical c_T (Buhl 2005)*

3.3.2 Tip and root losses

One of the limitations of the BEM theory is that it does not take into account the circulation that falls to zero at the blade tip and root, which results in reduced torque and power (Burton et al. 2001, p.78). The tip power loss is expressed as the tip-loss factor (Moriarty & Hansen 2005):

$$F_T(x) = \frac{2}{\pi}\cos^{-1} e^{-\frac{N}{2}\left(\frac{R-r}{r\sin(\phi)}\right)} \tag{3.21}$$

The loss factor at the blade root is

$$F_R(x) = \frac{2}{\pi}\cos^{-1} e^{-\frac{N}{2}\left(\frac{r-R_{hub}}{R_{hub}\sin(\phi)}\right)} \tag{3.22}$$

The combined loss factor is $F(x) = F_T(x)F_R(x)$ (Figure 3.5).

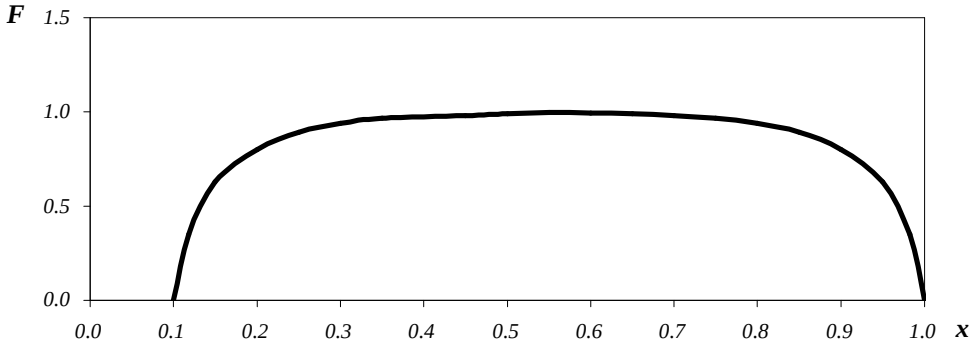

Figure 3.5 *Combined tip-loss and root loss factors across the normalized length of the blade*

The momentum part of equations (3.10) and (3.11) are modified with the combined loss-factor (Moriarty & Hansen 2005):

$$\frac{1}{2}\rho W^2 N c\left(C_L\cos(\phi) + C_D\sin(\phi)\right)\cdot\delta r = \pi\rho r\left(C_T V_\infty^2 + \left(2a'\Omega r\right)^2\right)\cdot F\cdot\delta r \tag{3.23}$$

$$\frac{1}{2}\rho W^2 N c\left(C_L\sin(\phi) - C_D\cos(\phi)\right)\cdot r\cdot\delta r = \left(4\pi\rho V_\infty\left(\Omega r\right)a'\left(1-a\right)r^2\right)\cdot F\cdot\delta r \tag{3.24}$$

3.4 Wind speed distribution

The wind speed variation of a specific area is described by its Weibull probability distribution (Burton et al. 2001, p14):

$$f = \frac{k}{c} \cdot \left(\frac{V_\infty}{c} \right)^{k-1} \cdot e^{-\left(\left(\frac{V_\infty}{c} \right)^k \right)} \qquad (3.25)$$

$$\text{with} \quad c = \frac{\Gamma\left(1 + \frac{1}{k}\right)}{\bar{V}_\infty}$$

k is the shape factor, $\bar{V}_\infty$ the mean annual wind speed and Γ the gamma function. An example of a Weibull probability distribution is shown in Figure 3.6.

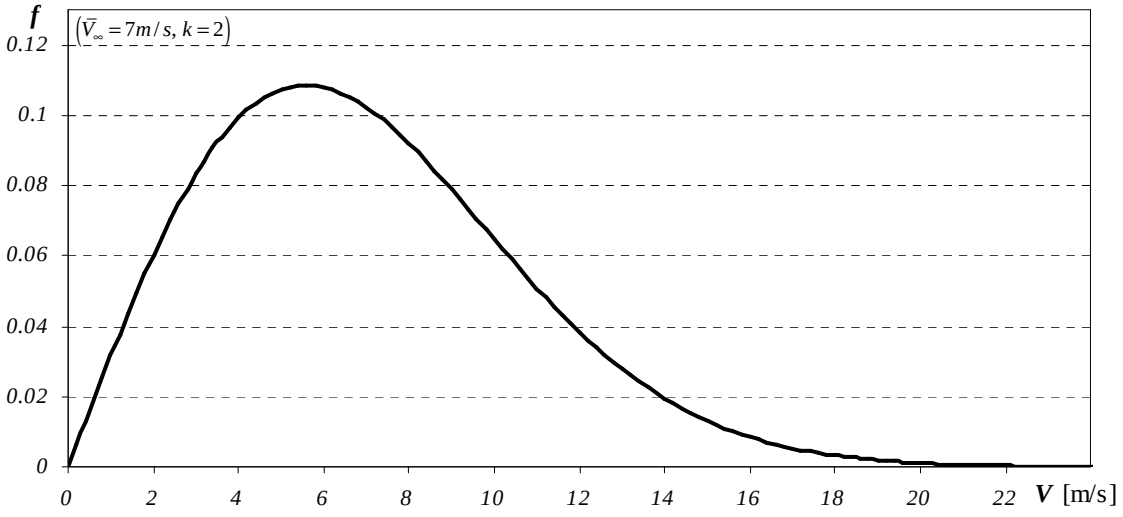

Figure 3.6 *Example of a Weibull probability distribution with $\bar{V}_\infty$ = 7 m/s and k=2*

As seen from Figure 3.6, the wind speed distribution is skewed. High wind speeds seldom occur.

3.5 Centrifugal governor

Figure 3.7 shows the flow diagram of a wind turbine with a centrifugal governor. Notice that with the added governor to the system, the pitch is now dependant on the rotor speed (Gasch & Twele 2005, p.328).

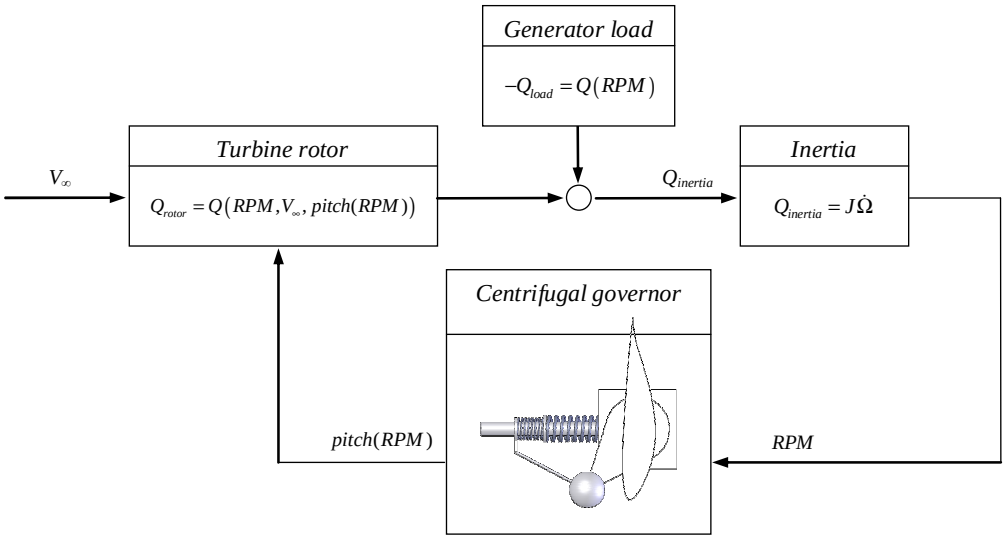

Figure 3.7 *Block diagram for a wind turbine with a centrifugal governor*

As a first concept, a home-made 3-bladed centrifugal governor concept was used to develop the model (Figure 3.8 and Figure 3.9).

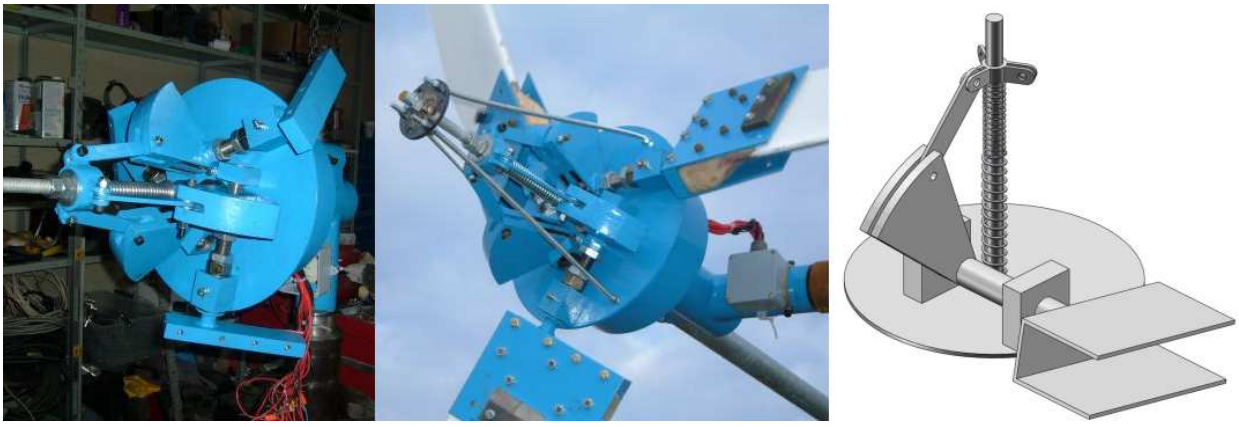

Figure 3.8 *Centrifugal governor concept*

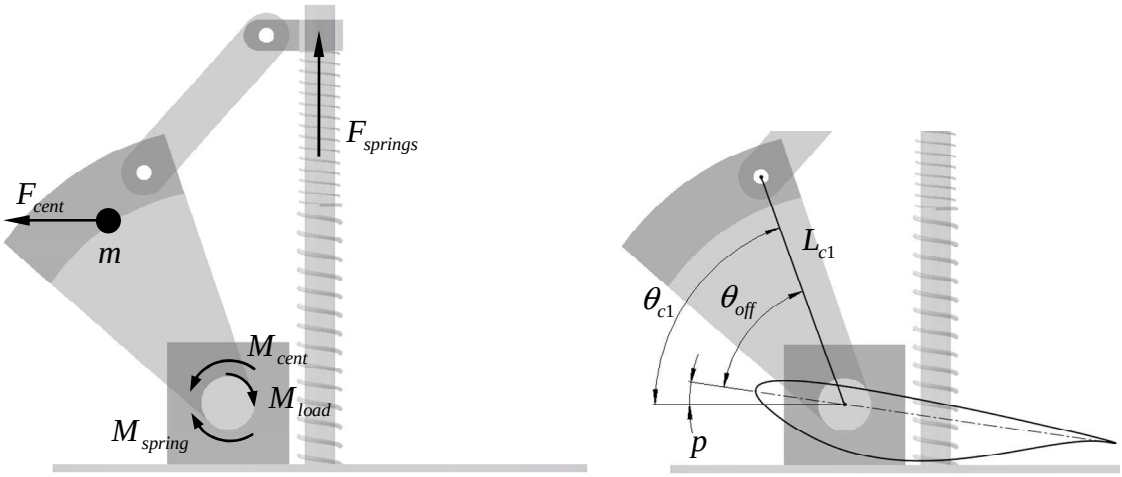

Figure 3.9 *Governor forces, moments and angle conventions*

At a specific rotational speed Ω, the equilibrium of the moments around the pitching axis caused by the mass and spring determines the pitch (Figure 3.9):

$$M_{cent} - M_{spring} - M_{load} = 0 \tag{3.26}$$

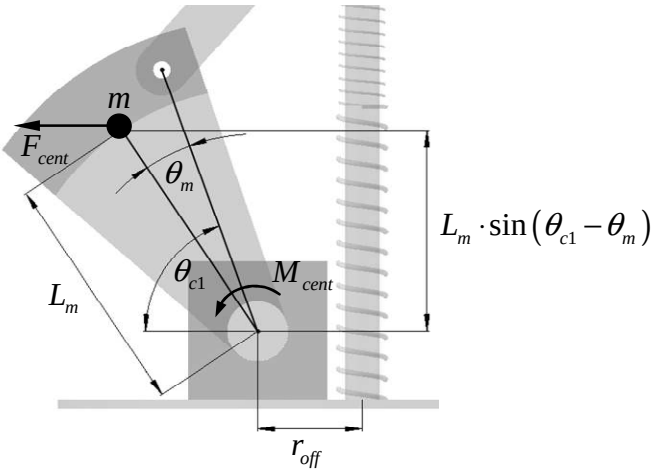

Figure 3.10 *Moment caused by centrifugal force*

From Figure 3.10, the moment caused by the centrifugal force of the mass for a specific θ_{c1} is

$$M_{cent} = F_{cent} \cdot L_m \cdot \sin\left(\theta_{c1} - \theta_m\right) \tag{3.27}$$

with

$$\begin{aligned} F_{cent} &= m \cdot \Omega^2 \cdot r_{effective} \\ &= m \cdot \Omega^2 \cdot \left(r_{off} + L_m \cdot \cos\left(\theta_{c1} - \theta_m\right)\right) \end{aligned} \tag{3.28}$$

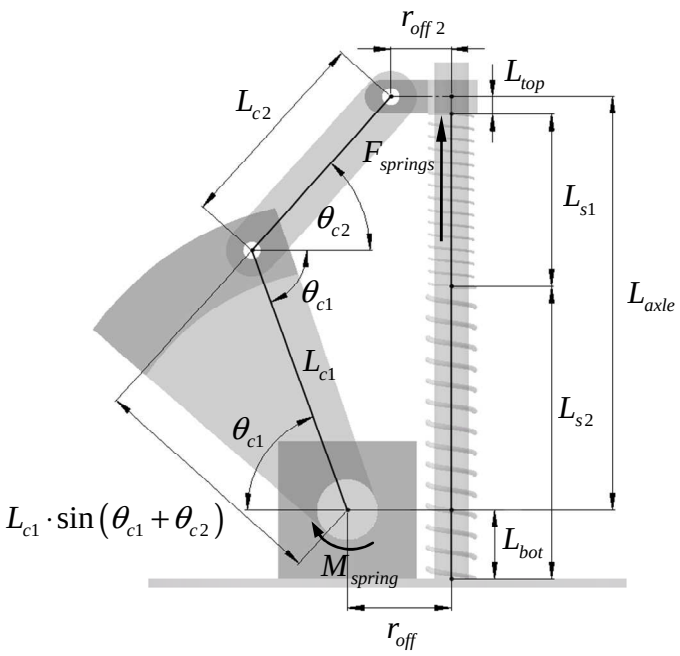

Figure 3.11 *Moment caused by spring force*

From Figure 3.11, the moment caused by the spring forces for a specific θ_{c1} is

$$M_{spring} = \left(\frac{F_{springs}}{\sin\theta_{c2}}\right) \cdot L_{c1} \cdot \sin\left(\theta_{c1} + \theta_{c2}\right) \tag{3.29}$$

with

$$\theta_{c2} = \cos^{-1}\left(\frac{L_{c1} \cdot \cos\left(\theta_{c1}\right) + r_{off} - r_{off\,2}}{L_{c2}}\right) \tag{3.30}$$

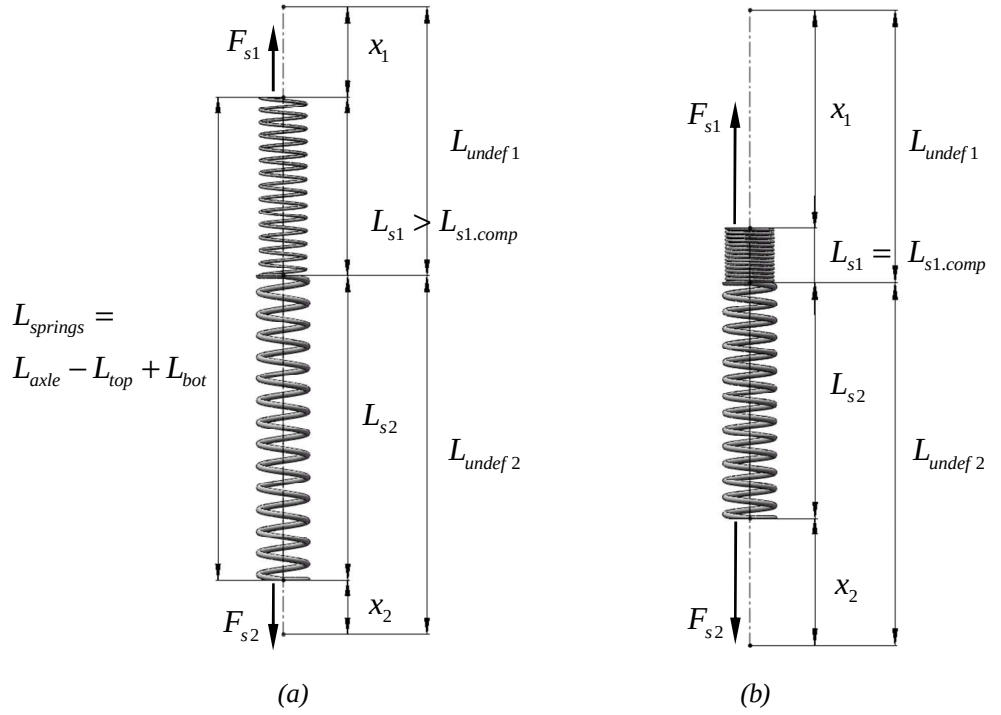

Figure 3.12 *Spring forces and displacements*

$F_{springs}$ is calculated from the displaced length of the springs at a specific θ_{c1} (Figure 3.11):

$$\begin{aligned} L_{springs} &= L_{s1} + L_{s2} \\ &= L_{axle} - L_{top} + L_{bot} \\ &= \left(L_{c1} \cdot \sin\theta_{c1} + L_{c2} \cdot \sin\theta_{c2}\right) - L_{top} + L_{bot} \end{aligned} \tag{3.31}$$

The spring forces are (Figure 3.12)

$$\begin{aligned} F_{springs} &= F_{s1} + F_{s2} \\ F_{s1} &= -k_1 \cdot x_1 = -k_1 \cdot \left(L_{undef\,1} - L_{s1}\right) \\ F_{s2} &= -k_2 \cdot x_2 = -k_2 \cdot \left(L_{undef\,2} - L_{s2}\right) \end{aligned} \tag{3.32}$$

If both springs are not fully compressed (Figure 3.12(a)), the forces in the springs will be equal:

$$\begin{aligned} F_{s1} &= F_{s2} \\ k_1 \cdot L_{undef\,1} - k_2 \cdot L_{undef\,2} &= k_1 \cdot L_{s1} - k_2 \cdot L_{s2} \end{aligned}$$

Rearranging to use equation (3.31):

$$\begin{aligned} k_1 \cdot L_{undef\,1} - k_2 \cdot L_{undef\,2} &= k_1 \cdot \left(L_{s1} + L_{s2}\right) - k_1 \cdot L_{s2} - k_2 \cdot L_{s2} \\ &= k_1 \cdot L_{springs} - k_1 \cdot L_{s2} - k_2 \cdot L_{s2} \\ -k_2 \cdot L_{undef\,2} + k_2 \cdot L_{s2} &= k_1 \cdot L_{springs} - k_1 \cdot L_{s2} - k_1 \cdot L_{undef\,1} \\ L_{s2} \cdot \left(k_1 + k_2\right) &= k_1 \cdot L_{springs} - k_1 \cdot L_{undef\,1} + k_2 \cdot L_{undef\,2} \\ L_{s2} &= \frac{k_1 \cdot L_{springs} - k_1 \cdot L_{undef\,1} + k_2 \cdot L_{undef\,2}}{k_1 + k_2} \end{aligned}$$

and from (3.31), with both springs not completely compressed, the displacements are

$$\begin{aligned} L_{s1} &= L_{springs} - L_{s2} \\ &= L_{springs} - \frac{k_1 \cdot L_{springs} - k_1 \cdot L_{undef\,1} + k_2 \cdot L_{undef\,2}}{k_1 + k_2} \\ &= \left(\left(L_{c1} \cdot \sin\theta_{c1} + L_{c2} \cdot \sin\theta_{c2}\right) - L_{top} + L_{bot}\right) \\ &\quad - \frac{k_1 \cdot \left(\left(L_{c1} \cdot \sin\theta_{c1} + L_{c2} \cdot \sin\theta_{c2}\right) - L_{top} + L_{bot}\right) - k_1 \cdot L_{undef\,1} + k_2 \cdot L_{undef\,2}}{k_1 + k_2} \\ L_{s2} &= \left(\left(L_{c1} \cdot \sin\theta_{c1} + L_{c2} \cdot \sin\theta_{c2}\right) - L_{top} + L_{bot}\right) - L_{s1} \end{aligned} \tag{3.33}$$

If $L_{s1} \le L_{s1.comp}$ (Figure 3.12(b)), the displacements are

$$\begin{aligned} L_{s1} &= L_{s1.comp} \\ L_{s2} &= \left(\left(L_{c1} \cdot \sin\theta_{c1} + L_{c2} \cdot \sin\theta_{c2}\right) - L_{top} + L_{bot}\right) - L_{s1.comp} \end{aligned} \tag{3.34}$$

With L_{s1} and L_{s2} known, equations (3.32) can be evaluated to get $F_{springs} = F_{s1} + F_{s2}$ and M_{spring} from equation (3.29).

M_{load} from equation (3.26) can consist of any external moments that influences the governor, including aerodynamic forces, centrifugal forces, inertia and friction. Under ideal circumstances the governor's only governing variable will be the rotation speed. With the addition of the external moment M_{load}, the angular displacement will no longer be only a function of the rotational speed. The sense of M_{load} will determine whether the rotational speed that is reached is higher or lower than the target rotational speed for a specific wind speed.

The sense of M_{load} in Figure 3.9 will result in a higher rotational speed. The different components of M_{load} will be discussed in the next section.

For a specific rotational speed Ω, the angle θ_{c1} must be found that satisfies the equilibrium of equation (3.26). (3.26), including (3.27) through (3.34), must be solved iteratively for θ_{c1}. With θ_{c1} known, the pitch can be calculated with the pitch offset angle θ_{off}:

$$p = \theta_{c1} - \theta_{off} \tag{3.35}$$

The limits of the governor can either be reached when $\theta_{c2}=0°$, with L_{c2} horizontal (Figure 3.13(a)) or when both the springs are compressed to a solid height (Figure 3.13(b)).

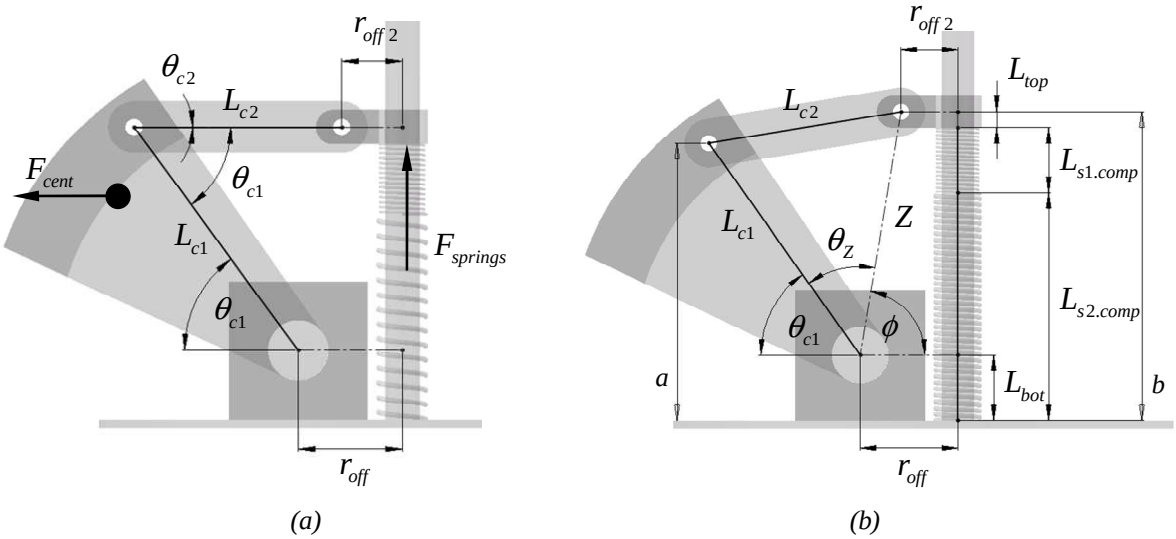

Figure 3.13 *Governor limit with (a) L_{c2} horizontal and (b) springs solid compressed*

From Figure 3.13(a), with L_{c2} horizontal, the minimum angle θ_{c1} will be

$$\theta_{c1.\min} = \cos^{-1}\left(\frac{L_{c2} + r_{off\,2} - r_{off}}{L_{c1}}\right) \tag{3.36}$$

From Figure 3.13(b), when the springs are compressed to a solid height:

$$Z = \sqrt{\left(L_{top} - L_{bot} + L_{s1.comp} + L_{s2.comp}\right)^2 + \left(r_{off} - r_{off\,2}\right)^2} \tag{3.37}$$

$$\phi = \cos^{-1}\left(\frac{r_{off} - r_{off\,2}}{Z}\right)$$

Using the cosine rule:

$$L_{c2}^2 = Z^2 + L_{c1}^2 - 2 \cdot Z \cdot L_{c1} \cdot \cos\left(\theta_Z\right)$$
$$\theta_Z = \cos^{-1}\left(\frac{Z^2 + L_{c1}^2 - L_{c2}^2}{2 \cdot Z \cdot L_{c1}}\right)$$

When the springs are compressed to a solid height, the minimum angle will therefore be

$$\begin{aligned}\theta_{rc.\min 2} &= \pi - \theta_Z - \phi \\ &= \pi - \cos^{-1}\left(\frac{Z^2 + L_{c1}^2 - L_{c2}^2}{2 \cdot Z \cdot L_{c1}}\right) - \cos^{-1}\left(\frac{r_{off} - r_{off\,2}}{Z}\right)\end{aligned} \tag{3.38}$$

Note that $\theta_{c1.\min 2}$ is only valid when $a < b$ (Figure 3.13(b)), therefore

$$\begin{aligned} a \quad &< b \\ \therefore \left(r_c \cdot \sin\left(\theta_{rc.\min 2}\right)\right) &< \left(L_{top} - L_{bot} + L_{s1.comp} + L_{s2.comp}\right)\end{aligned}$$

and when equation (3.37) evaluates to a real number. The minimum limit of θ_{c1} will therefore be the maximum of $\theta_{c1.\min}$ and $\theta_{c1.\min 2}$.

The maximum angle $\theta_{c1.max}$, when the springs are uncompressed and at their full length, can be calculated by modifying equation (3.37):

$$Z = \sqrt{\left(L_{top} - L_{bot} + L_{undef\,1} + L_{undef\,2}\right)^2 + \left(r_{off} - r_{off\,2}\right)^2} \tag{3.39}$$

3.6 Blade forces

The interaction that the blades have on the control of the centrifugal governor must be taken into account. Some of the governor components must also be designed for strength. The forces and moments are calculated where the governor pitching shaft is connected to the blade at radius r_c (Figure 3.14).

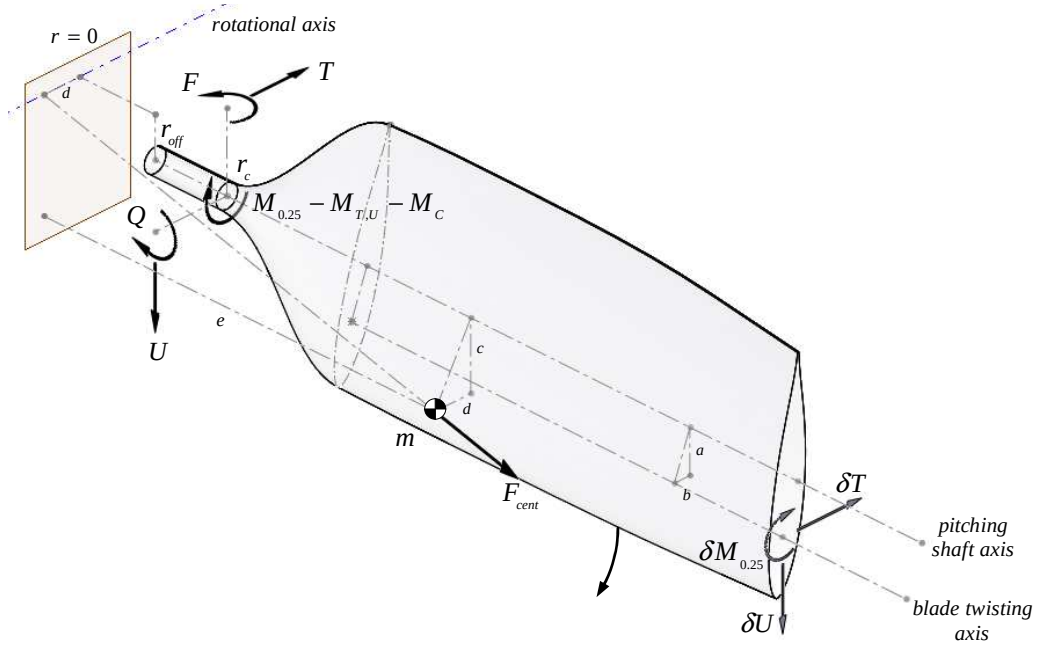

Figure 3.14 *The resolved blade forces and moments acting at point r_c*

The distribution of component δU causes a force U and moment Q at r_c in the plane of rotation. The out-of-plane δT distribution causes the thrust T and flapping moment F. The distribution of component $\delta M_{0.25}$ causes the pitching moment $M_{0.25}$ (Gasch & Twele 2005, p.174):

$$T = \int_{r_c}^{R} (\delta T)\, \delta r \tag{3.40}$$

$$F = \int_{r_c}^{R} \left(\delta T \cdot (r - r_c)\right) \delta r \tag{3.41}$$

$$U = \int_{r_c}^{R} (\delta U)\, \delta r \tag{3.42}$$

$$Q = \int_{r_c}^{R} \left(\delta U \cdot (r - r_c)\right) \delta r \tag{3.43}$$

$$M_{0.25} = \int_{r_c}^{R} (\delta M_{0.25})\, \delta r = \int_{r_c}^{R} \left(\frac{1}{2} \rho W^2 c^2 C_M \right) \delta r \tag{3.44}$$

Note that the forces and moments are calculated the same way as equations (3.12) and (3.13), but now the moments are calculated at $r=r_c$ instead of $r=0$.

With e the perpendicular distance from the centre of gravity to the $r=0$ plane and c the perpendicular distance to the pitching shaft axis, the centrifugal force will be

$$F_{cent} = m \cdot \Omega^2 \cdot \sqrt{e^2 + \left(c + r_{off}\right)^2} \tag{3.45}$$

The rotor blade elements are usually arranged along their 25% chord points on the blade's twisting axis as to minimize the twisting caused by the aerodynamic forces (Gasch & Twele 2005, p.168). With a and b the perpendicular distances between the pitching shaft axis and the blade twisting axis, the additional moment caused by the thrust T and force U is

$$M_{T,U} = T \cdot a + U \cdot b \tag{3.46}$$

If the blade's centre of gravity is not in line with the pitching shaft axis, the additional moment is

$$M_C = \left(m \cdot \Omega^2 \cdot \left(c + r_{off}\right)\right) \cdot d \tag{3.47}$$

The external moment (as defined in Figure 3.9) will thus be

$$M_{load} = M_{0.25} - M_{T,U} - M_C \tag{3.48}$$

Note that the moment due to the blade weight does not contribute to M_{load}, since the pitch of each blade is synchronised and the weight's effect is cancelled out. Any moment due to friction is also neglected because only the steady-state of the governor is considered.

3.7 Summary

The blade element-momentum theory, with its limitations was discussed in detail. The Weibull probability distribution was discussed. The centrifugal control and kinematics were developed and discussed in detail.

Chapter 4 Model implementation and preliminary results

4.1 Introduction

This chapter discusses the implementation of the theory discussed in the previous chapter to model the performance of an ungoverned wind turbine and a wind turbine with a centrifugal governor. The preliminary modelling results are discussed.

4.2 Model implementation

The algorithm for the complete wind turbine system, which consists of the rotor blades and generator are shown in Figure 4.1. For a given wind turbine, wind speed V_∞ and pitch p, the rotational speed Ω must be found where the torque Q or power P of the blades matches that of the generator. The rotational speed Ω is solved iteratively until the condition is satisfied. The iterative solution is done by using Newton's method (Cheney & Kincaid 1999). The external moment M_{load} will later be used in the governor calculation.

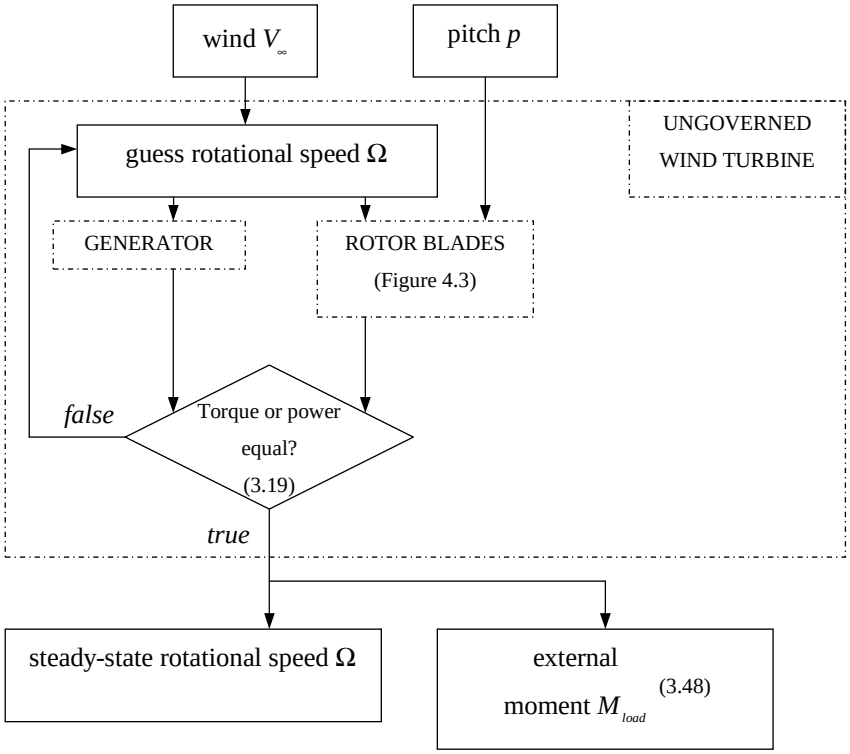

Figure 4.1 *Ungoverned wind turbine algorithm*

The algorithm for the wind turbine with a centrifugal governor is given in Figure 4.2. For a given governed wind turbine and wind speed, the rotational speed and pitch are solved iteratively until the whole system is in equilibrium.

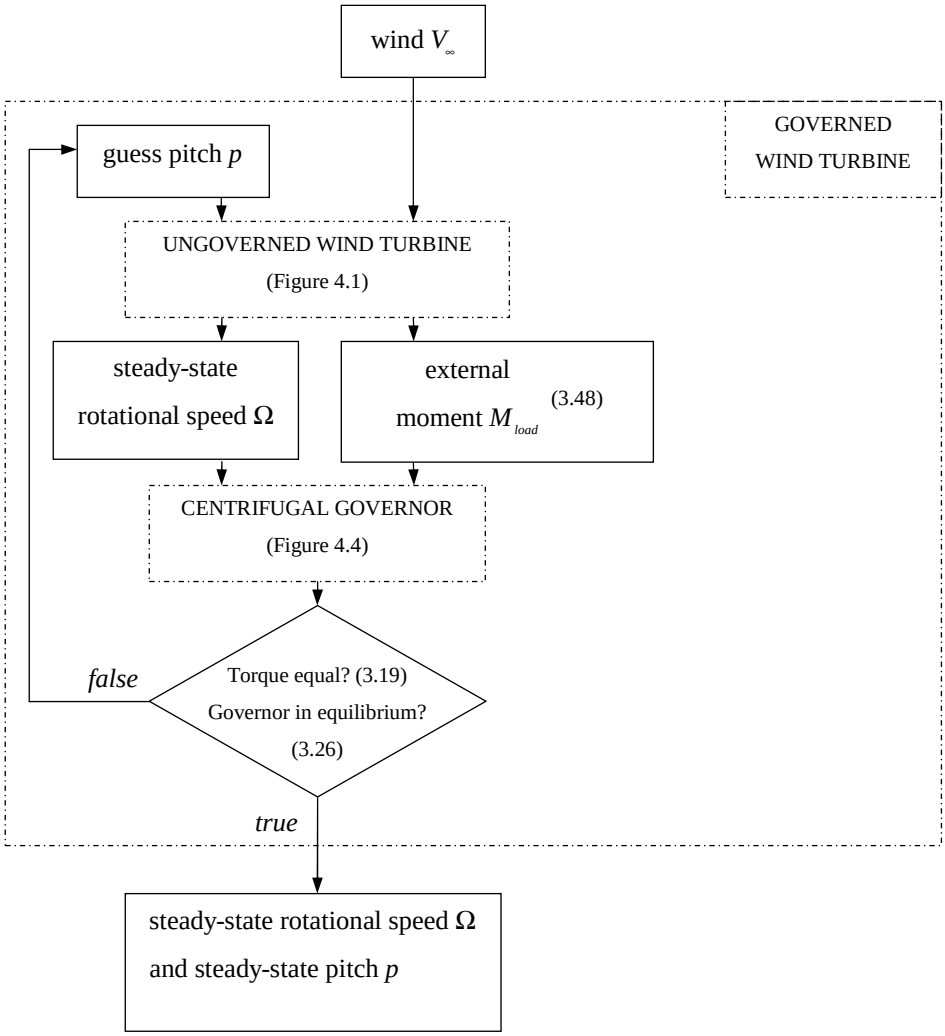

Figure 4.2 *Governed wind turbine algorithm*

The algorithm for the rotor blades is given in Figure 4.3. The wind speed, rotational speed and pitch are the inputs. For each blade element the induction factors are solved iteratively until the BEM conditions are satisfied. The distributions ∂T and ∂Q are integrated to get the thrust T, torque Q and power P. The accuracy of the integrals in equations (3.11) to (3.14) depends on the number of blade elements chosen.

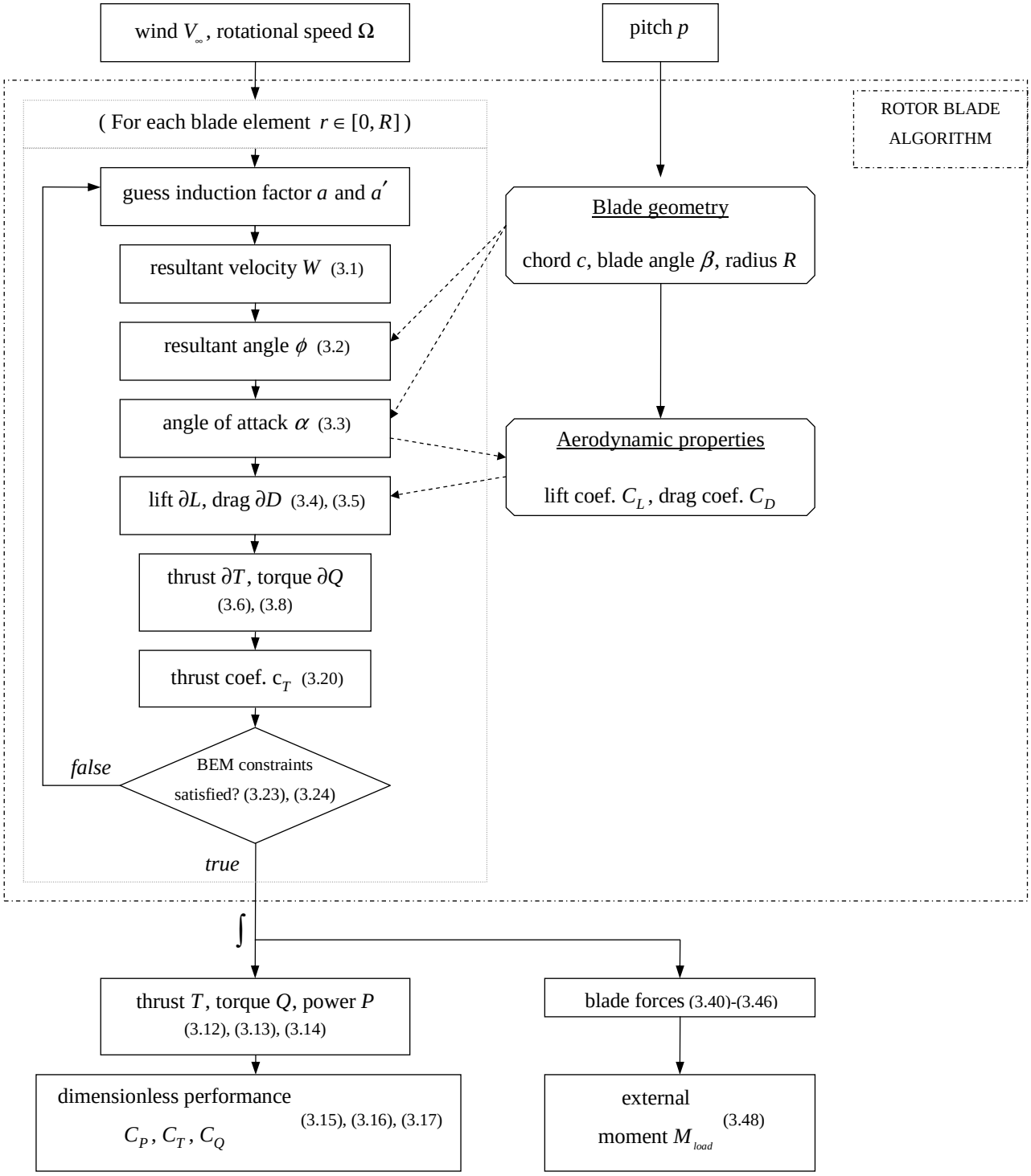

Figure 4.3 *Rotor blade algorithm*

The algorithm for the centrifugal governor is given in Figure 4.4. The rotational speed and the external moment M_{load} are the inputs. The pitch is solved iteratively until the governor is in equilibrium, with the conditions of equation (3.26) satisfied.

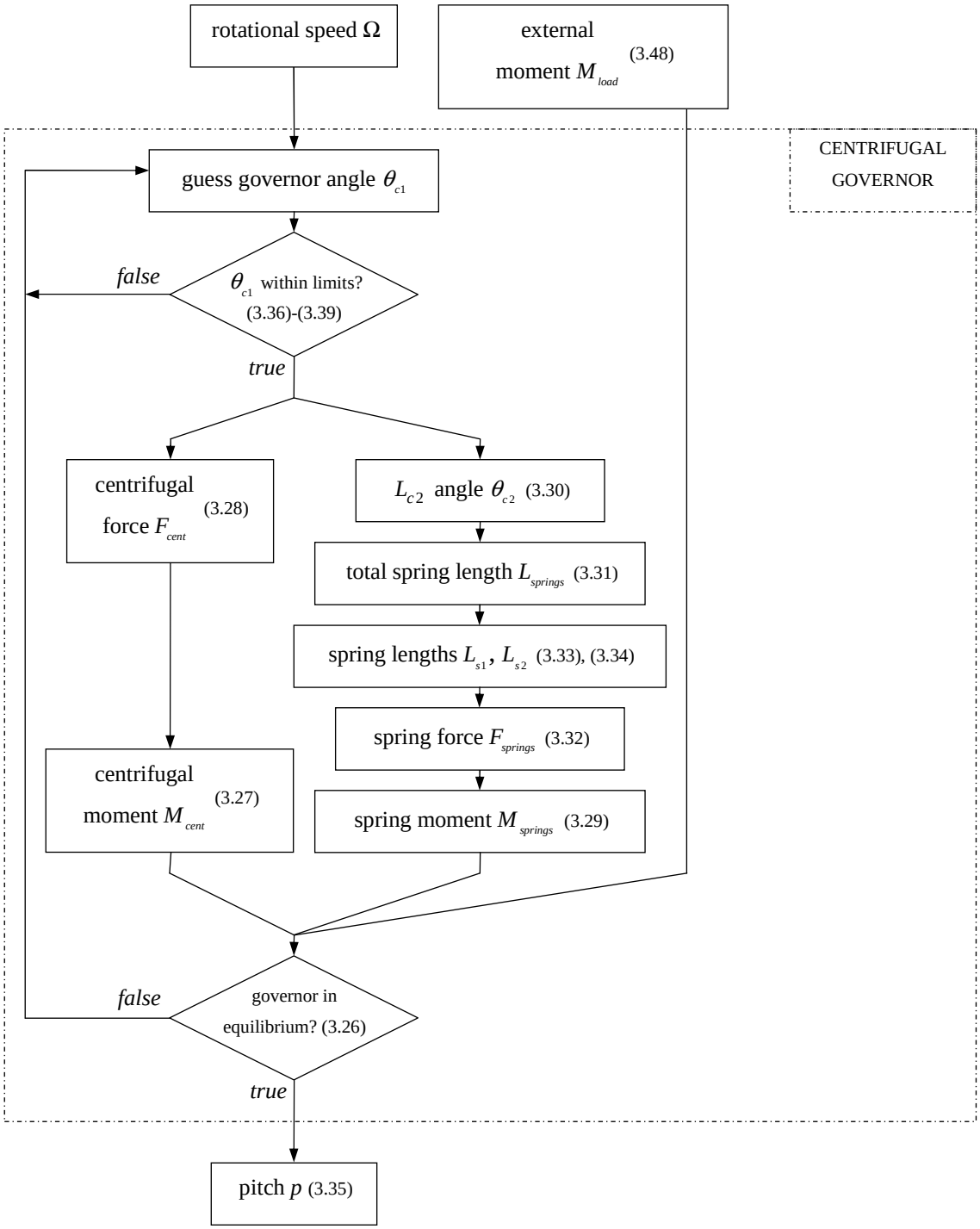

Figure 4.4 *Centrifugal governor algorithm*

The preliminary simulation results will be discussed next.

4.3 Ungoverned modelling results

The complete wind turbine system, which includes a generator, will first be modelled without the governor to establish a baseline for the start-up, power and rotational speed characteristics.

The AE1kW blades, which are used on 3-bladed horizontal-axis wind turbines, are going to be used for the governor. The specifications and the geometry of the blades are given in Table 4.1, Figure 4.5 to Figure 4.7 (Bosman 2003).

Table 4.1 *AE1kW blade specifications*

Diameter	3.6 m
No. of blades	3
Rated power at 10 *m/s*	1 kW
Airfoil	AE02-160ST
Optimal *TSR*	6

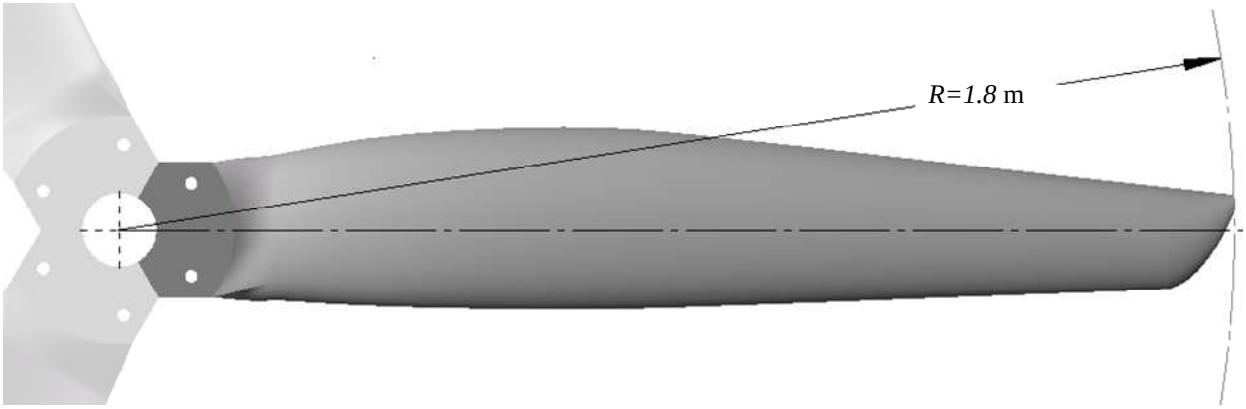

Figure 4.5 *AE1kW wind turbine blades*

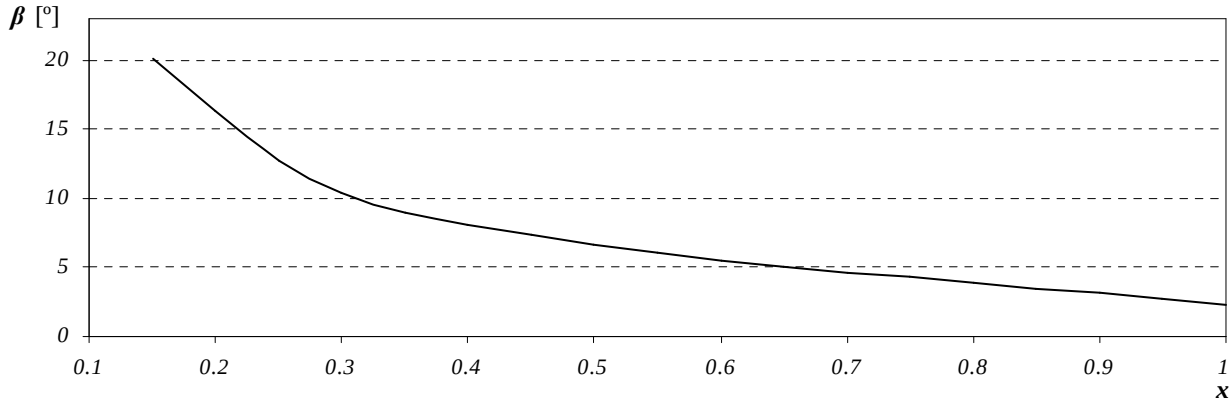

Figure 4.6 *Normalized blade angle distribution*

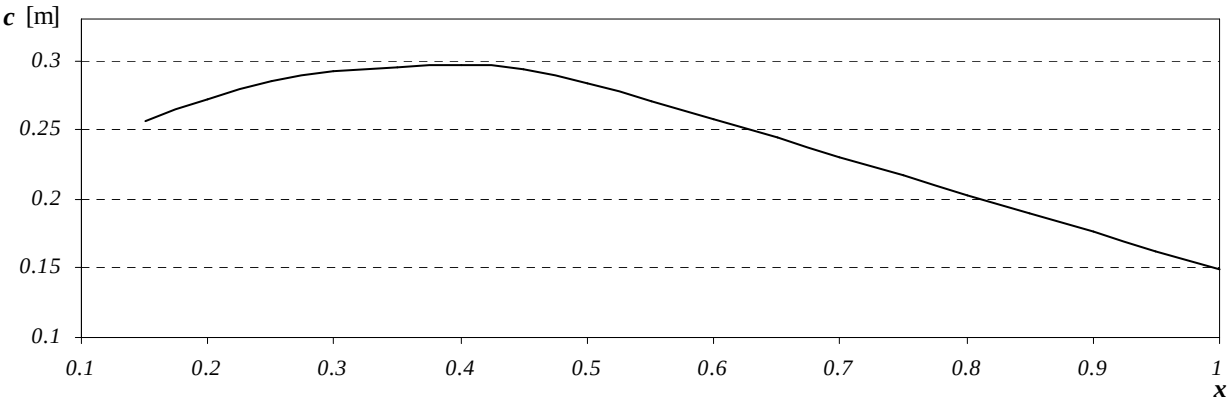

Figure 4.7 *Normalized chord distribution*

The safe rotational speed limit for the blades is 500 rpm. The generator used to model the performance is a permanent magnet alternator connected to a battery bank with a rectifier. The generator curve is shown with the results in Figure 4.9. The AE1kW blades were designed for this generator (Bosman 2003).

The wind turbine system is modelled at standard atmospheric conditions. The torque coefficient results are given in Figure 4.8.

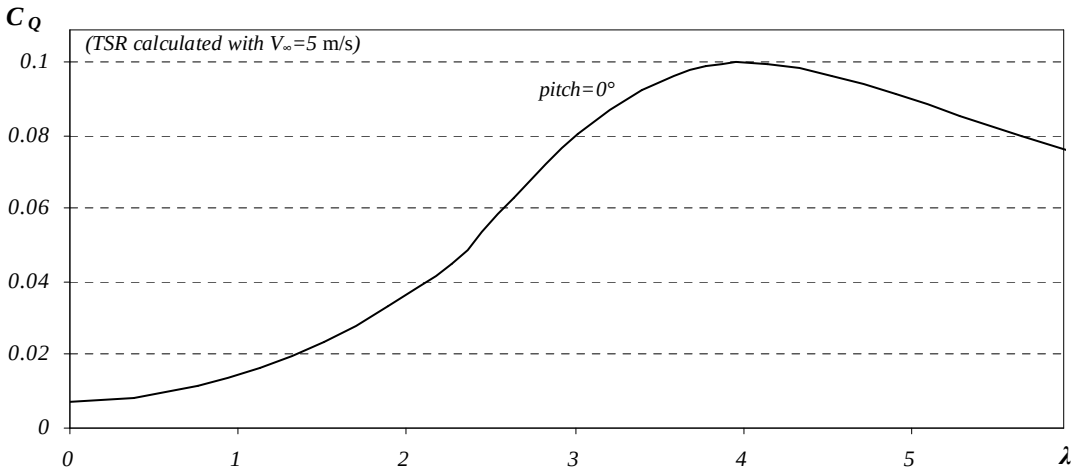

Figure 4.8 *Ungoverned torque coefficient C_Q vs. TSR*

The start-up torque coefficient is $C_Q = 0.007$. If the cut in wind speed is $V_\infty = 3\,\text{m/s}$, the start-up torque will be $Q = 0.718\,\text{Nm}$.

The power characteristics are given in Figure 4.9.

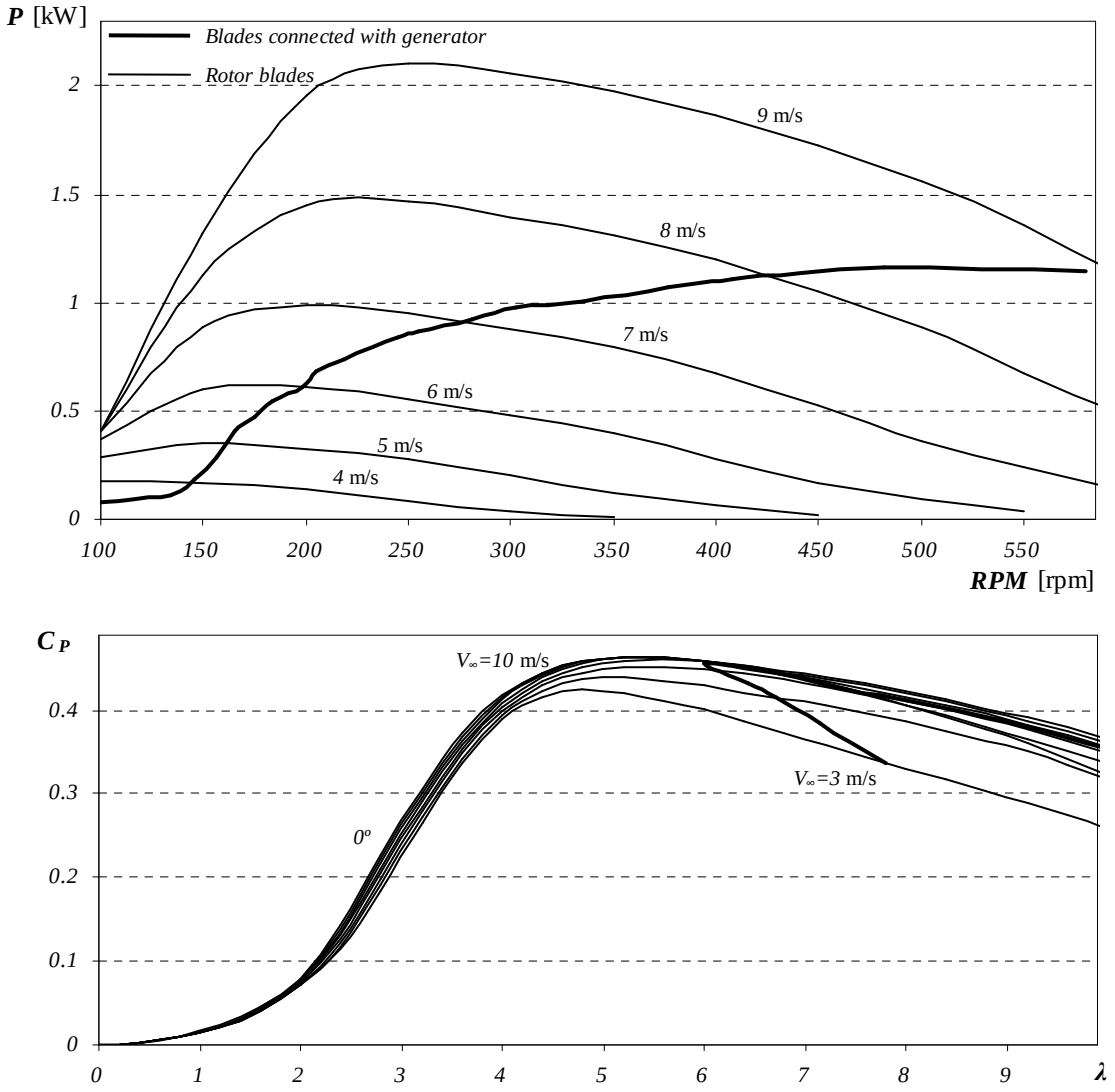

Figure 4.9 *Ungoverned wind turbine power characteristics*

In section 2.2 it was stated that if it is assumed that the aerodynamic performance does not deteriorate, the power coefficient C_P will only be a function of the tip speed ratio λ and the power curves can be represented by one C_P-*TSR* curve. The C_P-*TSR* curves from Figure 4.9 was made by calculating the power coefficient C_P at various rotational speeds Ω and wind speeds V_∞, with the tip speed ratio determined by the rotational speed and wind speed (equation (3.18)). From Figure 4.9 the power coefficient is not only a function of the tip speed ratio, but also of the wind speed. For lower wind speeds the deviation of the power coefficient is larger. The power and rotational speed as a function of wind speed are given in Figure 4.10.

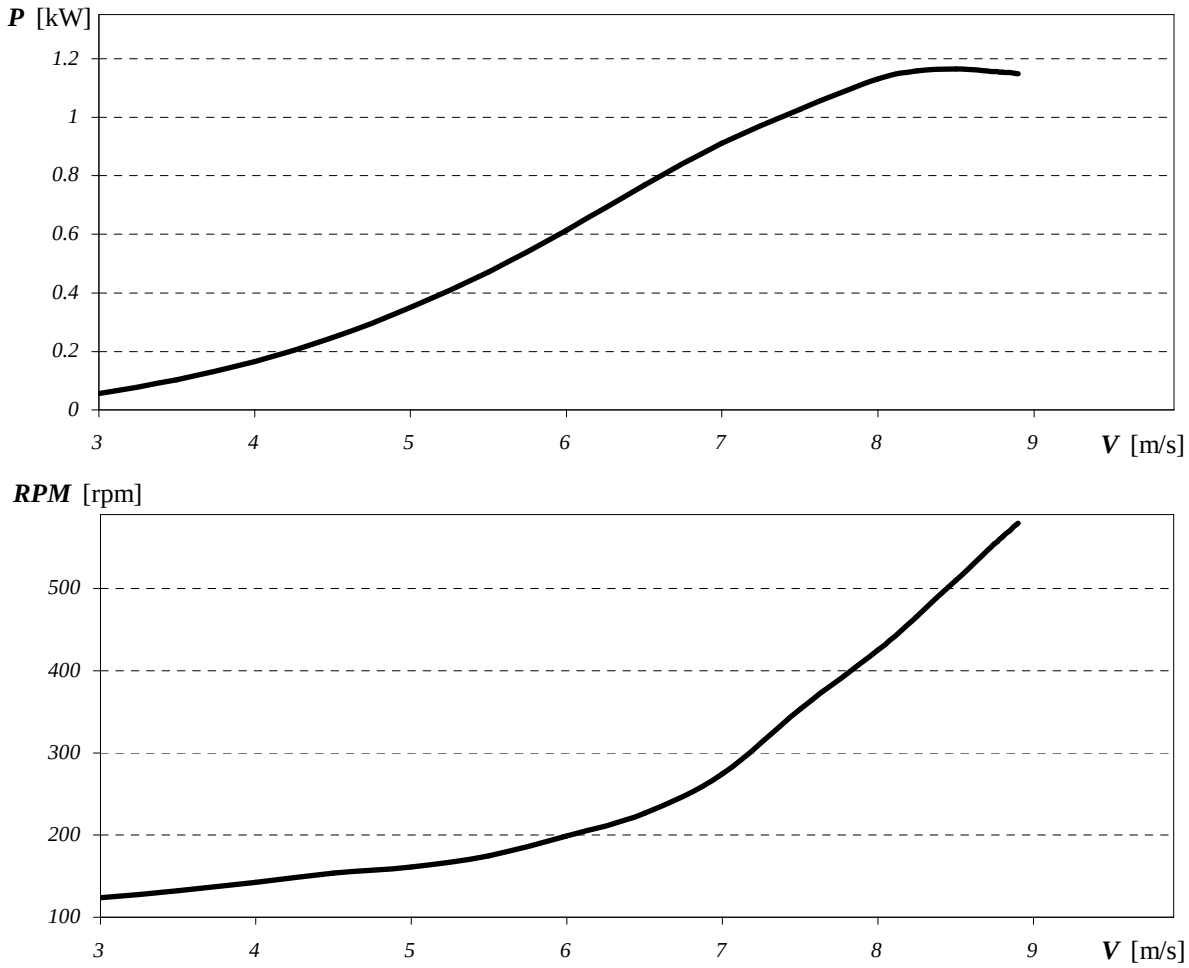

Figure 4.10 *RPM and power vs. wind speed for the ungoverned wind turbine*

The speed limit of the blades of 500 rpm is already reached at V_∞=8.4 m/s. The detailed calculation steps for V_∞=7 m/s are given in Appendix A, section A.1.

4.4 Governed modelling results

The centrifugal governor concept from section 2.4 and section 3.5 is simulated with the theory developed in section 3.5 and the algorithm in Figure 4.4. The concept must achieve both the control objectives of improved start-up performance and over-speed protection by pitching from a positive pitch angle towards stall. It uses a soft spring to provide better start-up and then a harder spring to provide power and speed regulation. Figure 4.11 shows one of the three masses and the chosen model inputs.

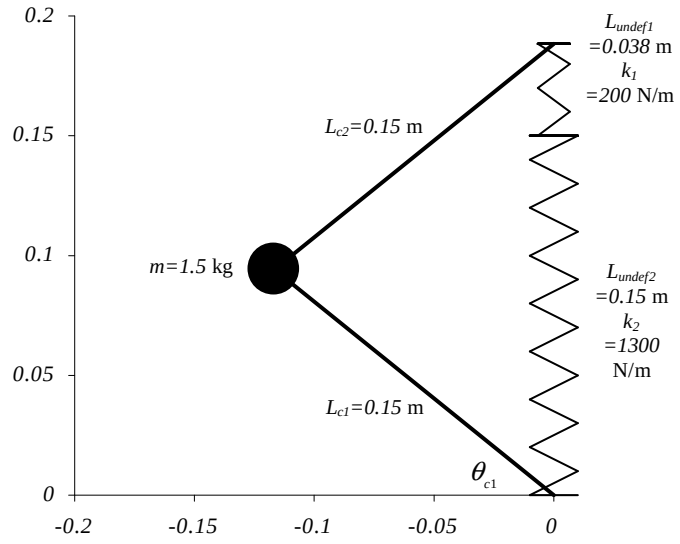

Figure 4.11 *Two-spring centrifugal governor*

Solving M_{spring} as a function of θ_{c1} and solving M_{cent} as a function of θ_{c1} and RPM, both at the origin of Figure 4.11, the results in Figure 4.12 are obtained.

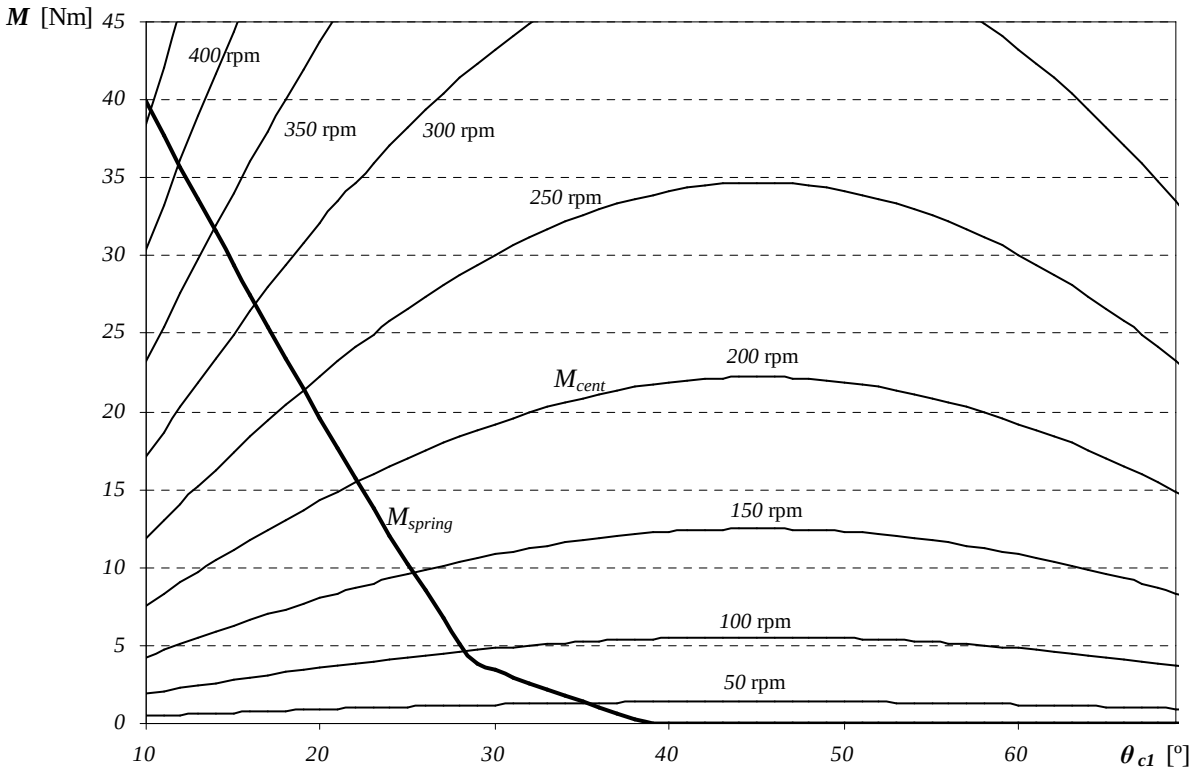

Figure 4.12 *Two-spring centrifugal governor moments*

The intersection of M_{spring} and M_{cent} gives the θ_{c1} vs. RPM curve of the centrifugal governor (Figure 4.13). Note that the effect of the external moment M_{load} is neglected to determine only the characteristic of the governor.

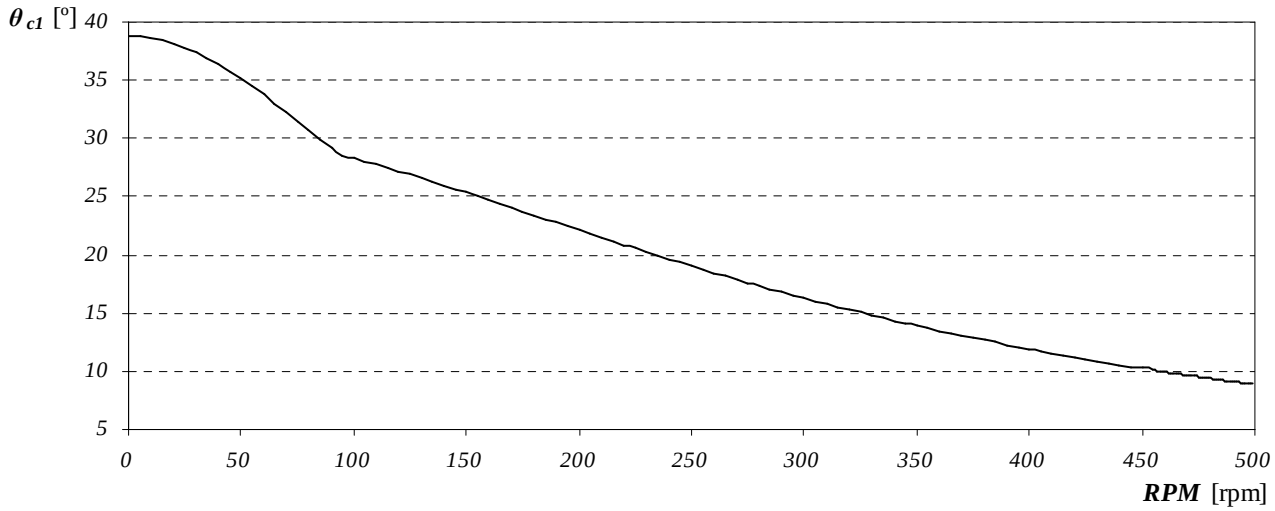

Figure 4.13 *θ_{c1} vs. RPM for the two-spring centrifugal governor*

Choosing $\theta_{off} = 28.8^{\circ}$ so that the start-up pitch will be p=10°, the pitch range is given in Figure 4.14. The stiffness of the springs determines the slope of the pitch curves, while the length of the springs determines the amount of pitch change per spring. The stiffness and length of the springs were selected by trail and error so that the small spring will be solid at $p = 0^{\circ}$ at 95 rpm and $p = -20^{\circ}$ at 500 rpm. The detailed calculation steps for 50 rpm are given in Appendix A, section A.2

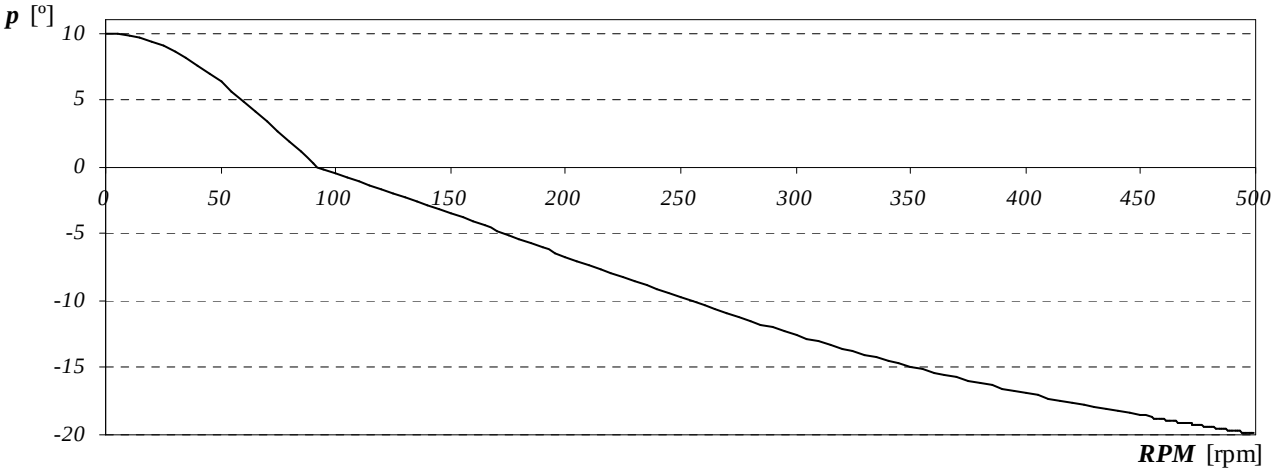

Figure 4.14 *Pitch vs. RPM for the two-spring centrifugal governor*

The complete wind turbine system is modelled with the two-spring governor. The torque coefficient results are given in Figure 4.15 and Table 4.2.

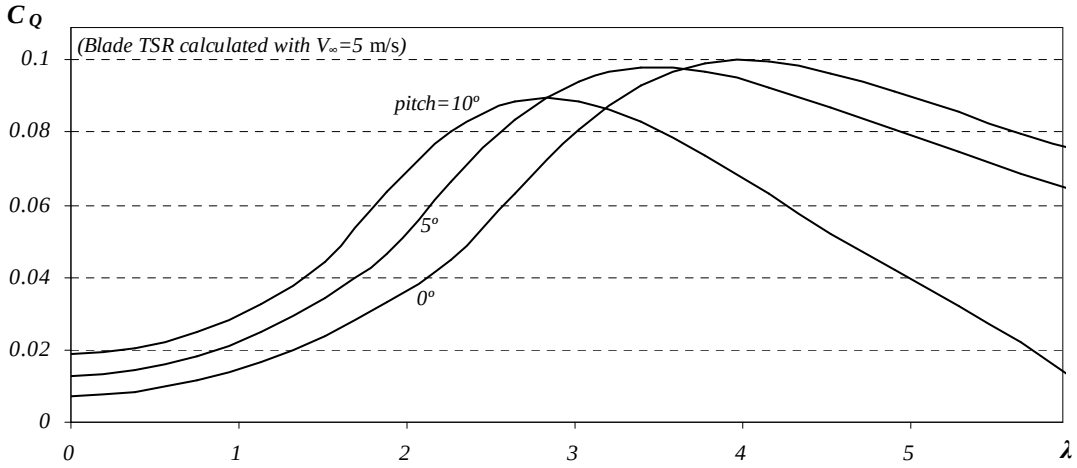

Figure 4.15 *Governed torque coefficients C_Q vs. TSR*

Table 4.2 *Start-up results for the two-spring centrifugal governor*

Pitch	0º	10º
C_Q ($\lambda=0$)	0.007	0.019
Q($\lambda=0$, V_∞=3 m/s)	0.718 Nm	1.874 Nm

The increased pitch of p=10º at start-up will more than double the start-up torque coefficient and start-up torque. The power and rotational speed characteristics are given in Figure 4.16 and Figure 4.17.

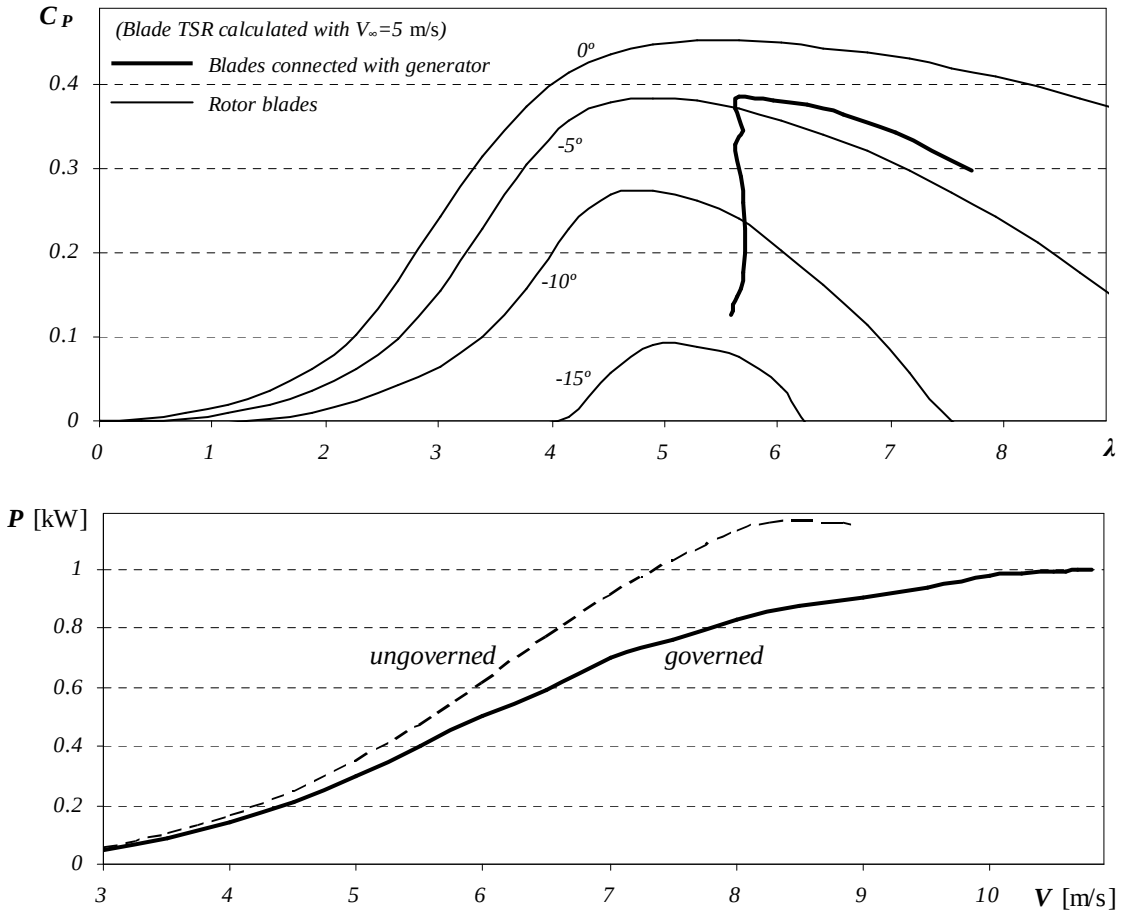

Figure 4.16 *Governed and ungoverned wind turbine power characteristics*

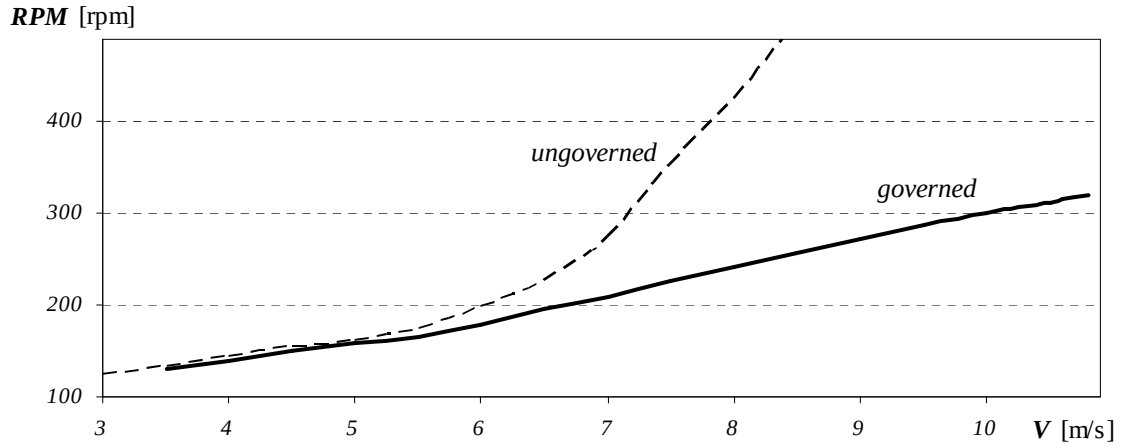

Figure 4.17 *Governed and ungoverned wind turbine RPM vs. wind speed*

From Figure 4.16 and Figure 4.17 it can be seen that the governor does limit the rotational speed, but also the power. This is because the continuous negative pitch change from 95 rpm results in a power and speed reduction (Figure 4.14). From the control objectives and required pitch curve from Figure 2.7, the governor must keep the pitch zero during normal operation and only near 500 rpm the pitch must become negative to limit the speed.

4.5 Summary

In this chapter all the algorithms of the model were discussed. The preliminary modelling results were discussed and it was established that the first centrifugal governor concept from section 3.5 is not adequate to achieve the control objectives because of the power loss during normal operation.

Chapter 5 Concept modification and results

5.1 Introduction

This chapter discusses the modification of the first concept so that it will be more suitable for over-speed protection without the loss of power during normal operation. The further conceptual design of the governor and the results are discussed.

5.2 The Sliding concept

The first concept from section 3.5 is modified by letting the end of connector L_{c2} slide or roll across L_{c1}. As long as the roller remains unconstrained, connector L_{c2} remains perpendicular to L_{c1} (Figure 5.1). Where L_{c1} remained constant with the first concept from section 3.5, it now varies continuously with the sliding concept.

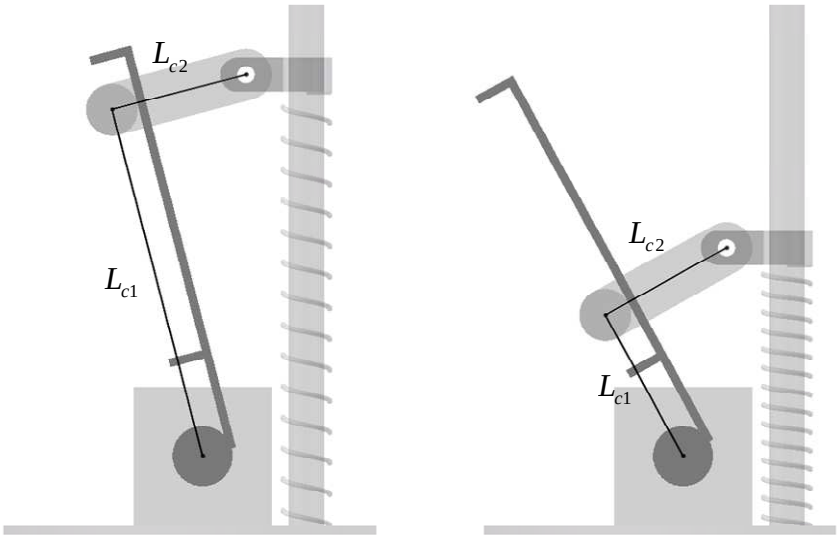

Figure 5.1 *Sliding centrifugal governor concept*

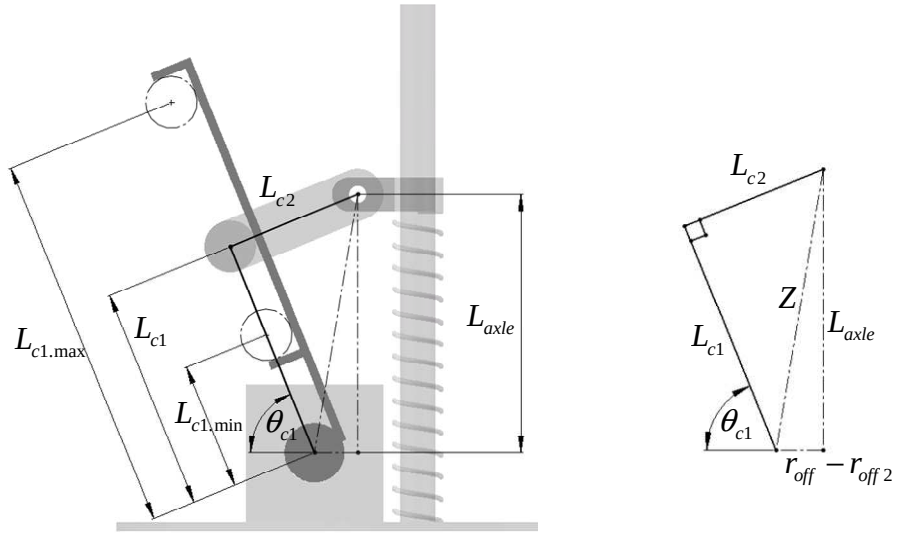

Figure 5.2 *Sliding centrifugal governor concept*

The existing model is modified to accommodate the new concept. From Figure 5.2, the new L_{c1} is calculated:

$$L_{axle} = L_{c1}\sin\theta_{c1} + L_{c2}\cos\theta_{c1}$$

$$Z^2 = \left(r_{off} - r_{off\,2}\right)^2 + L_{axle}^2 = L_{c1}^2 + L_{c2}^2$$

$$\left(r_{off} - r_{off\,2}\right)^2 + \left(L_{c1}\sin\theta_{c1} + L_{c2}\cos\theta_{c1}\right)^2 = L_{c1}^2 + L_{c2}^2$$

$$\left(r_{off} - r_{off\,2}\right)^2 + L_{c1}^2\left(\sin^2\theta_{c1} - 1\right) + L_{c2}^2\left(\cos^2\theta_{c1} - 1\right) + 2L_{c1}L_{c2}\sin\theta_{c1}\cos\theta_{c1} = 0$$

$$L_{c1}^2 + \left(\frac{2L_{c2}\sin\theta_{c1}\cos\theta_{c1}}{\sin^2\theta_{c1} - 1}\right)\cdot L_{c1} + \left(\frac{\left(r_{off} - r_{off\,2}\right)^2 + L_{c2}^2\left(\cos^2\theta_{c1} - 1\right)}{\sin^2\theta_{c1} - 1}\right) = 0$$

$$p \equiv \left(\frac{2L_{c2}\sin\theta_{c1}\cos\theta_{c1}}{\sin^2\theta_{c1} - 1}\right), \quad q \equiv \left(\frac{\left(r_{off} - r_{off\,2}\right)^2 + L_{c2}^2\left(\cos^2\theta_{c1} - 1\right)}{\sin^2\theta_{c1} - 1}\right)$$

$$L_{c1} = -\frac{p}{2} \pm \sqrt{\frac{p^2}{4} - q}$$

thus

$$L_{c1} = L_{c1\perp} = -\frac{\left(\frac{2L_{c2}\sin\theta_{c1}\cos\theta_{c1}}{\sin^2\theta_{c1}-1}\right)}{2} \pm \sqrt{\frac{\left(\frac{2L_{c2}\sin\theta_{c1}\cos\theta_{c1}}{\sin^2\theta_{c1}-1}\right)^2}{4} - \left(\frac{\left(r_{off}-r_{off\,2}\right)^2 + L_{c2}^2\left(\cos^2\theta_{c1}-1\right)}{\sin^2\theta_{c1}-1}\right)} \qquad (5.1)$$

when $L_{c1.\min} < L_{c1} < L_{c1.\max}$

Equation (5.1) is substituted into equations (3.29) to (3.38) where applicable.

Figure 5.3 shows one of the three masses and the chosen model inputs. There are no constraints for the roller so, L_{c1} is unconstrained.

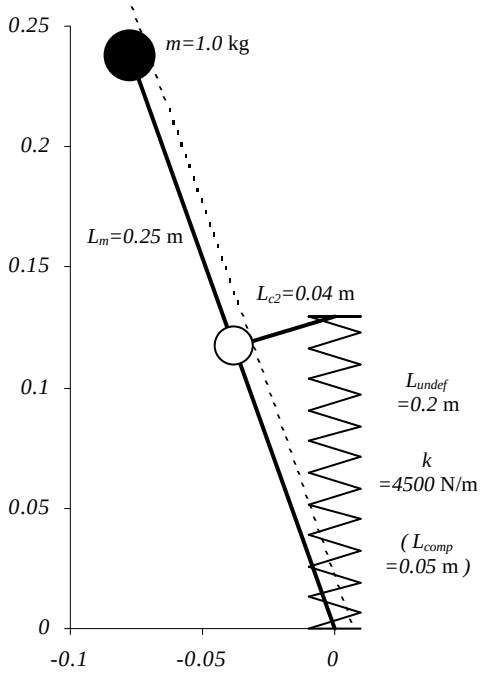

Figure 5.3 *Sliding centrifugal governor concept parameters*

Solving M_{spring} as a function of θ_{c1} and then solving M_{cent} as a function of θ_{c1} and *RPM*, the results in Figure 5.4 are obtained. Note that where M_{spring} was linear in the first concept (Figure 4.12) and it is now non-linear.

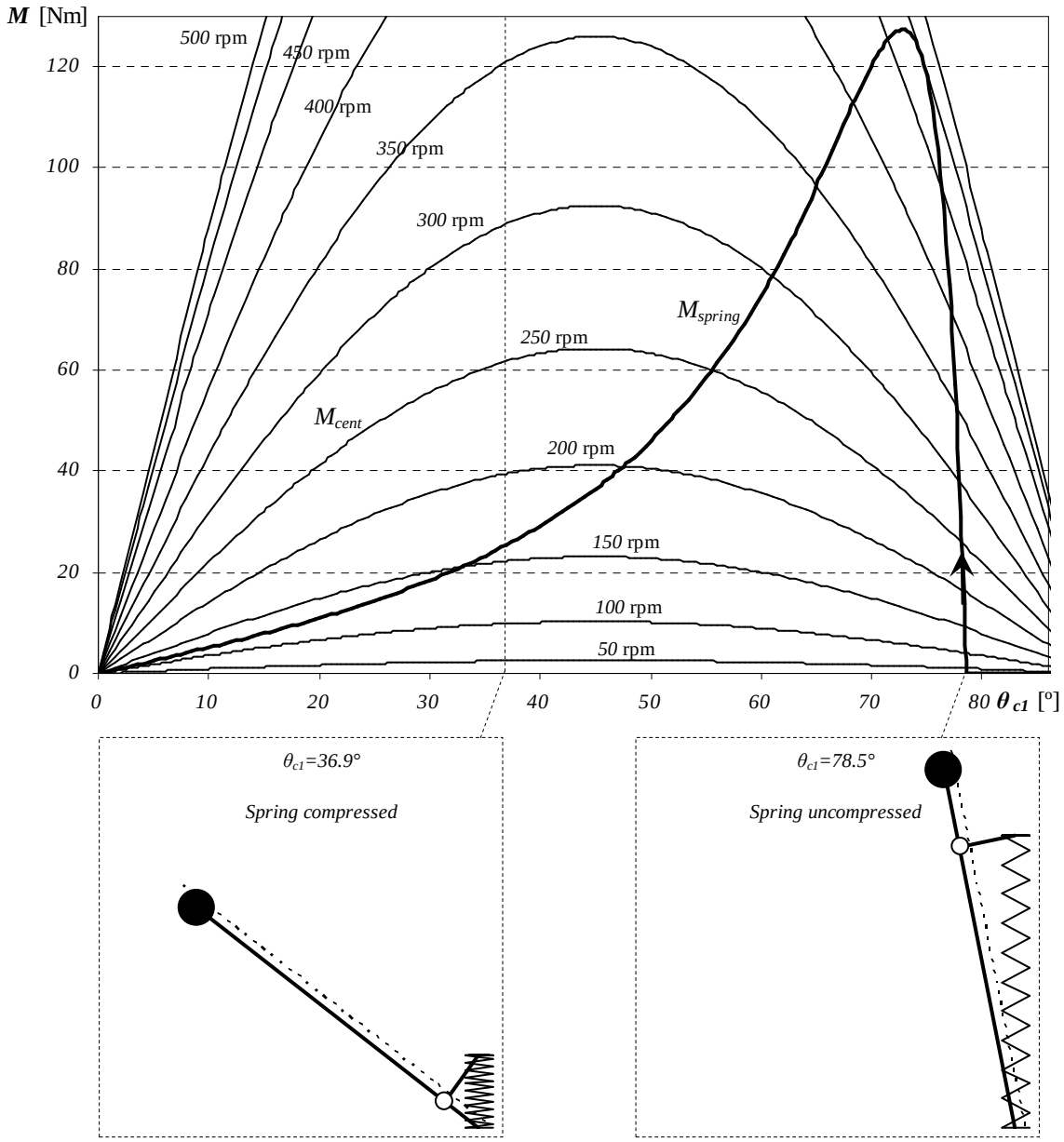

Figure 5.4 *Governor moments of the sliding concept*

The intersection of M_{spring} and M_{cent} gives the θ_{c1} vs. RPM curve of the governor. The pitch offset of $\theta_{off} = 78.5^{\circ}$ was chosen so that the start-up pitch will be $p = 0^{\circ}$ and the pitch results are given in Figure 5.5.

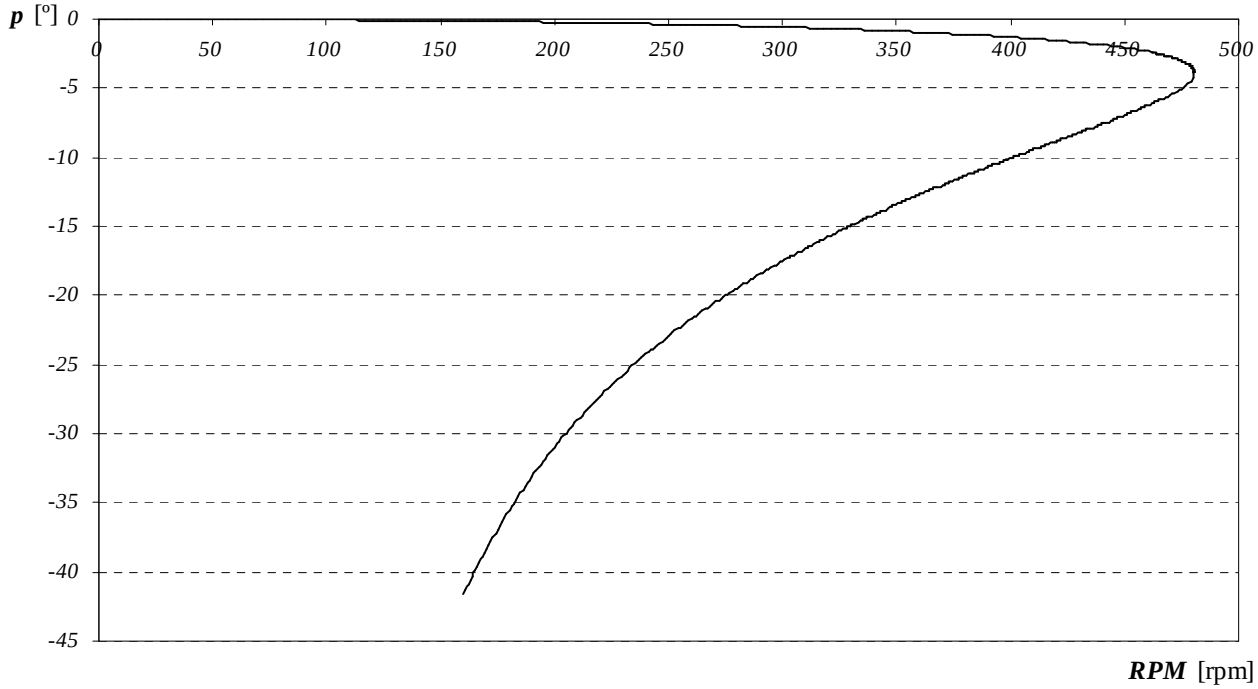

Figure 5.5 *Pitch vs. RPM for the sliding concept*

Starting with $p = 0^\circ$ ($\theta_{c1} = 78.5^\circ$) at standstill, the pitch decreases very little with an increasing rotational speed until $p = -3.9^\circ$ ($\theta_{c1} = 74.6^\circ$) and 480 rpm, where after the rotational speed actually decreases with a decreasing pitch. The detailed calculation steps for 400 rpm are given in Appendix A, section A.3.

The power and rotational speed results are given in Figure 5.6.

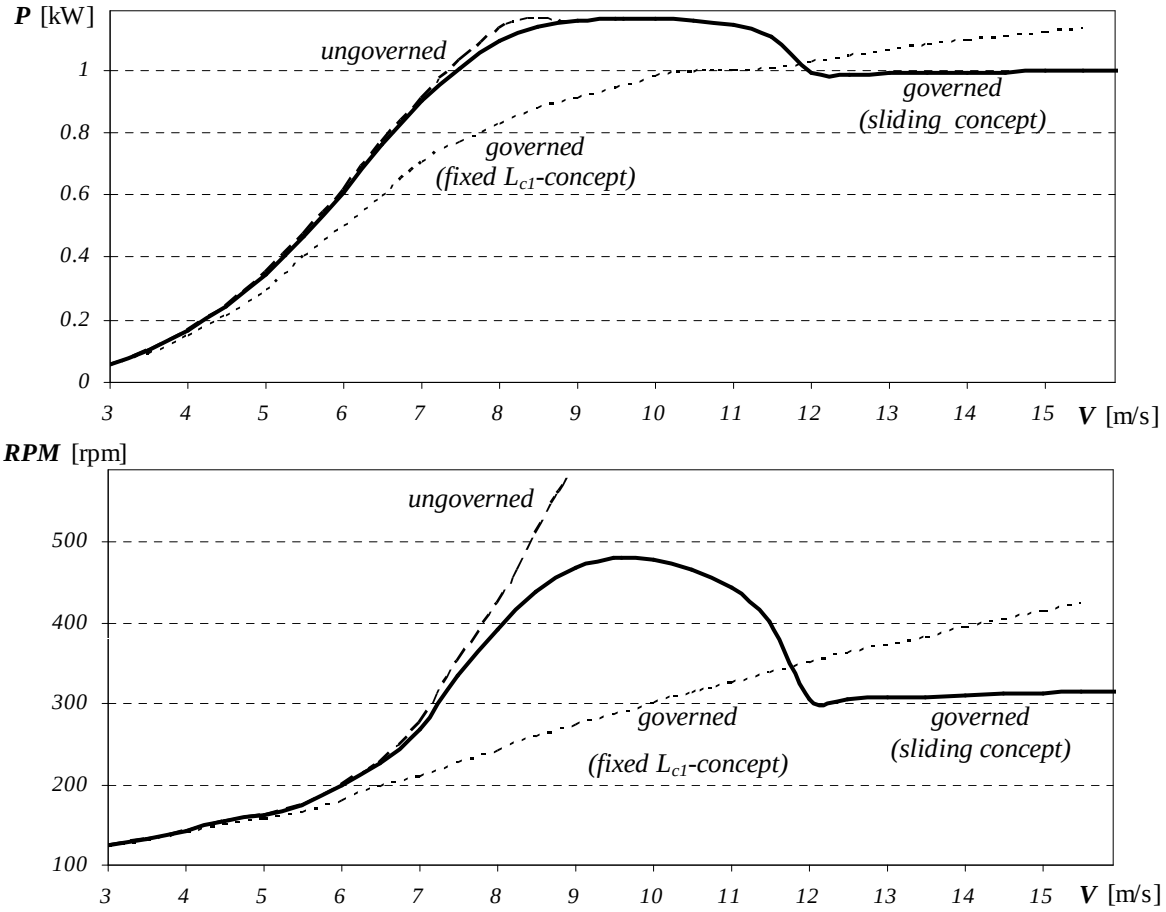

Figure 5.6 *RPM and power vs. wind speed for the sliding concept*

Because of the sliding concept's non-linear behaviour, it provides very effective over-speed protection. The pitch changes very little up to 480 rpm and V_∞=9.7 m/s, resulting in a minimum loss of power as compared to the fixed-L_{c1} concept. If the wind speed increases further, the power and rotational speed are limited, with the rotational speed even decreasing if the hard spring is long enough.

The fixed-L_{c1} concept from section 3.5 with a soft spring is combined with the non-linear sliding concept using a hard spring. At start-up, the roller presses against a stop so that $L_{c1} = L_{c1.\max}$ (Figure 5.7 (a)). L_{c1} remains constrained and for an increasing rotational speed there is an almost linear angular displacement until the soft spring is compressed and L_{c2} is perpendicular to L_{c1} (Figure 5.7 (b)). With a further increase in rotational speed the end of connector L_{c2} will slide across L_{c1} and the governor will behave like the sliding concept governor (Figure 5.7 (c)).

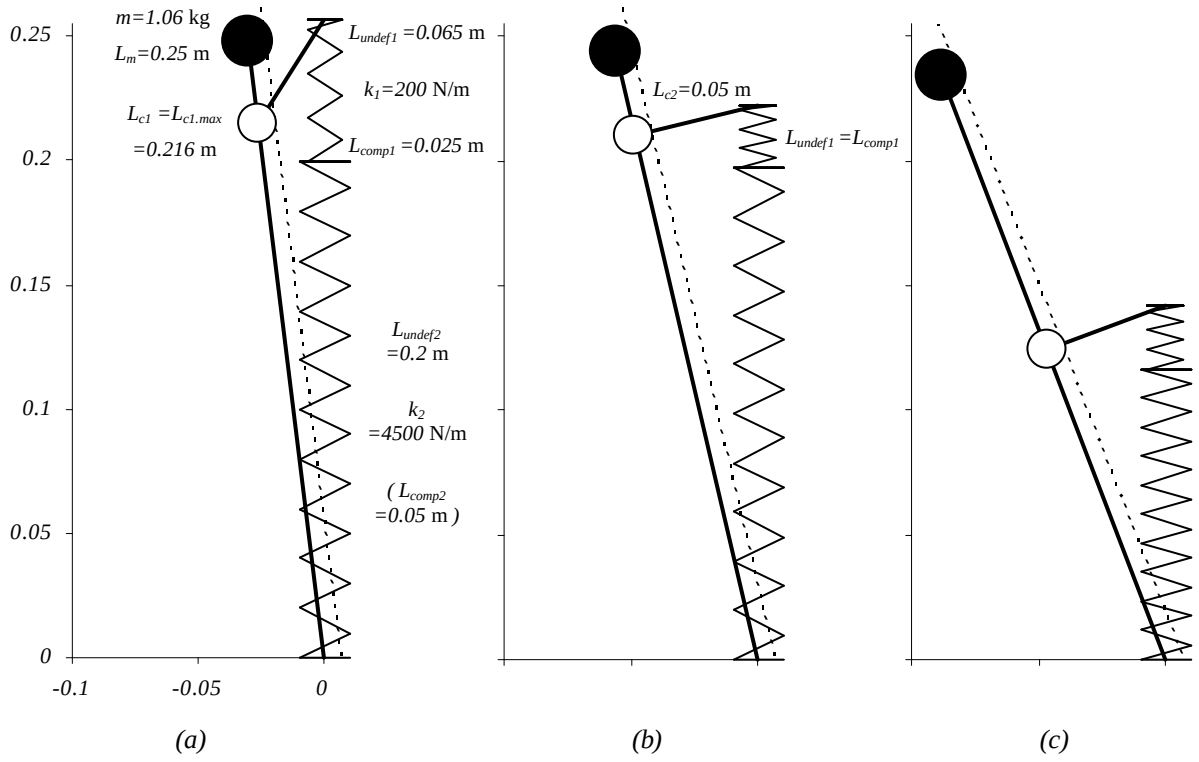

Figure 5.7 *Combined centrifugal governor concept at different stages*

Choosing $\theta_{off} = 87.6^{\circ}$ so that the start-up pitch will be p=10°, the pitch results are given in Figure 5.8.

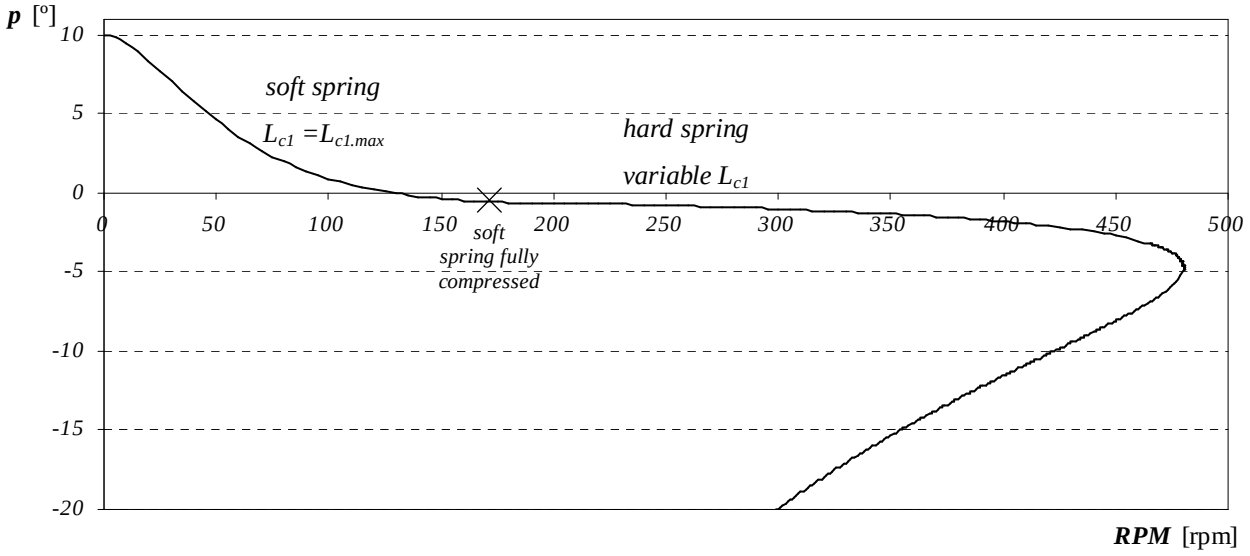

Figure 5.8 *Pitch vs. RPM for the combined concept*

Note that the soft spring is fully compressed at 169.1 rpm and p=-0.55°. After 169.1 rpm the governor will behave like the sliding concept governor.

The complete wind turbine system is modelled with the combined concept governor and the start-up results are given in Table 5.1.

Table 5.1 *Start-up results for the combined concept*

Pitch	0º	10º
C_Q (λ=0)	0.007	0.019
Q(λ=0, V_∞=3 m/s)	0.718 Nm	1.874 Nm

The increased start-up pitch of p=10° will more than double the start-up torque coefficient and torque. The power and rotational speed characteristics are given in Figure 5.9.

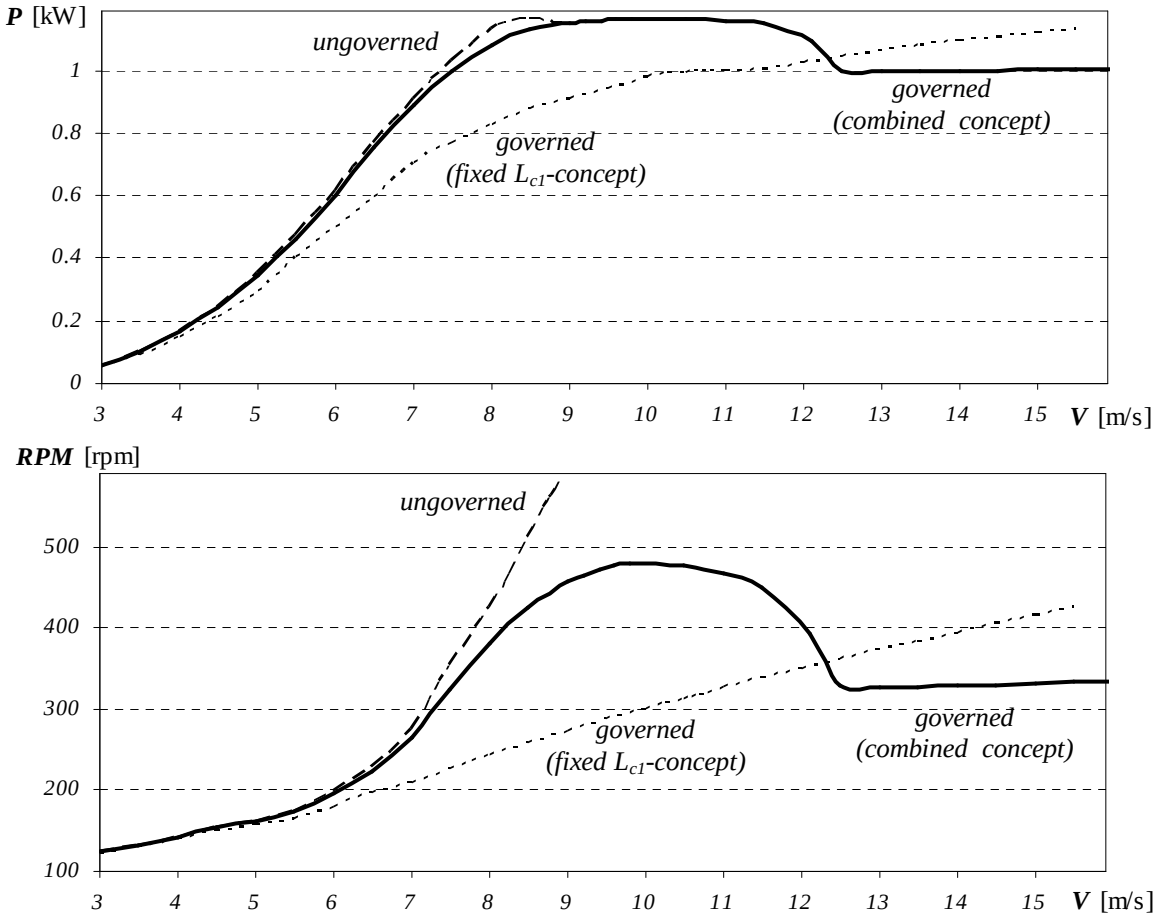

Figure 5.9 *RPM and power vs. wind speed for the combined concept*

As with the sliding concept, the combined concept provides very effective over-speed protection without the loss of power associated with the fixed-L_{c1} concept.

Because of the non-linear behaviour of the sliding concept, the governor will limit the rotational speed to the same level irrespective of the load of the generator. The wind turbine with the combined concept's power and rotational speed curves for the generator with different loads are shown in Figure 5.10.

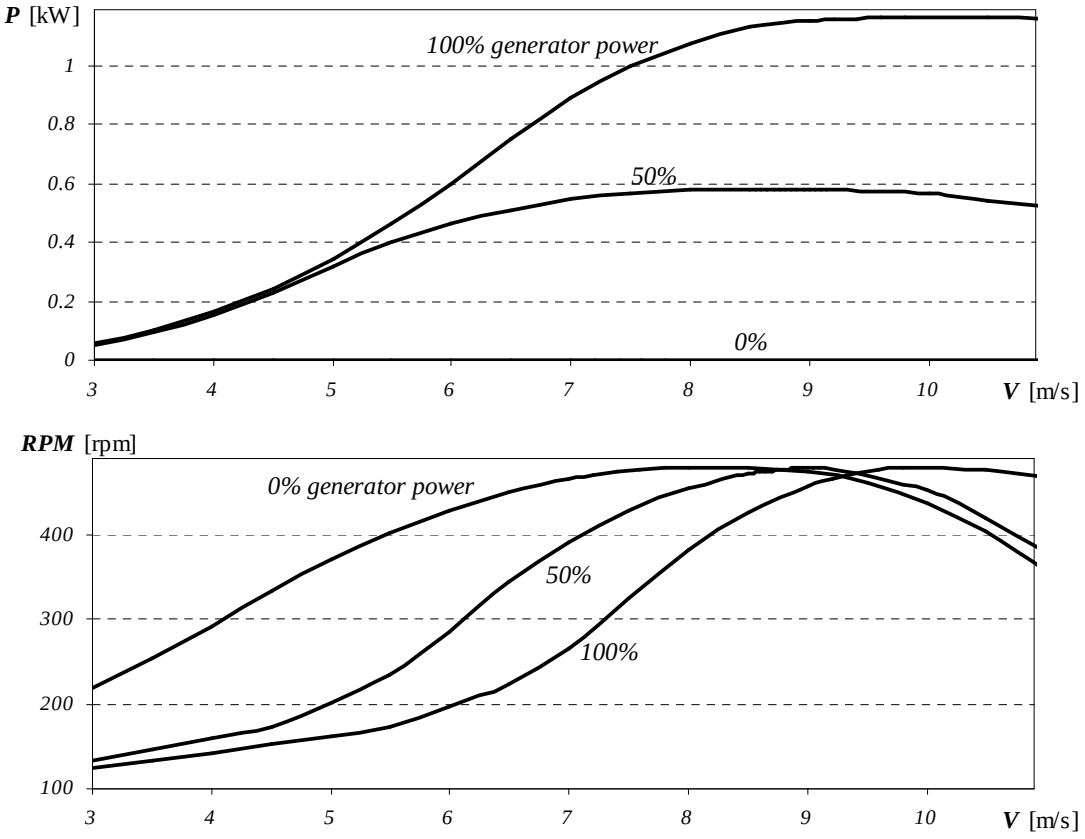

Figure 5.10 *Power and RPM speed at different generator loads*

The combined concept is ideally suited to achieve both the control objectives and will be used in the detail design of the prototype.

5.3 Summary

A two-stage centrifugal governor concept was developed, which will be used in the detail design. The governor pitches towards stall, with the first linear stage using a soft spring to provide improved start-up performance. The second non-linear stage uses a hard spring to provide over-speed protection without the loss of power associated with the linear over-speed protection. The governor will limit the rotational speed to the same level irrespective of the load of the generator.

Chapter 6 Detail design and results

6.1 Introduction

This chapter discusses the detail design of the centrifugal governor prototype. The effect the external moment M_{load} has on the control and how it can be minimized are discussed. The design of the governor hub with the strength design of the governor pitching shaft is discussed. The control system design is discussed.

6.2 Minimizing the external governor moment

The external governor moment M_{load} (equation (3.48)) must be minimized in relation to the governor's moments as to limit its effect on the control:

$$M_{cent} - M_{spring} - M_{load} = 0$$
$$M_{load} = M_{cent} - M_{spring} \qquad (3.26)$$

The effect of M_{load} can be minimized by decreasing M_{load} or by increasing M_{cent} and M_{spring}. M_{load} will first be minimized by finding the optimal position of the blade relative to the governor pitching shaft axis (distance a). The components of M_{load} are again shown in Figure 6.1.

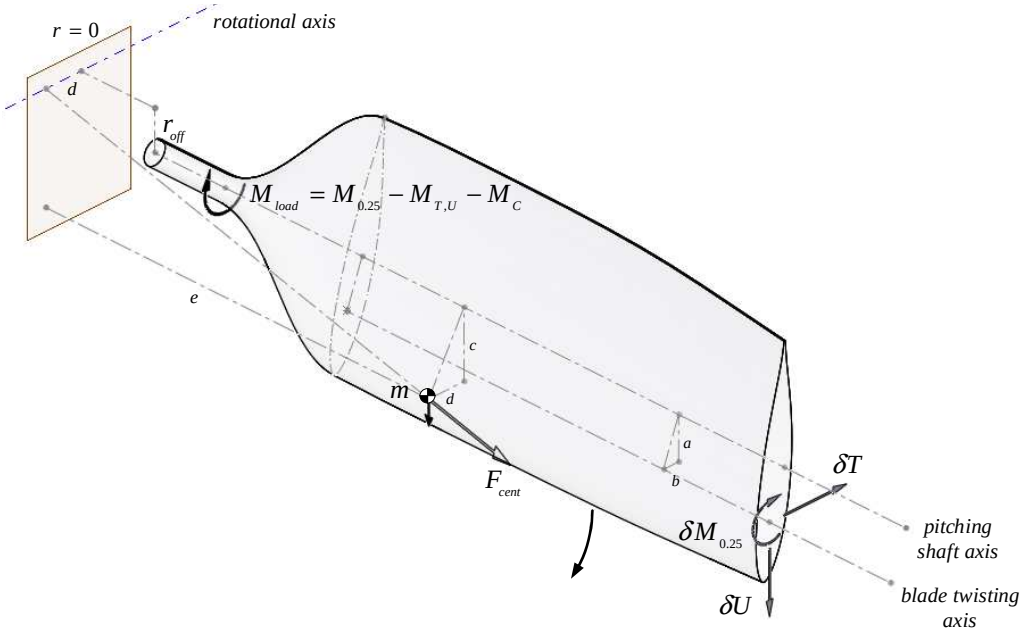

Figure 6.1 *External moment components*

M_{load} is a function of the blade's position relative to the governor pitching shaft axis and the rotational axis. $M_{T,U}$ (3.46) is a function of the position of the blade's twisting axis relative to the pitching shaft axis (distances a and b). M_C (3.47) is a function of the offset r_{off} of the pitching shaft axis relative to the rotational axis (as defined in Figure 3.10) and the position off the blade's centre of gravity (distances c and d).

$$\begin{aligned} M_{load} &= M_{0.25} - M_{T,U} - M_C \\ &= M_{0.25} - \left(T \cdot a + U \cdot b\right) - \left(m \cdot \Omega^2 \cdot \left(c + r_{off}\right)\right) \cdot d \end{aligned} \tag{3.48}$$

Figure 6.2 shows the location of the AE1kW blade's twisting axis and its centre of gravity with the pitching shaft located at the centre of the blade root. The distance d could not be accurately determinded. The method that was used to determine the centre of gravity is discussed in Appendix B.

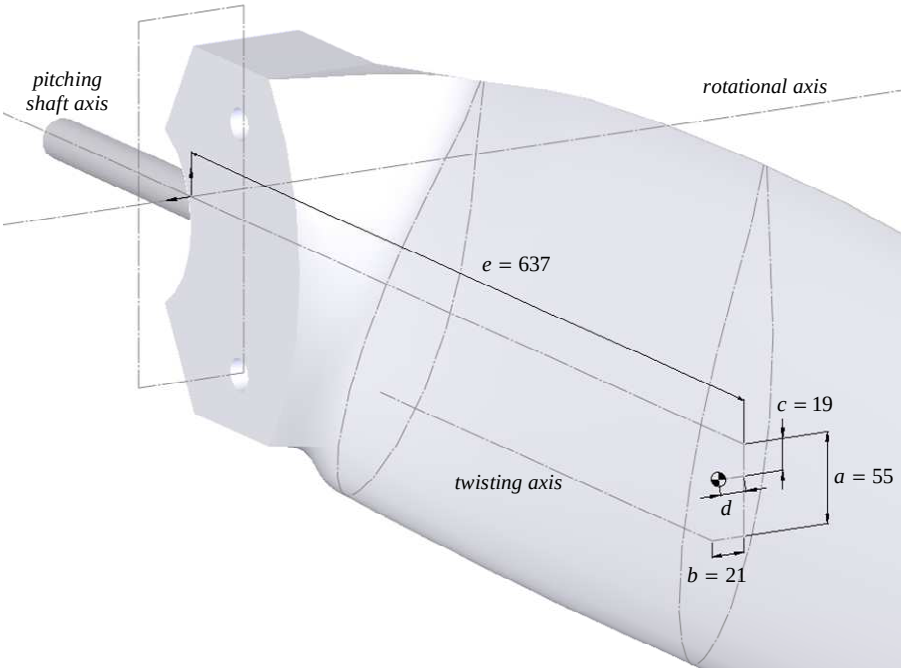

Figure 6.2 *AE1kW centre of gravity and twist axis locations*

Figure 6.3 shows M_{load} as a function of the blade position a at one of the operating points of the wind turbine with the combined concept governor (Figure 5.9, V=7 m/s at 264.5 rpm, $p = -0.83^{\circ}$). M_{load} and M_C are calculated for three values of d. Note the circled points where $M_{load} = 0$. The detailed calculation steps for $a = 55$ are given in Appendix A, section A.4.

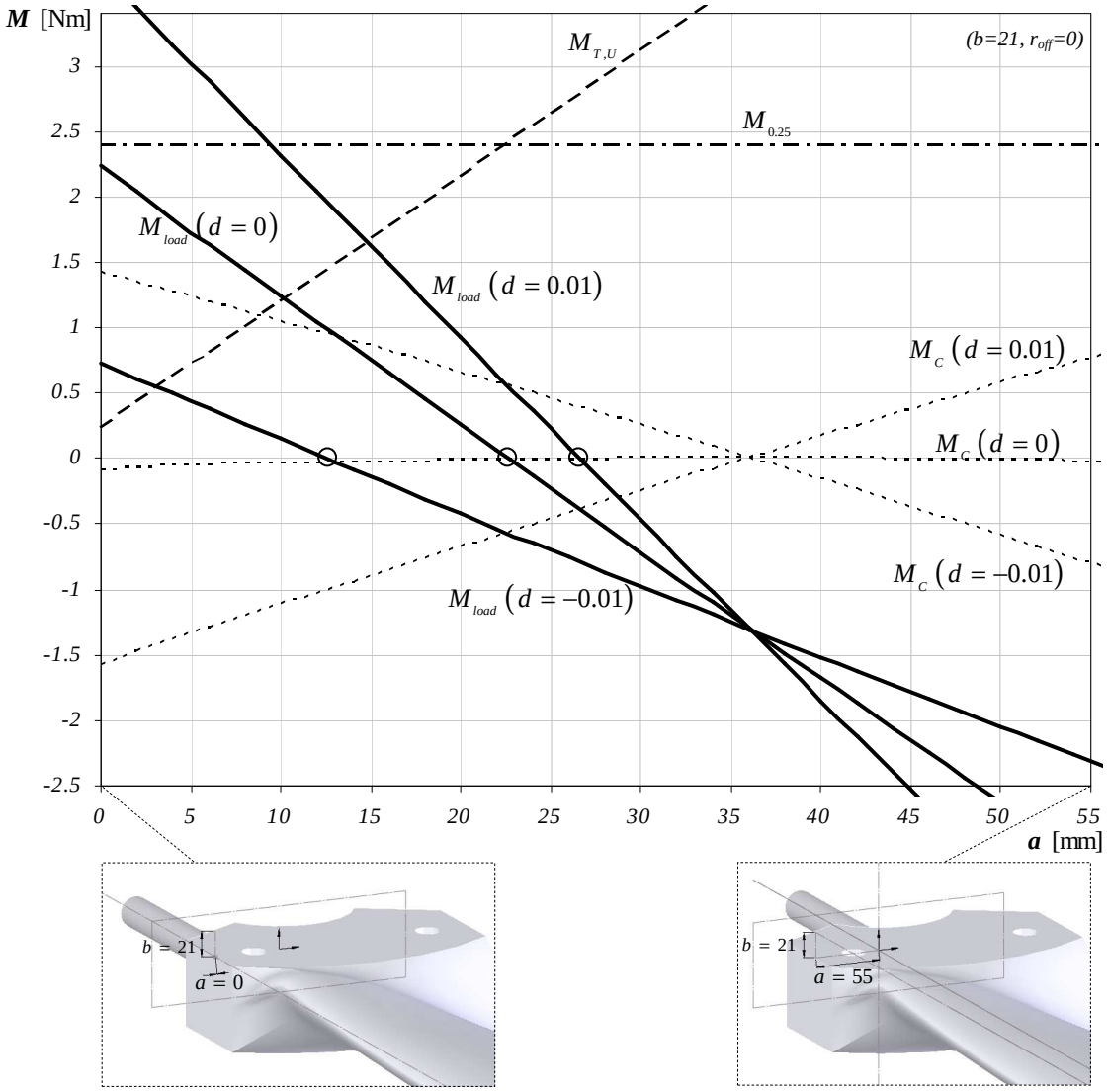

Figure 6.3 *M_{load} as a function of the blade position (a) relative to the governor pitching shaft*

Figure 6.4 shows the blade positions where M_{load} would be equal to zero for various generator loads.

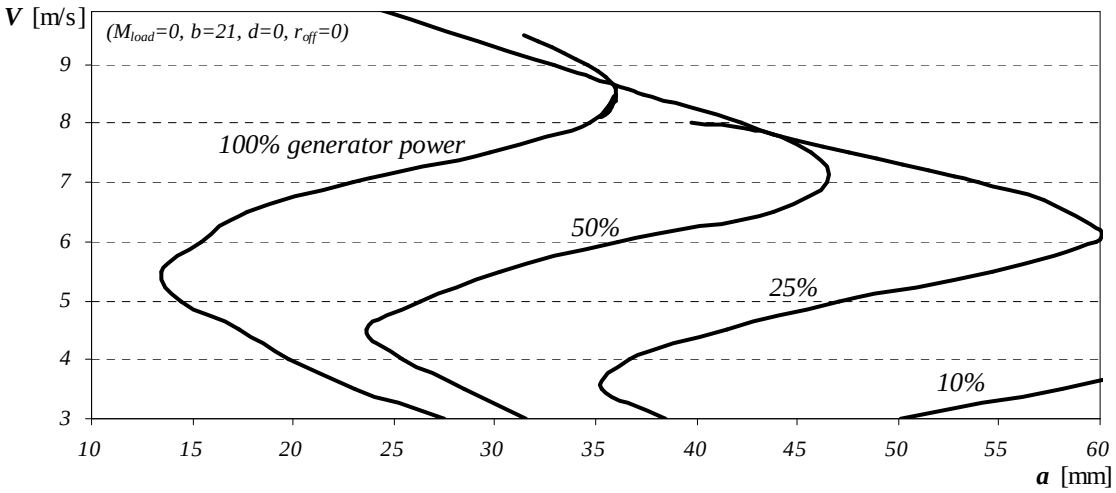

Figure 6.4 *Pitching shaft location (a) where M_{load}=0 for various generator loads*

From Figure 6.4 it can be seen that there are optimal ranges of the position a where $M_{load} = 0$. These are largely dependant on the wind speed and generator load. M_{load} will next be minimized by increasing M_{cent} and M_{spring}.

Figure 6.5 shows M_{load} compared to the governor moments M_{cent} and M_{spring}. The blades are connected as in Figure 6.2.

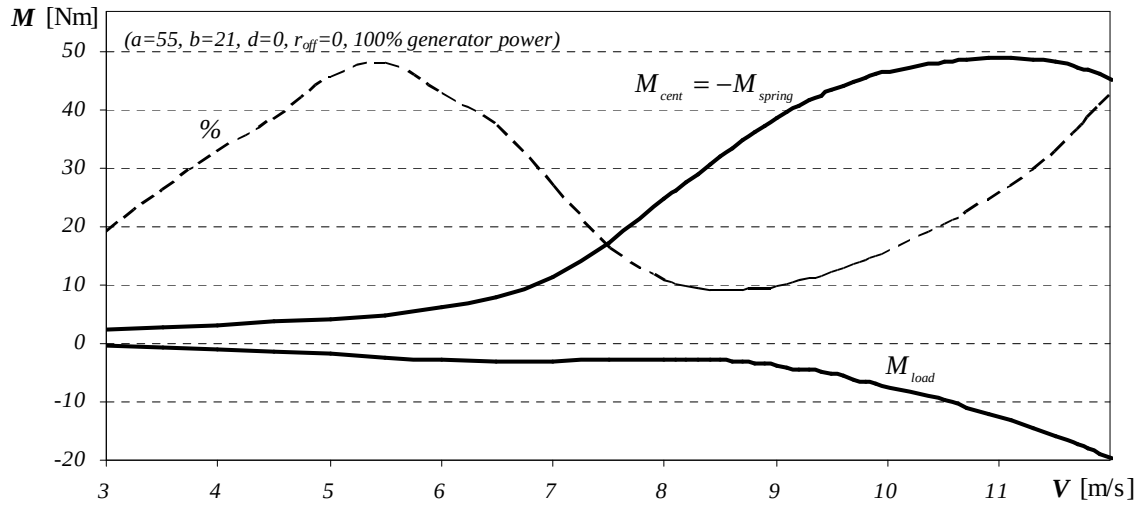

Figure 6.5 *M_{load} compared to M_{cent} and M_{spring}*

From Figure 6.5 it can seen that M_{load} is large compared to M_{cent} and M_{spring} and will have a large effect on the control. The maximum percentage of M_{load} relative to M_{cent} is 48%.

M_{cent} is a function of the governor's masses (equations (3.27) and (3.28)) and M_{spring} is a function of the spring's stiffness (equations (3.29) and (3.32)). By scaling the mass and the stiffness, M_{cent} and M_{spring} increases, while the control characteristics of the governor stays the same. M_{load} stays the same, therefore its effect will be decreased. Figure 6.6 shows the results with a scaling factor of 4.

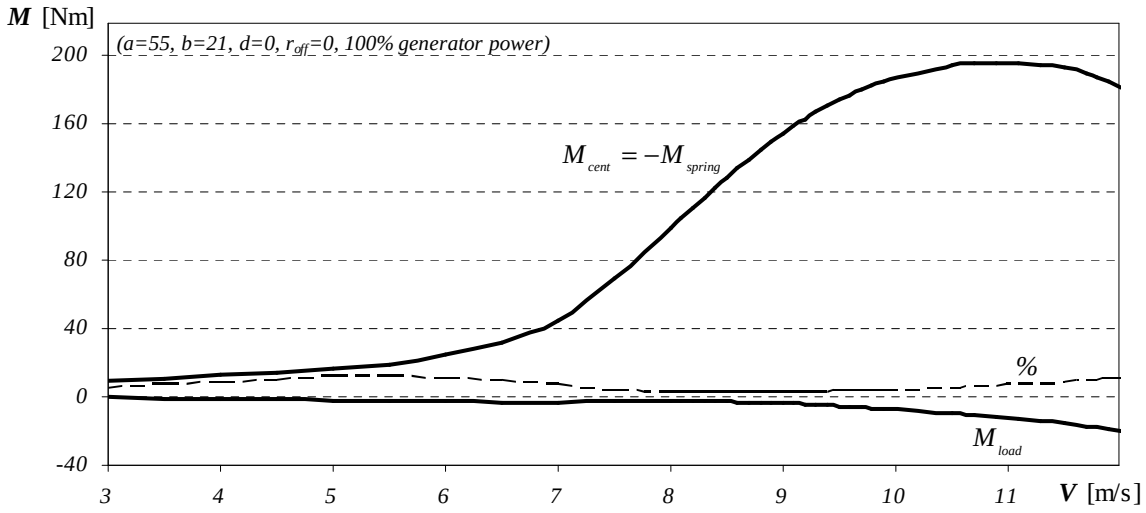

Figure 6.6 *M_{load} compared to M_{cent} and M_{spring}*

Increasing M_{cent} and M_{spring} works very well and the external moment percentage is now 12%. The design of the governor hub with the pitching shaft must first be done before the detail design of the control can be done.

6.3 Governor hub design

The prototype will be tested without a generator, so from Figure 6.4 the best position for the blade to minimize M_{load} is close to $a = 60$. The reason for testing without a generator will be discussed shortly. M_{load} will further be minimized by scaling the governor's mass and springs' stiffness. The pitching shaft can therefore be centred ($r_{off} = 0$) and connected to the centre of the blade's

root with $a = 55$ and $b = 21$. The only unknown variable is *d*. It was chosen as $d = 0$, because the influence of M_C on M_{load} is small compared to the influence of $M_{T,U}$ and $M_{0.25}$ (Figure 6.3). Because $r_{off} = 0$, the blades must be offset radially to make space for the shaft with its bearings (Figure 6.7).

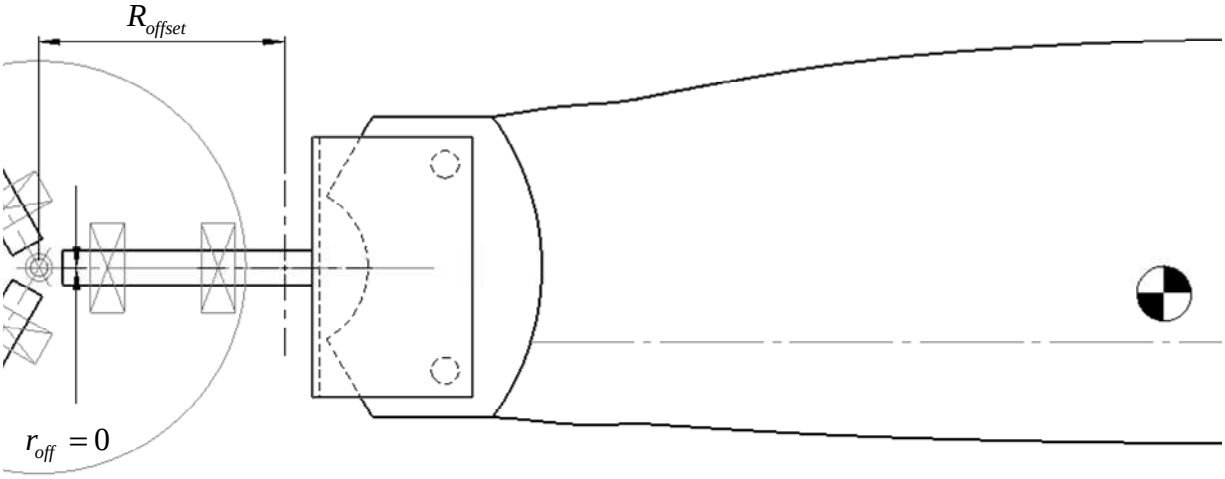

Figure 6.7 *Blades in new position*

Because the blade is offset, its radius, chord distribution and blade angle distribution will change. The chord and blade angle are given as a function of the normalized radius $x = \frac{r}{R}$ at each blade station. With an offset R_{offset}, the new stations of the chord and blade angle are calculated with the following equations:

$$x_{new} = \frac{x_{old} \cdot R_{old} + R_{offset}}{R_{old} + R_{offset}}$$
$$R_{new} = R_{old} + R_{offset} \qquad (6.1)$$
$$r_{new} = \frac{x_{new}}{R_{new}}$$

Figure 6.8 shows the AE1kW blade's new chord for an offset of $R_{offset} = 100\,\text{mm}$.

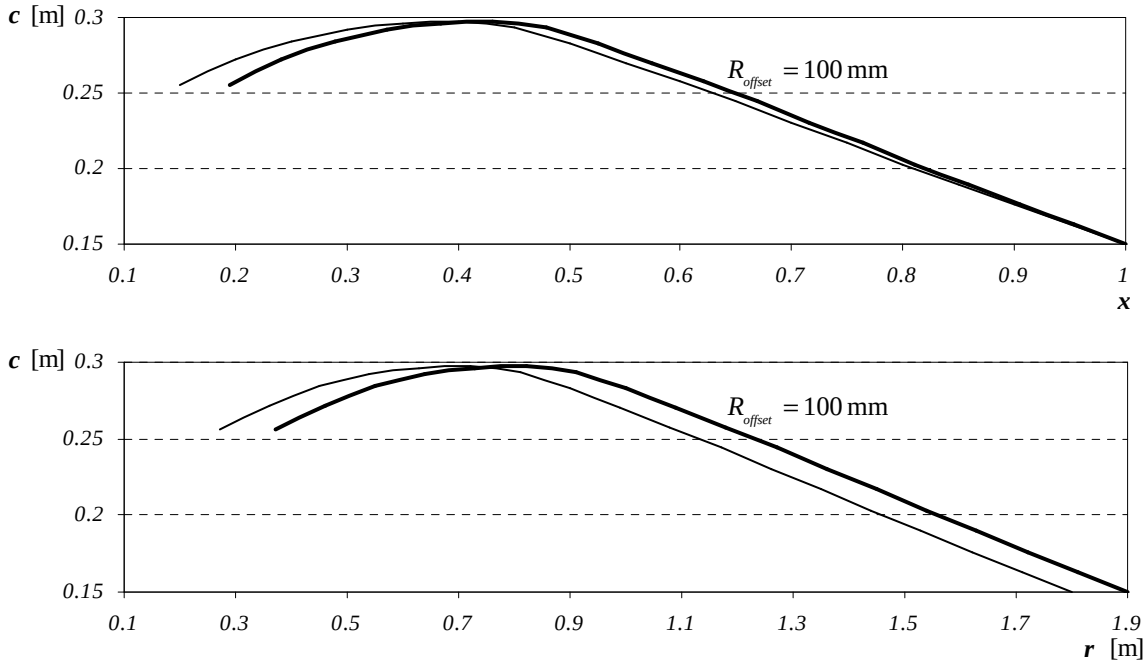

Figure 6.8 *Offset chord with R_{offset}=100 mm*

Instead of mounting the bearing holders on one base plate, they will be mounted between two plates because of the large thrust loads during negative pitching and the large centrifugal loads. For the same reasons the blades will also be attached to the pitching shaft using two plates. The pitching shaft of the governor is located with two tapered bearings (Figure 6.9).

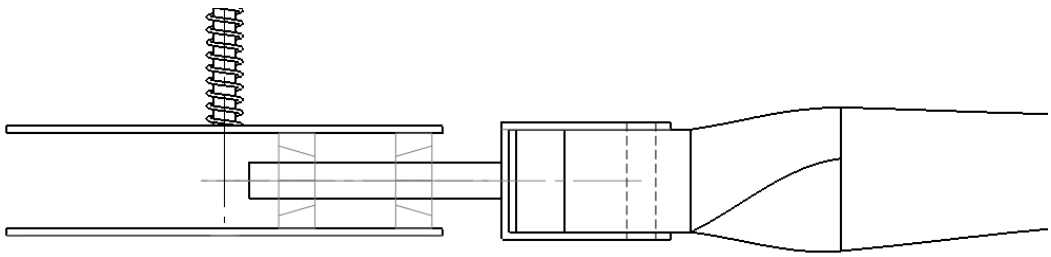

Figure 6.9 *Two plates for the bearing holders and the blades*

The governor must be designed for strength with a specific maximum wind speed in mind. To find this maximum wind speed the wind speed variation must be known. The governor is going to be tested in the North-West province, Potchefstroom. The wind conditions are low, with the mean annual wind speed below 3 m/s (Knecht 2004, p.69).

The shape factor k was chosen as the average of the three sites in South Africa given in Knecht (2004, p.71) and is k=2. The frequency distribution for the wind speeds are in given in Figure 6.10.

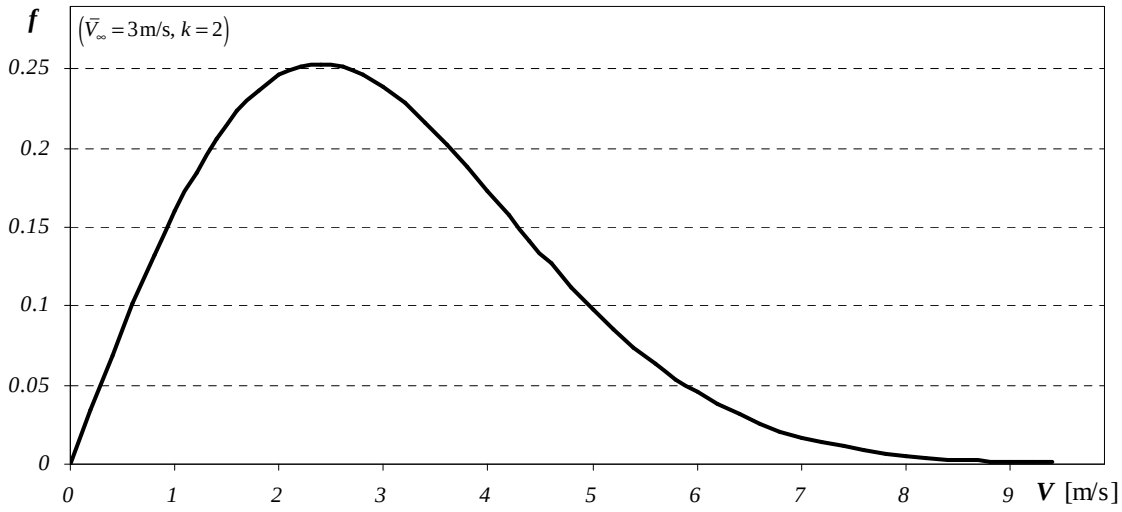

Figure 6.10 *Wind speed frequency distribution in Potchefstroom*

From Figure 6.10 the design strength wind speed was chosen as 9 m/s. The safe rotational speed limit of the blades is 500 rpm. Because no generator was available, the low wind conditions in Potchefstroom and the sliding governor's ability to limit to the same rotational speed independent of the load of the generator, the system is going to be tested without a generator. The rotor will reach its rotational speed limit at a lower wind speed, which will allow the whole pitch range of the governor to be tested. The pitch of the wind turbine with the combined concept governor with no generator at 9 m/s and 474 rpm is $p = -5.3^\circ$ (Figure 5.10 and Figure 5.8). The design pitch limit of $p = -5.5^\circ$ was therefore chosen.

The governor pitching shaft is the most critical part. For a smaller R_{offset} the centrifugal force F_{cent} is smaller, but the supports of the pitching shaft are closer together and bending moments therefore larger. These two conditions are traded of against each other.

The inner bearing holder is put as close as possible to the centre. Figure 6.11 shows the final design of the governor hub.

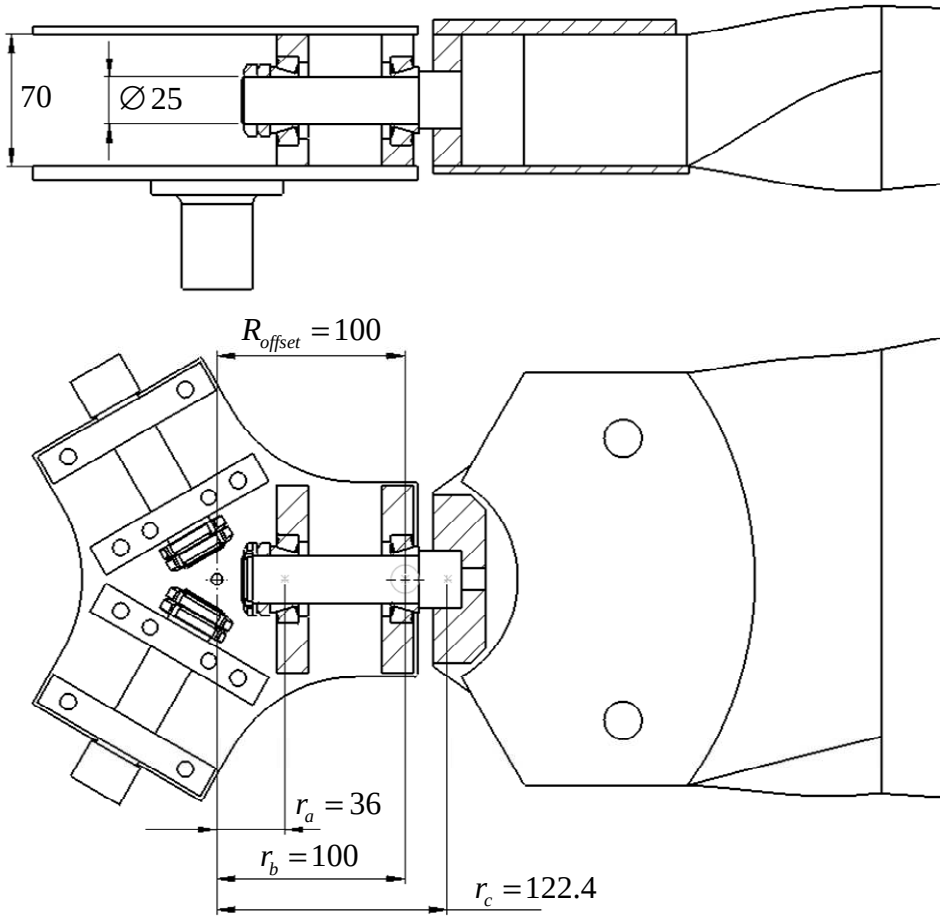

Figure 6.11 *Hub design of the governor*

The ambient atmospheric pressure in Potchefstroom is 652 mmHg (NWUSP 2006), which equates to an air density of ρ=1 kg/m^3 at 25°C. All the subsequent results are calculated at this air density.

The out-of-plane thrust T and flapping moment F causes the largest stresses in the pitching shaft during negative pitching. These forces acting at r_c are given in Table 6.1.

Table 6.1 *Design loads for the governor pitching shaft*

V_∞=9 m/s	T=273.4 kN
Ω=500 rpm	F=343.5 Nm
p= -5.5º	F_{cent}=12.9 kN

The out-of-plane bending moments of the pitching shaft are given in Figure 6.12.

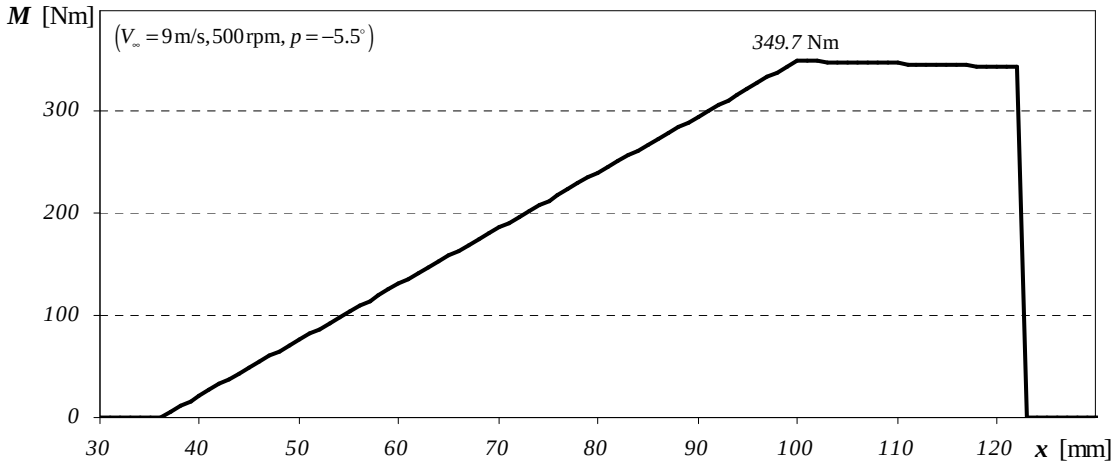

Figure 6.12 *Out-of-plane bending moment diagram of the pitching shaft*

The stresses caused by the bending moments and F_{cent} are given in Figure 6.13.

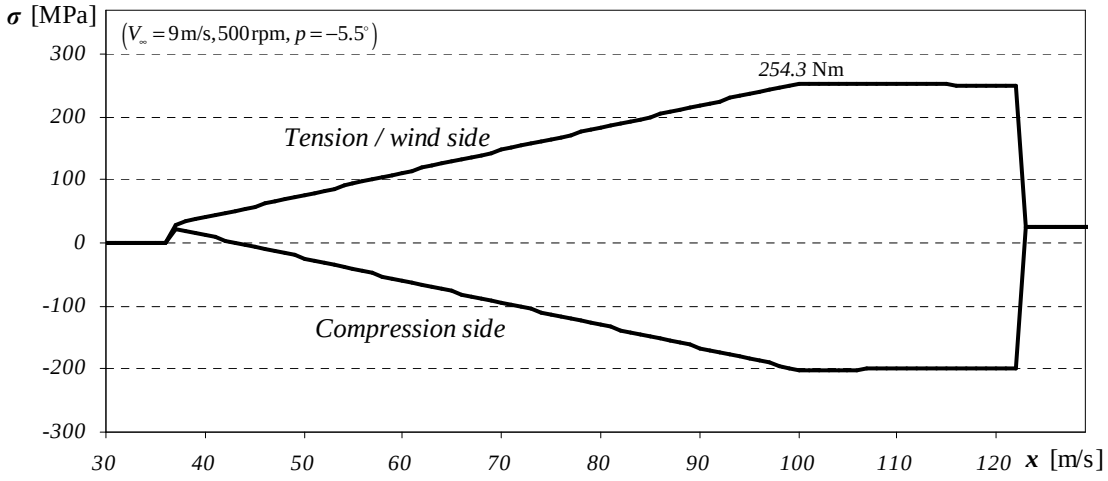

Figure 6.13 *Out-of-plane stresses of the pitching shaft*

The maximum stress of $\sigma = 254.3\,\text{MPa}$ is at r_b at the outer bearing. The governor pitching shaft is manufactured from normalized EN8 steel, with a yield stress of $370\,\text{MPa}$ (Matweb 2008). This gives a minimum safety factor of *SF*=1.5. The detailed calculation steps for the stress at r_b are given in Appendix A, section A.5.

6.4 Control system design

The end of connector L_{c2} slides or rolls across L_{c1} (Figure 5.1). A track and hanger used on hanging sliding doors will be used as a slide for L_{c1} (Figure 6.14).

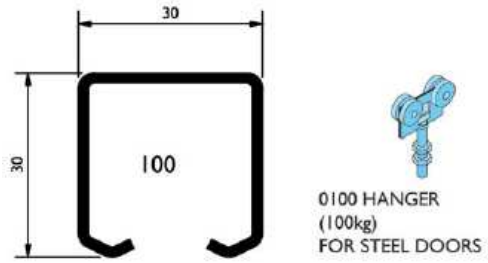

Figure 6.14 *Hillaldam 100 steel door track and hanger*

The tracks are centered radialy to the rotational axis as to cause no twist on the 3-legged connector. The track roller will be connected to the 3-legged connector with rod ends and a clevis. The tracks are connected to the pitching axis with rectangular tubing as close as possible to the generator axis (Figure 6.15).

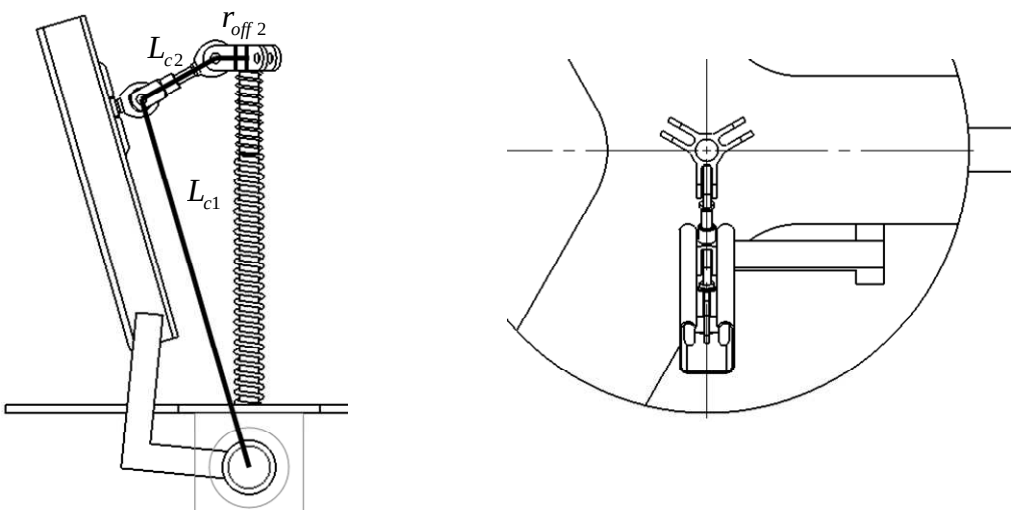

Figure 6.15 *Position of the track*

Instead of permanently welding the tracks with the rectangular tubing to the pitching axis, they are free to rotate so that adjustments can be made to the pitch offset θ_{off}. Figure 6.16 shows how the adjustment device works. The screw is fixed to the ball joint which is fixed to the blade. By turning the setting nut, the correct pitch offset can be finely adjusted.

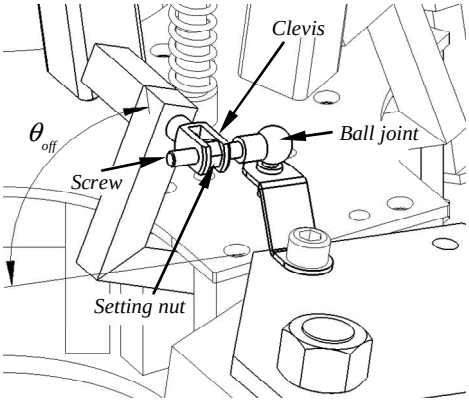

Figure 6.16 *Pitch adjustment*

It is very important that the pitch regulation of each blade be synchronized as to prevent aerodynamic imbalances and inconsistent control (Gasch & Twele 2005, p.85). Because of the sliding action of the three arms the blades will not be synchronised. Figure 6.17 shows how the tracks, which are connected to the blades, can be synchronised by connecting another set of links to a bush that runs over the springs.

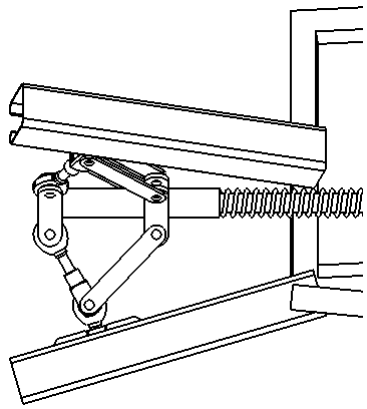

Figure 6.17 *Synchronisation of governor*

The most important aspect of the design is the governor's control characteristics. A start-up range of 150 rpm was arbitrarily chosen. A start-up pitch close to $p = 10^{\circ}$ will more than double the torque coefficient (Table 5.1). The AE1kW blades' over-speed limit is 500 rpm, so the governor's over-speed limit is chosen as 490 rpm at a maximum negative pitch of $p = -5.5^{\circ}$. The required pitch characteristic is given in Figure 6.18.

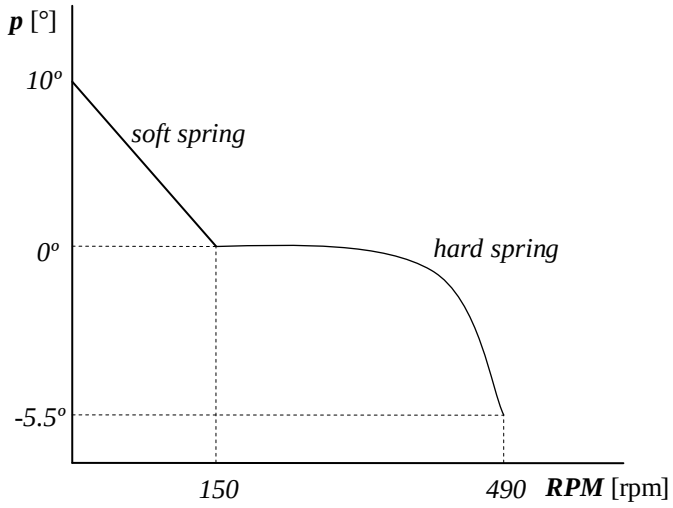

Figure 6.18 *Required pitch characteristic for the final design*

Because the governor model can only analyse an existing governor and not do inverse design, trail and error was used in the selection of the spring parameters and length of the connector L_{c2}. The limit $L_{c1.\max}$ is positioned so that when the soft spring is compressed, L_{c2} will be perpendicular to L_{c1}. The trail and error observations that are used to get the required pitch characteristic are compared to the final pitch curve:

- Decreasing the stiffness k_1 and k_2 of the springs or increasing the governor's mass m decreases the *RPM*-range (Figure 6.19).

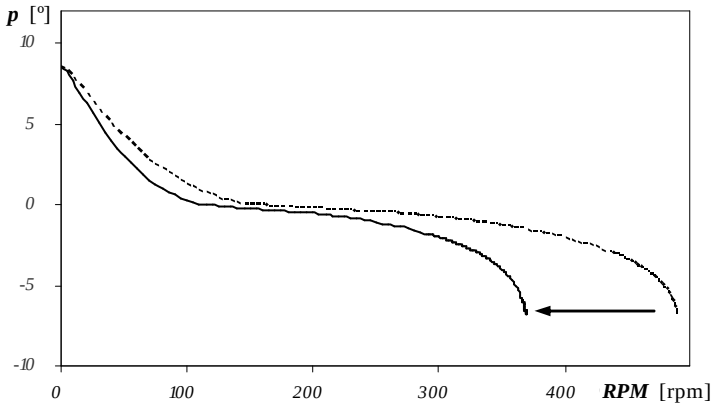

Figure 6.19 *Decreasing the RPM-range by decreasing the stiffness or by increasing the mass*

- Increasing the soft spring's length $L_{undef\,1}$ increases the start-up pitch.

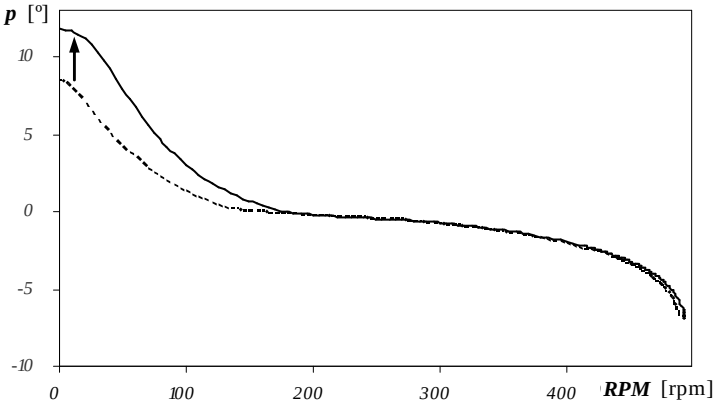

Figure 6.20 *Increasing the start-up pitch by increasing the soft spring's length*

- Increasing the hard spring's length $L_{undef\,2}$ and the limit $L_{c1.\max}$ by the same amount, increases the hard spring's *RPM*-range (Figure 6.21).

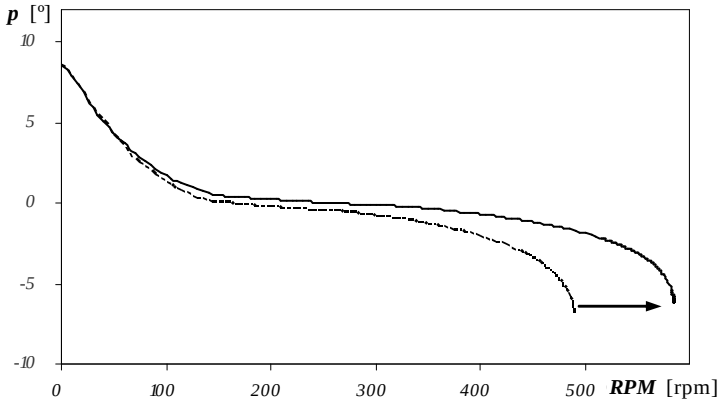

Figure 6.21 *Increasing the RPM-range of the hard spring by increasing its length and* $L_{c1.max}$

- Increasing the length of connector L_{c2} increases the maximum negative pitch (Figure 6.22 (a)). The *RPM*-limit and the start-up pitch also decreases, but if these effects are not wanted, they can be minimized. By increasing the hard spring's stiffness k_2 the *RPM*-limit is increased. By increasing the short spring's length $L_{undef\,1}$ and decreasing its stiffness k_1, the start-up pitch is restored (Figure 6.22 (b)).

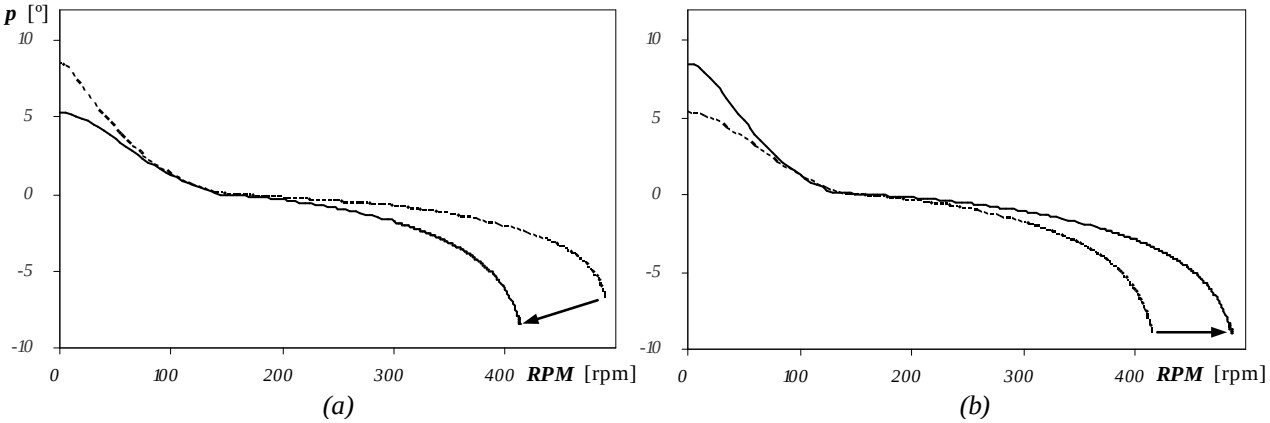

Figure 6.22 *Increasing the maximum negative pitch by increasing* L_{c2}

The effect of the external governor moment is considered next. By scaling the springs' stiffness and the mass, M_{load} is minimized to an acceptable level below 10% while the required pitch curve stays the same. The springs are selected out of a catalogue and manufactured to exact specification. Spacers are used if the exact spring can not be found.

The selection of the mass is done last, because its position can easily be changed by changing its size as long as the M_{cent} stays the same. The effect of the track's mass and roller's mass were also included in the calculation of M_{cent} (Figure 6.23 (a)).

After many design iterations the design of the governor prototype is shown in Figure 6.23. The manufacturing drawings of the governor prototype are given in Appendix C.

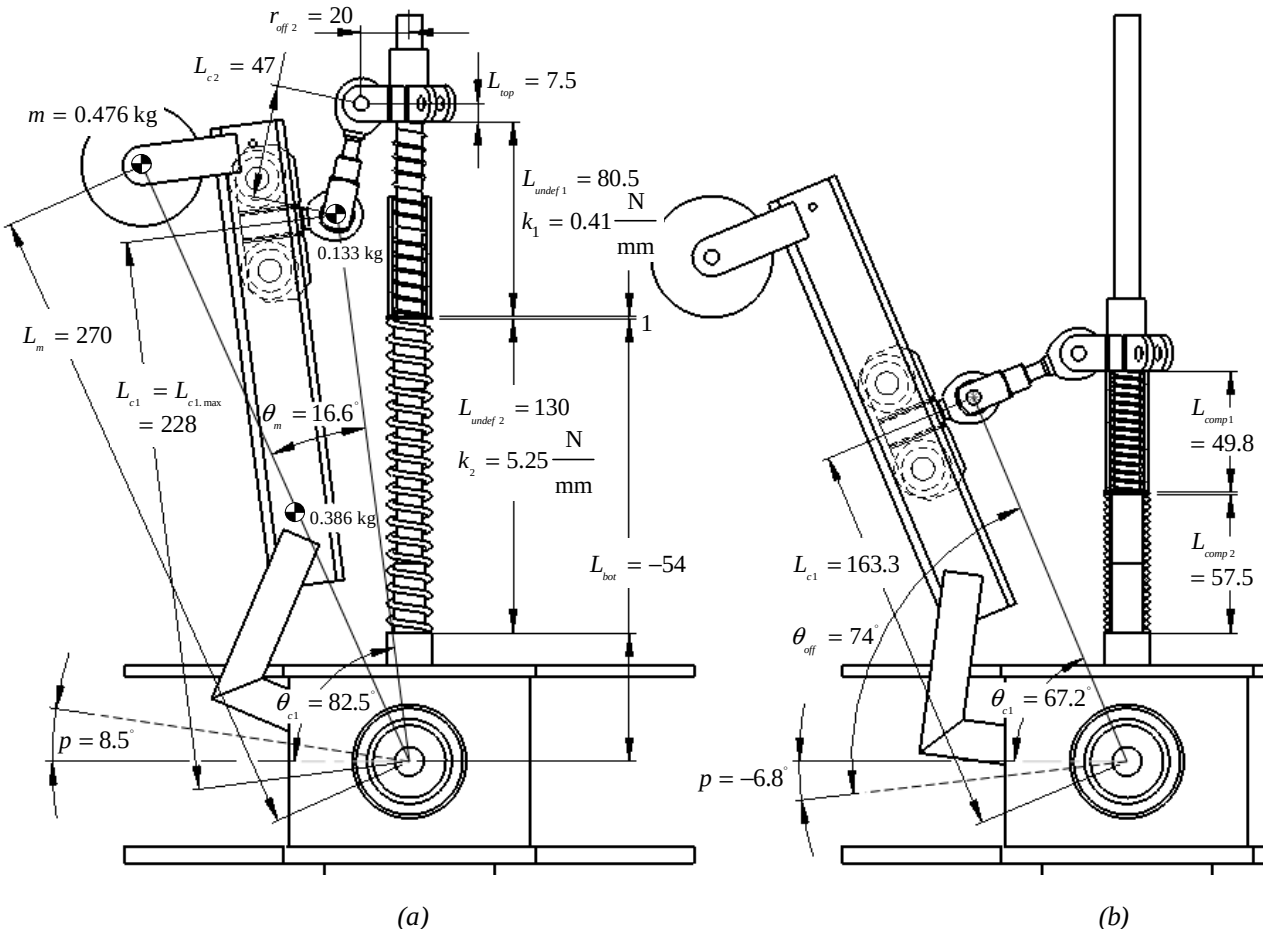

Figure 6.23 *(a) Governor prototype at the start-up position and (b) at the compressed position*

Note from Figure 6.23 the distance $L_{bot} = -54\,\text{mm}$ is negative because L_{bot} was defined in Figure 3.11 as the distance of the pitching shaft above the bottom of the hard spring. The 1 mm distance between the soft and the hard spring is included in L_{bot}.

With θ_{off}=74°, the pitch curve is shown in Figure 6.24.

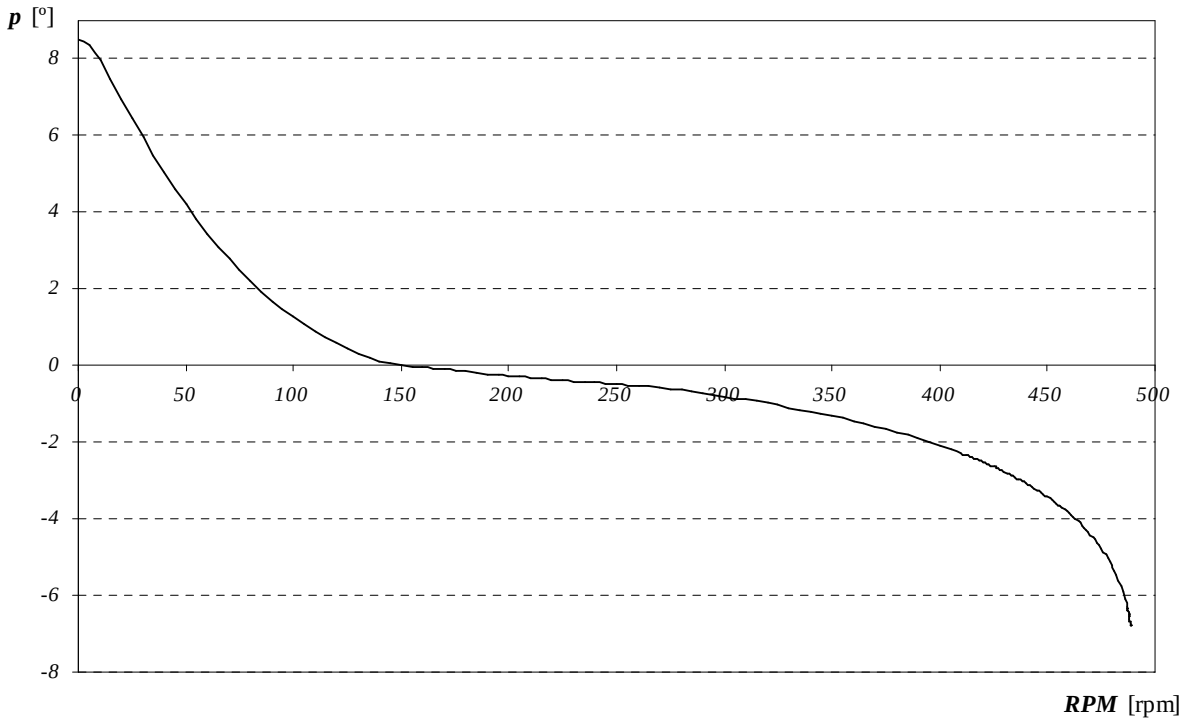

Figure 6.24 *Pitch vs. RPM for the governor prototype*

The increased start-up coefficient and moment results are given in Table 6.2. The start-up moment is calculated for a cut-in wind speed of $V_\infty = 3\,\text{m/s}$. The start-up torque is more than double for a start-up pitch of $p = 8.5^\circ$.

Table 6.2 *Start-up results for the governor prototype*

Pitch	0º	8.5º
C_Q ($\lambda=0$)	0.007	0.017
$Q(\lambda=0, V_\infty=3$ m/s)	0.709 Nm	1.613 Nm

The rotational speed characteristics without the generator are given in Figure 6.25. The governor limits the rotational speed below 484 *RPM*. With the governor disabled and $p = 0^\circ$ the limit of 500 rpm is reached at V_∞=6.5 m/s.

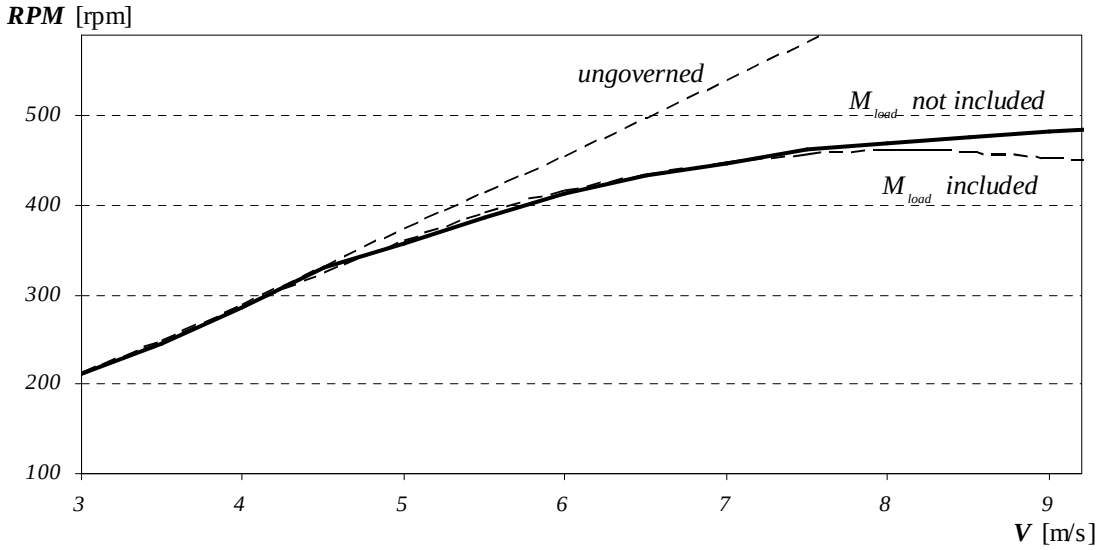

Figure 6.25 *RPM vs. wind speed for the governor design without the generator*

The safety factor of the pitching shaft at V_∞=9 m/s, 482.4 rpm and $p = -5.52^\circ$ is *SF*=1.5.

The effect that M_{load} has on the control characteristics is very small and is more than acceptable, since it lowers the maximum rotational speed. Figure 6.26 shows M_{load} compared to the governor moments M_{cent} and M_{spring}. M_{load} is below 11% up to 9 m/s.

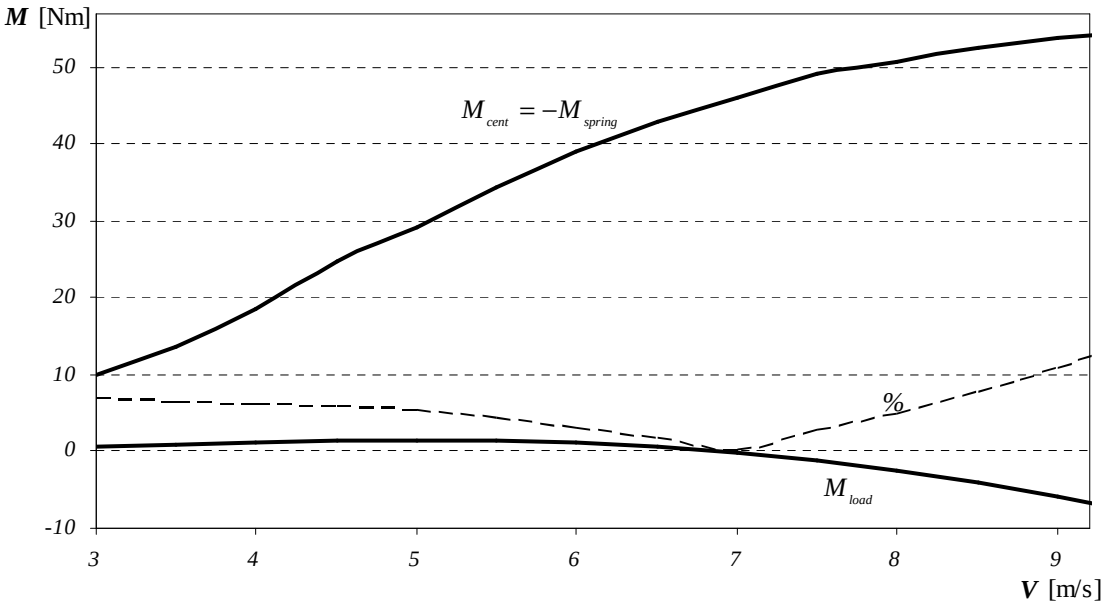

Figure 6.26 *M_{load} compared to M_{cent} and M_{spring}*

Even though the prototype was not designed with a generator and will not be tested with one, the simulation results for the prototype with the generator are given in Figure 6.27.

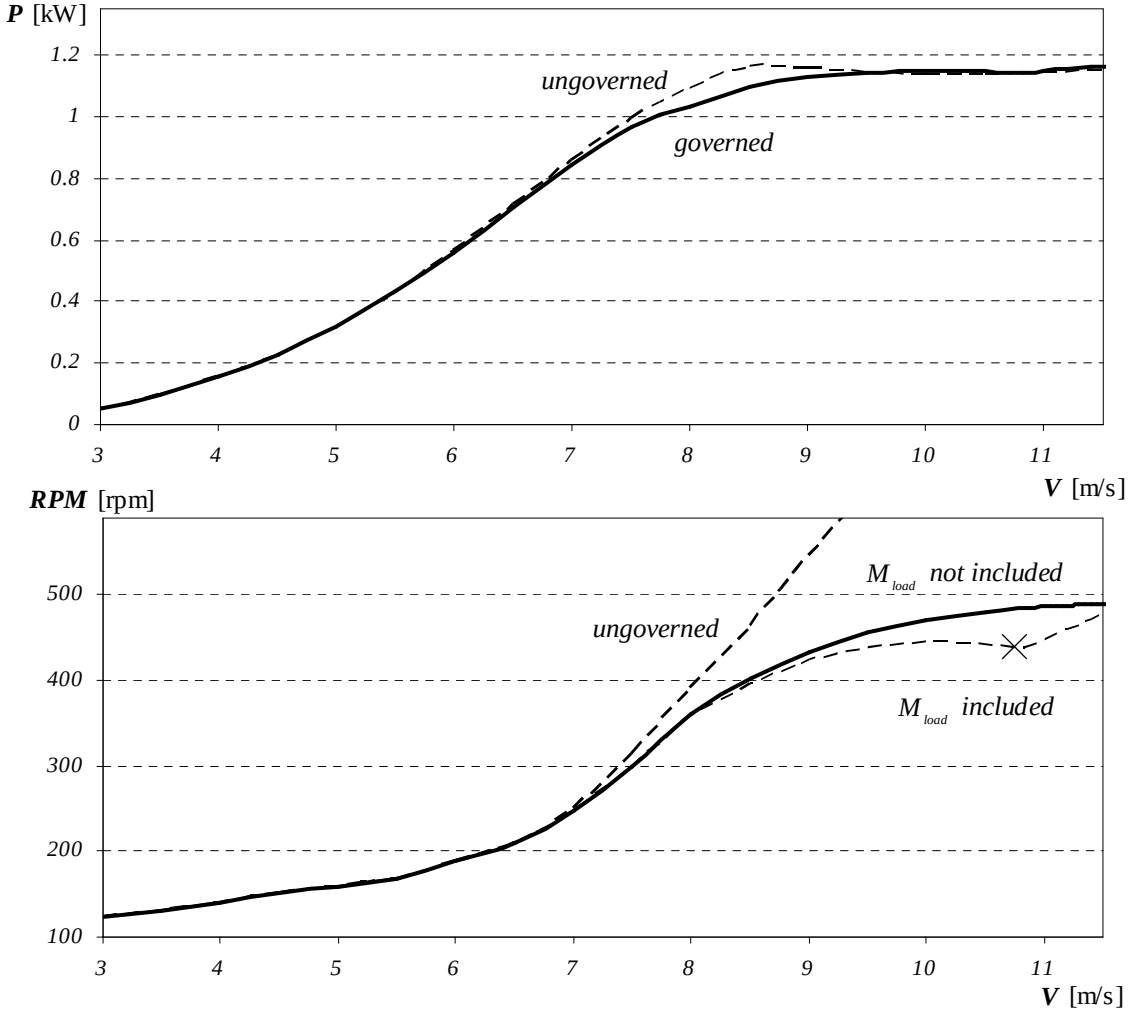

Figure 6.27 *RPM and power vs. wind speed for the governor prototype with the generator*

Either with or without a generator, the governor will limit the rotational speed. The effect of M_{load} is a larger because of the higher wind speeds. The governor's limit of p=-6.8°, when all the springs are compressed to a solid height, is reached at V_∞=10.8 m/s. With the generator the governor will limit the rotational speed with a minimum loss of power.

6.5 Summary

The detail design of the governor prototype was done. The governor prototype was designed to achieve the control objectives with the specific control characteristics of Figure 6.18. The effect of the external moment on the control was minimized. The strength design of governor's pitching shaft was done.

Chapter 7 Testing and results

7.1 Introduction

This chapter discusses the initial testing of the stand-alone governor and its results. The modification of the governor prototype from the initial testing results will be discussed. The final testing of the wind turbine blades with the governor is discussed with its results.

A summary of all the tests are given in Table 7.1.

Table 7.1 *Test summary*

Initial testing	**Final testing**			
	Governed over-speed	**Ungoverned over-speed**	**Governed start-up**	**Ungoverned start-up**
Establish the *pitch vs. RPM* characteristics and validate the model.	Perform comparative tests to see if the governor can achieve the control objective of over-speed protection. Establish the *RPM vs. V* characteristics and validate the model.		Perform comparative tests to see if the governor can achieve the control objective of improved start-up performance.	

7.2 Initial testing and results

The governor prototype is first tested on a dc-motor without the blades. This experiment is used to establish the following:

- Establish the governor's pitch vs. rotational speed characteristics
- Compare the results with Figure 6.24 to validate governor model

Because no blades are connected to the governor, $M_{load} = 0$. Figure 7.1 shows the experimental setup of the governor prototype connected to the dc-motor.

Figure 7.1 *Initial test setup with the governor prototype in the start-up position without blades*

The pitch p is a function of the displacement x of the tip of the governor's centre shaft to the top of the bush (Figure 7.2). The displacement x is calculated for the entire pitch range and given in Figure 7.3. The pitch can therefore be determined by only measuring x and using Figure 7.3 to interpolate the pitch.

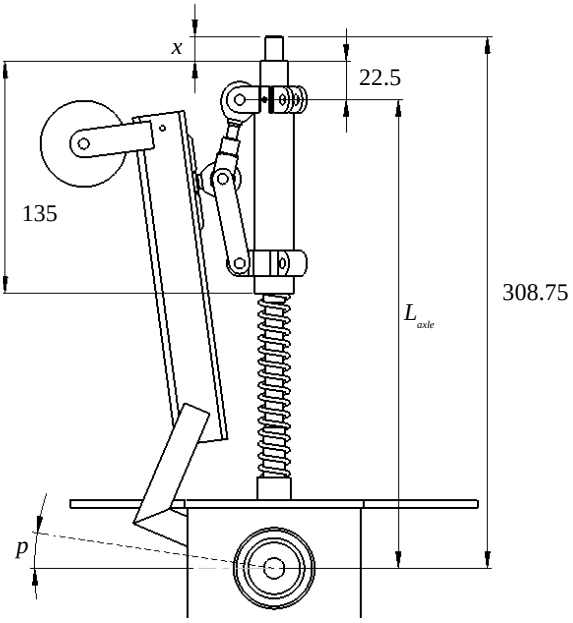

Figure 7.2 *Displacement x to determine the pitch p*

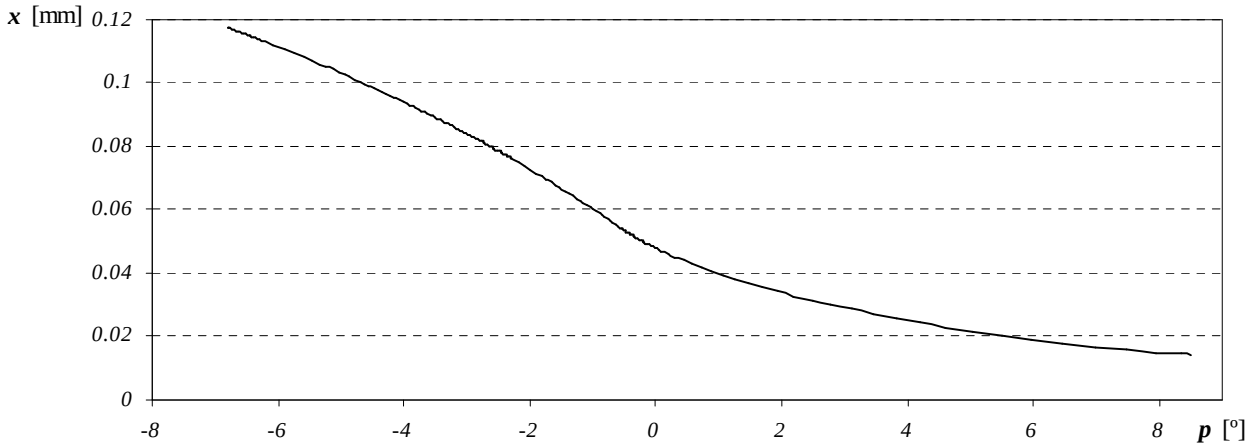

Figure 7.3 *Calculated displacement x relative to the pitch p*

The test is done by increasing the motor's speed in small increments while photos are taken from the side, with a tachometer indicating the speed (Figure 7.4).

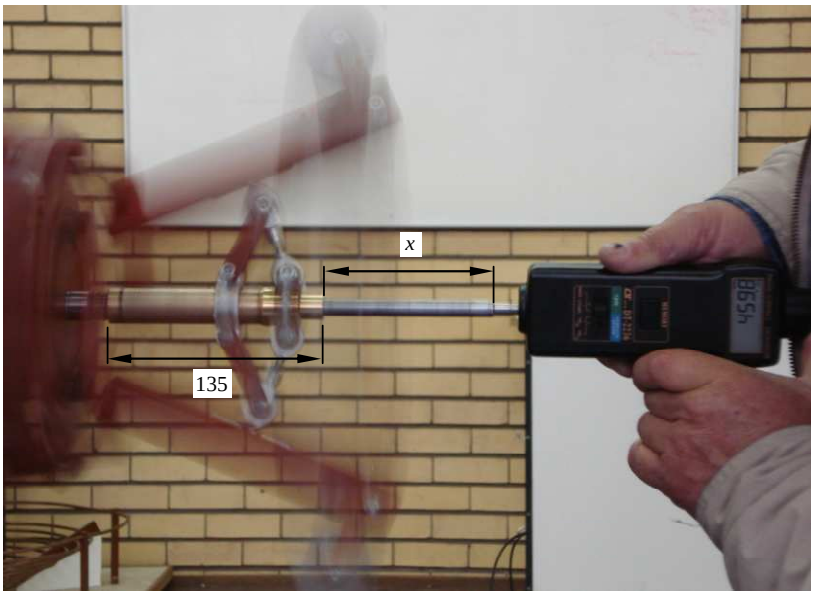

Figure 7.4 *Side view of governor at one test rotational speed*

The photos are digitized in a CAD application and scaled to the correct size using the length of the 135 mm bush to determine the displacement *x* (Figure 7.5).

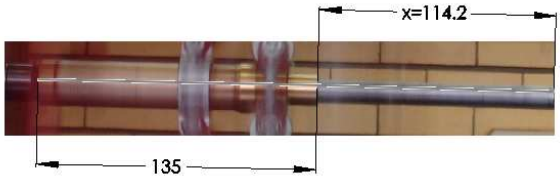

Figure 7.5 *Displacement at 459.8 RPM*

Figure 7.6 shows the measured displacement *x* compared to the calculated displacement *x* relative to the *RPM*.

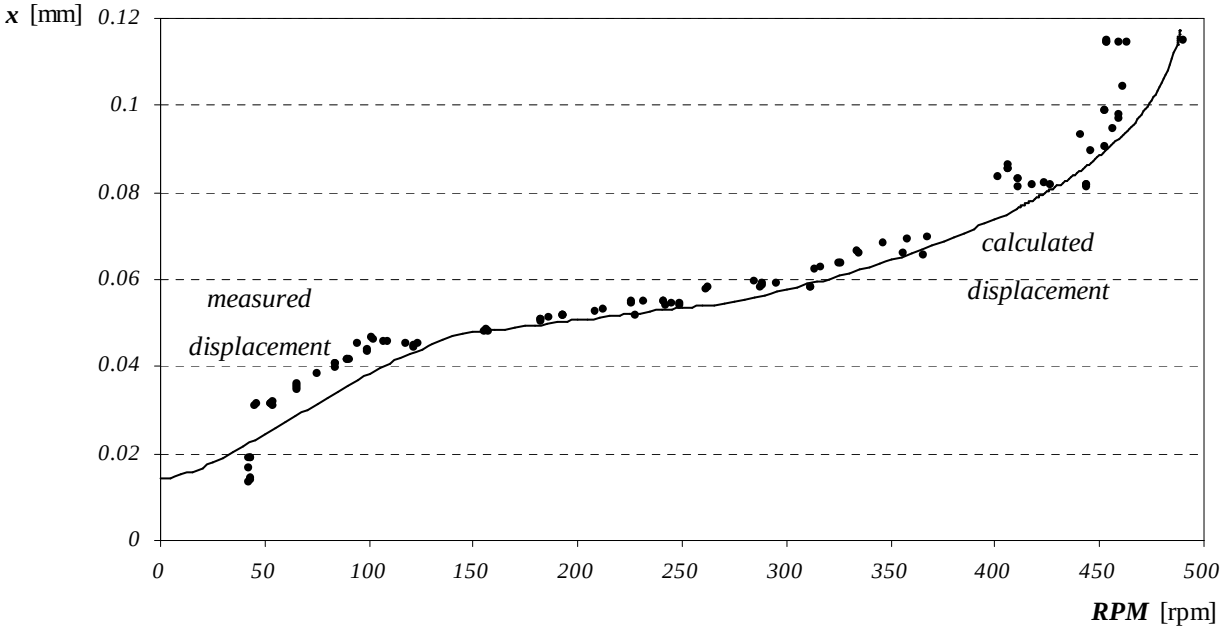

Figure 7.6 *Measured and calculated displacement x vs. RPM*

The pitch is interpolated from the displacement *x* using Figure 7.3 and the results are shown in Figure 7.7. The results are compared to the calculated results of the governor prototype in Figure 6.24.

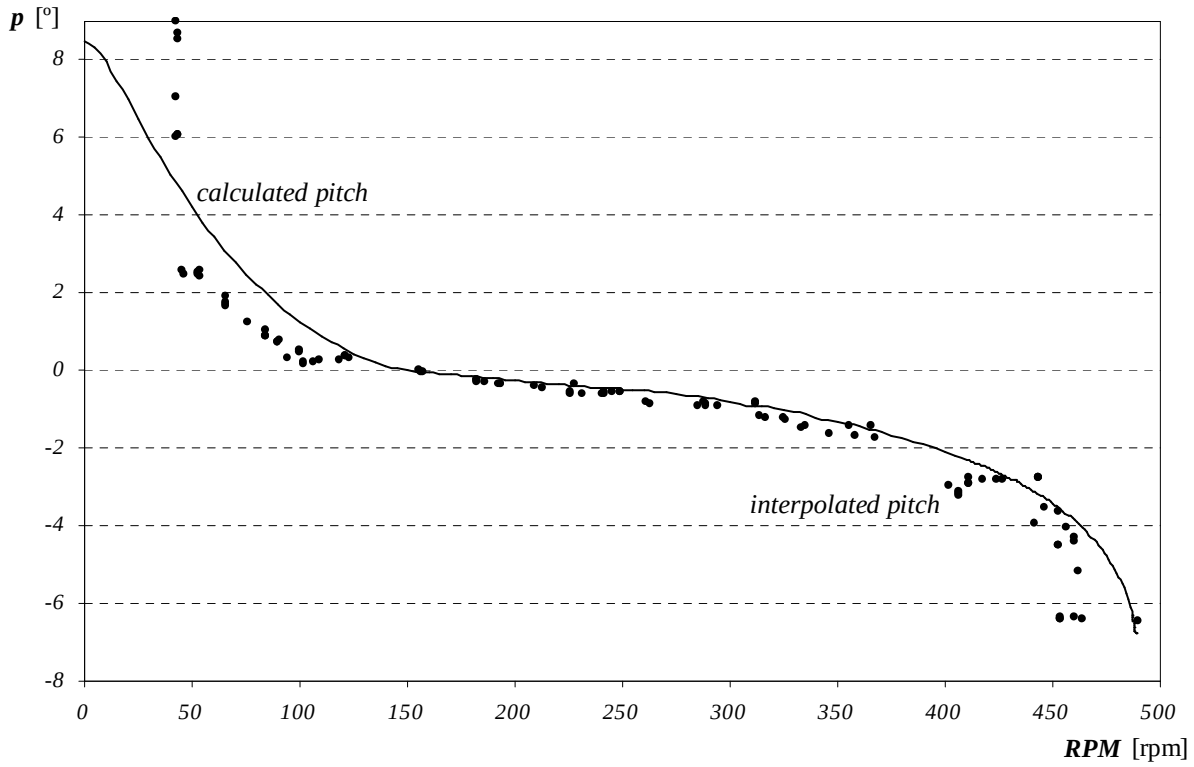

Figure 7.7 *Interpolated and calculated pitch vs. RPM*

From Figure 7.6 and Figure 7.7 it can be seen that there is a very good correlation between the calculated and measured results. The governor prototype behaves as predicted by the centrifugal governor model and the model is thus reliable.

One problem that was experienced during the testing was that the governor did not return to the start-up position of p=8.5°, but jammed at p=2.5°. This was due to the friction between synchronisation bush and connector as well as the small stiffness of the small spring (Figure 7.8).

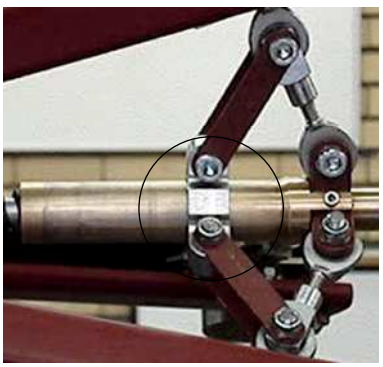

Figure 7.8 *Friction between synchronisation bush and connector*

To overcome the problem the prototype is modified by adding another identical small spring to the governor (Figure 7.9). Adding the spring results in an initial compression of the springs at the start-up position. Notice from Figure 7.9 the rod end pressing against the synchronization bush.

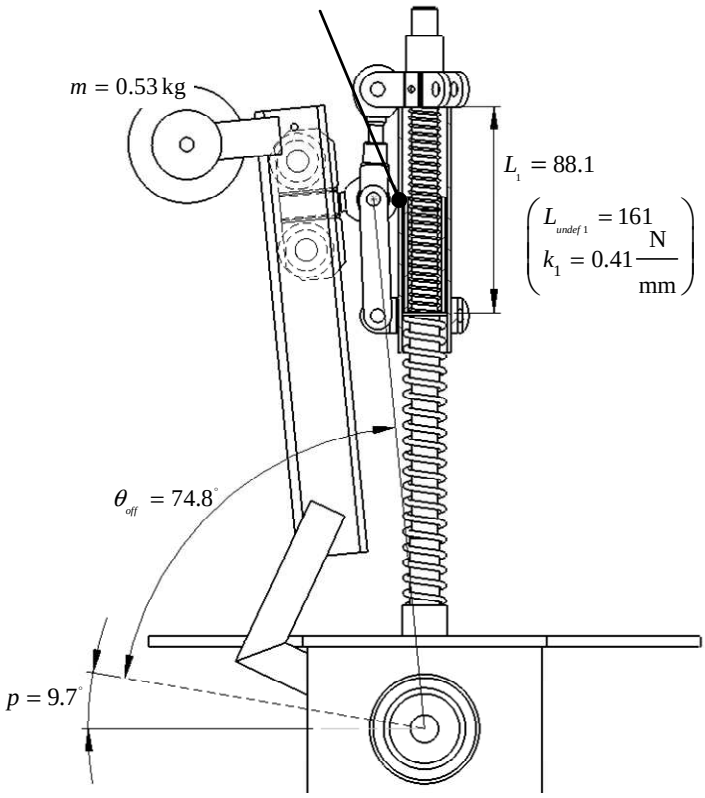

Figure 7.9 *Modified prototype design at the start-up position*

Adding the small spring increases the start-up pitch, but also slightly increases the *RPM*-range over the speed limit (Figure 7.10 (a)). Adding two $27\,\text{g}$ steel discs to each mass restores the *RPM*-range again (Figure 7.10 (b)).

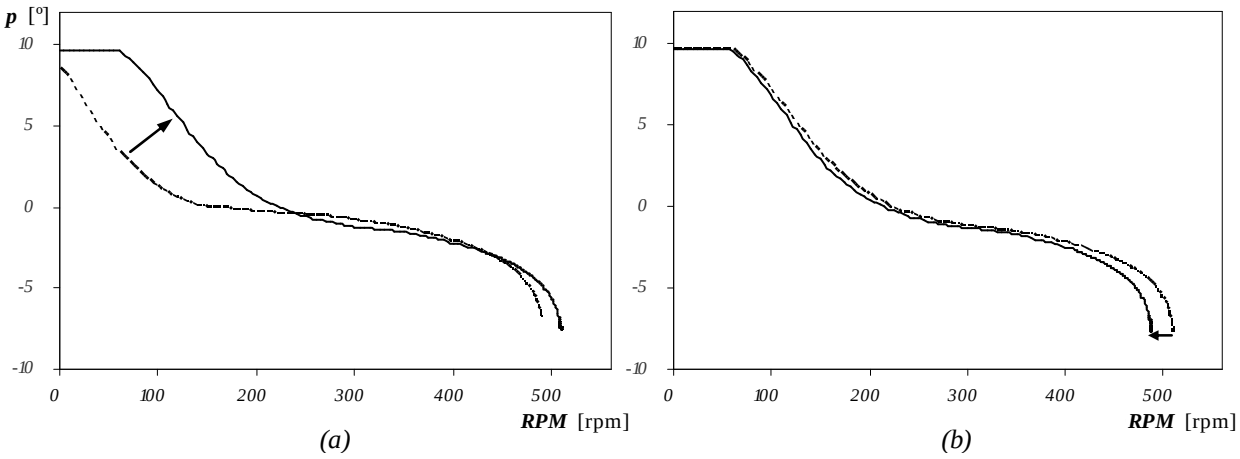

Figure 7.10 *(a) Adding an additional small spring and (b) adding mass to restore the RPM-range*

The new pitch curve compared to the previous one from Figure 6.24 is shown in Figure 7.11.

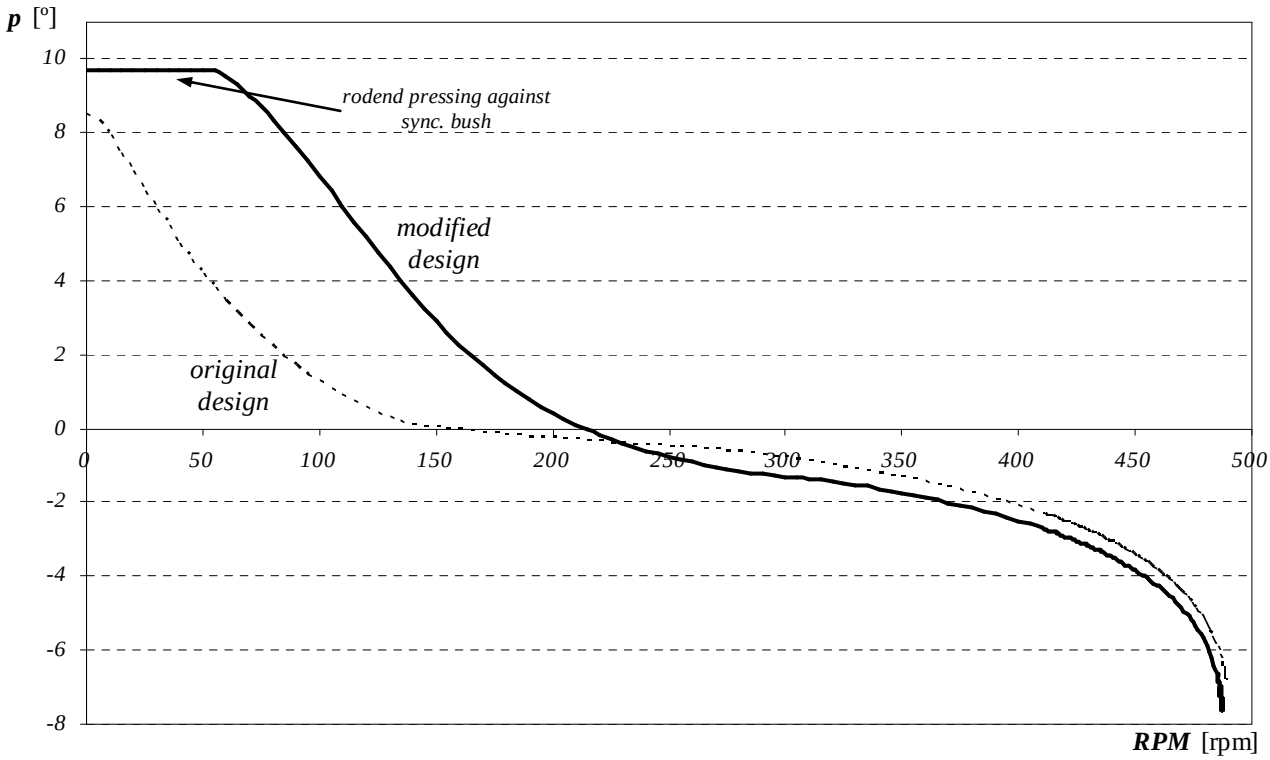

Figure 7.11 *Calculated pitch vs. RPM for the modified design compared to the original design*

The start-up coefficient and torque results for the modified prototype are given in Table 7.2.

Table 7.2 *Calculated start-up results for the modified design*

Pitch	0º	9.7º
C_Q ($\lambda=0$)	0.007	0.018
$Q(\lambda=0, V_\infty=3$ m/s)	0.709 Nm	1.735 Nm

The rotational speed characteristics are compared to those of the original design in Figure 6.25 and are given in Figure 7.12.

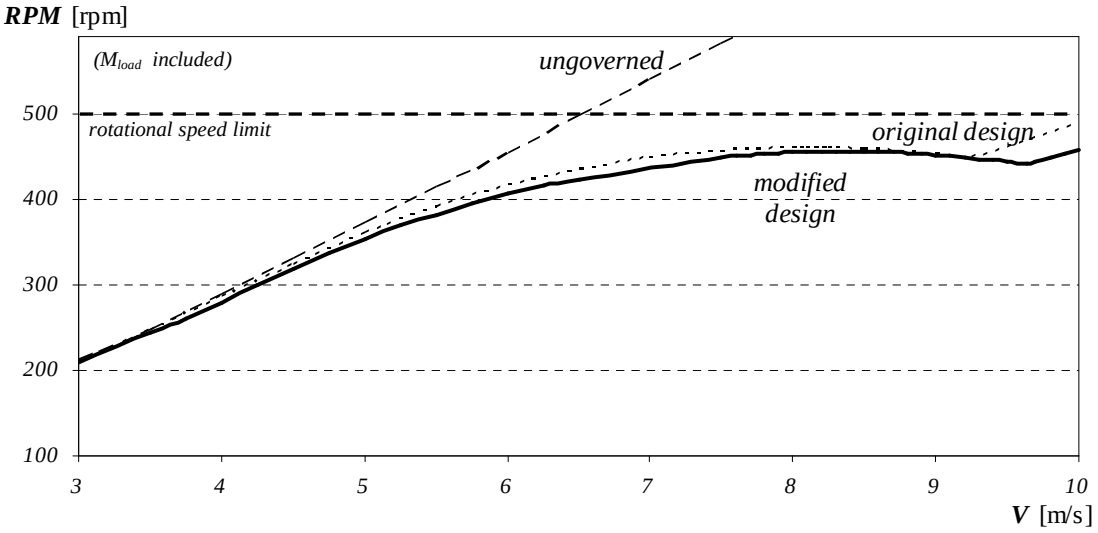

Figure 7.12 *Calculated RPM vs. wind speed for the modified design without a generator*

As seen from Figure 7.11 and Figure 7.12, the design modification has little effect on the normal and over-speed operation of the governor. The manufacturing drawings of the modified governor prototype are given in Appendix C.

7.3 Over-speed tests

7.3.1 Test setup

To test if the modified prototype can accomplish the control objective of over-speed protection, comparative tests are done between the governed and ungoverned wind turbine system. The tests are done without a generator and were motivated in section 6.3. The following tests are done:

- Establish the system's governed and ungoverned rotational speed vs. wind speed characteristics.
- Compare the governed test results to the ungoverned test results to test if the system can achieve the control objective of over-speed protection.
- Compare the governed and ungoverned test results to the calculated results of Figure 7.12 to validate the model.

The only variables that have to be measured are the rotational speed and the wind speed. The displacement of governor was not measured since the first test validated the governor model.

Figure 7.13 and Figure 7.14 shows the test setup.

Figure 7.13 *Experimental setup of the governor prototype with the AE1kW blades*

Figure 7.14 *Experimental setup of the governor prototype with the AE1kW blades*

The governor with the AE1kW blades are mounted on a 3 m tower on a free-running shaft. The v-belt and pulley function as an emergency brake when the v-belt is pulled into the pulley's groove with the rope.

To measure the wind speed an anemometer from a Davis Weather Wizard III is mounted to the side of the tower (Davis Instruments 2008). The rotational speed is measured by a small dc-motor modified to function as a tachometer.

The data is recorded by a Somat eDAQ lite data logger (SoMat Corporation 2008). The logger records the open-close periods of the circuit of the anemometer and the tachometer, from which respectively the wind speed and rotational speed can be calculated.

In one complete rotation the anemometer circuit opens once (Figure 7.15). Taking the inverse of the elapsed time between consecutive closed or open periods gives the frequency. Once the frequency is known, the wind speed can be calculated. For a wind speed of 1 mph the anemometer rotates at 1600 rev/h (Davis Instruments 2008). A wind speed of 1.006 m/s will thus cause the anemometer to rotate at 1 Hz. Figure 7.15 shows a calculation example of the frequency and the wind speed of the anemometer.

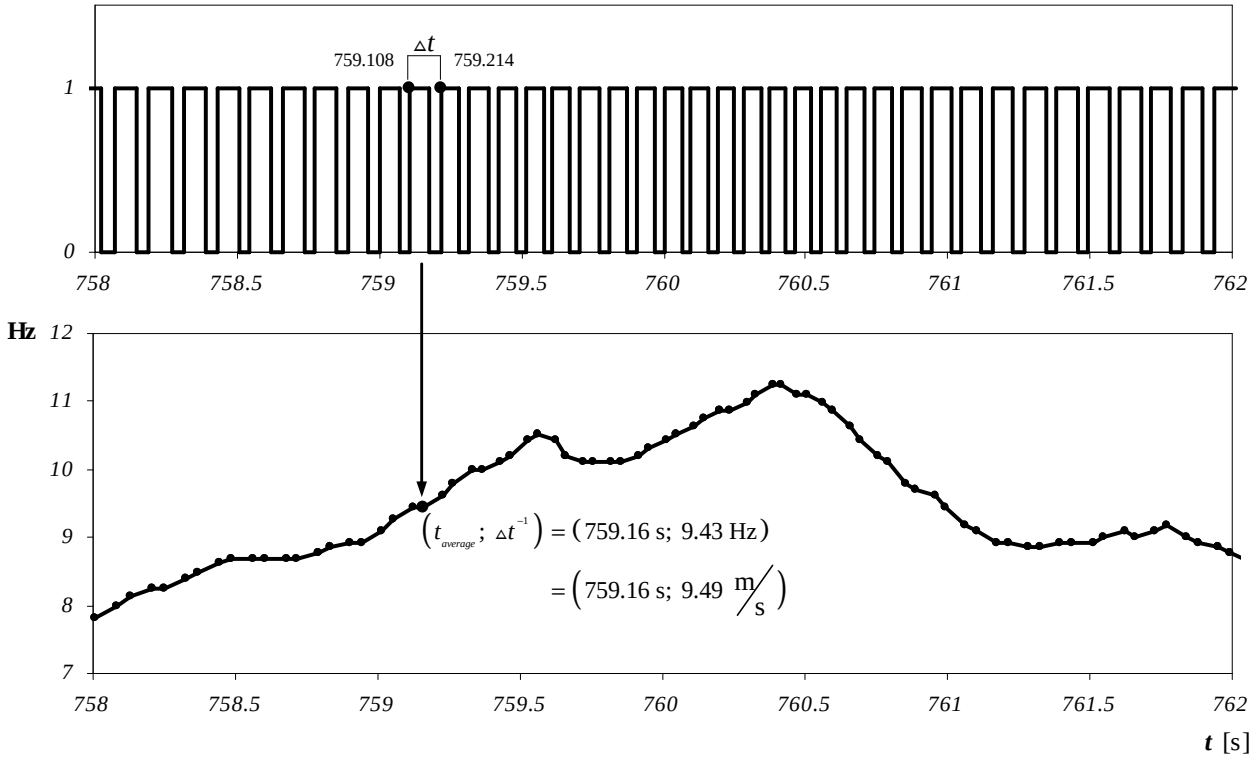

Figure 7.15 *Anemometer frequency and wind speed calculation example*

The tachometer circuit closes twice in one complete rotation. Figure 7.16 shows a calculation example of the frequency and rotational speed of the tachometer.

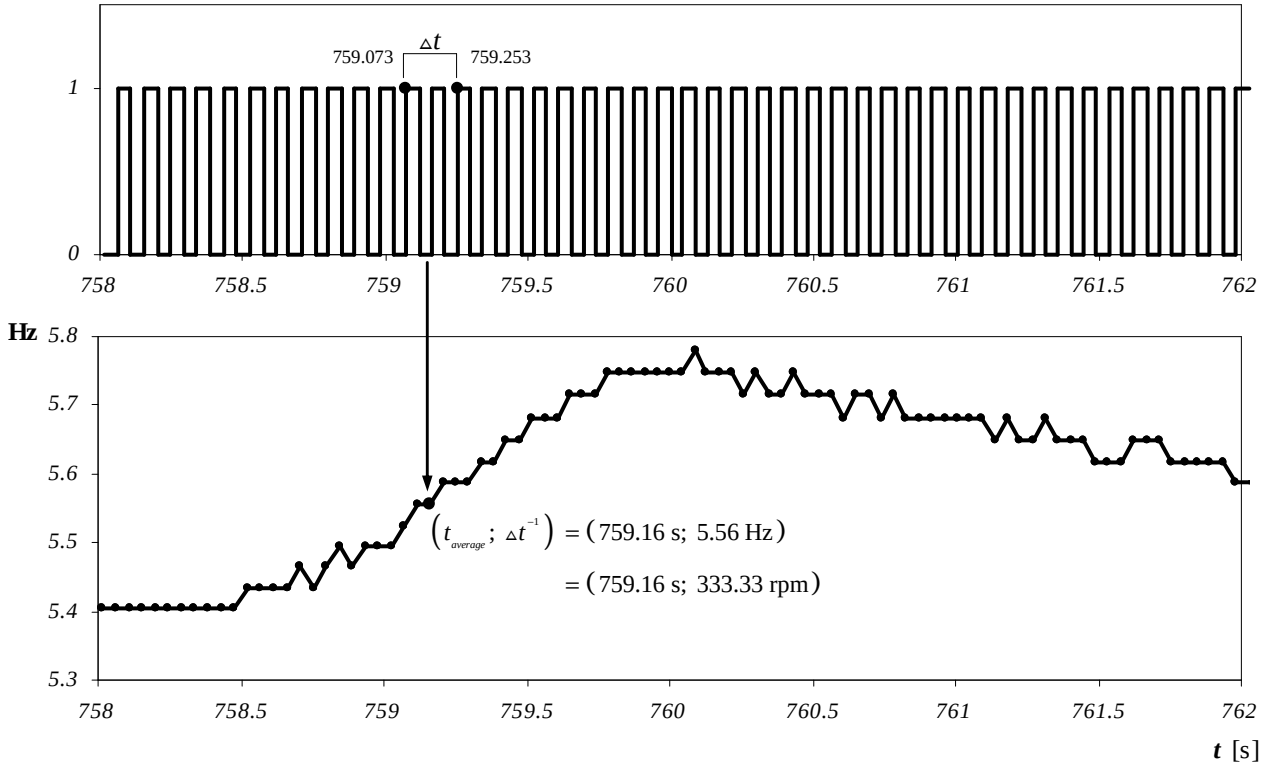

Figure 7.16 *Tachometer frequency calculation example*

Figure 7.17 shows the wind speed vs. the rotational speed for the time interval from 758 s to 762 s. The longer the sample time is, the denser the data will be.

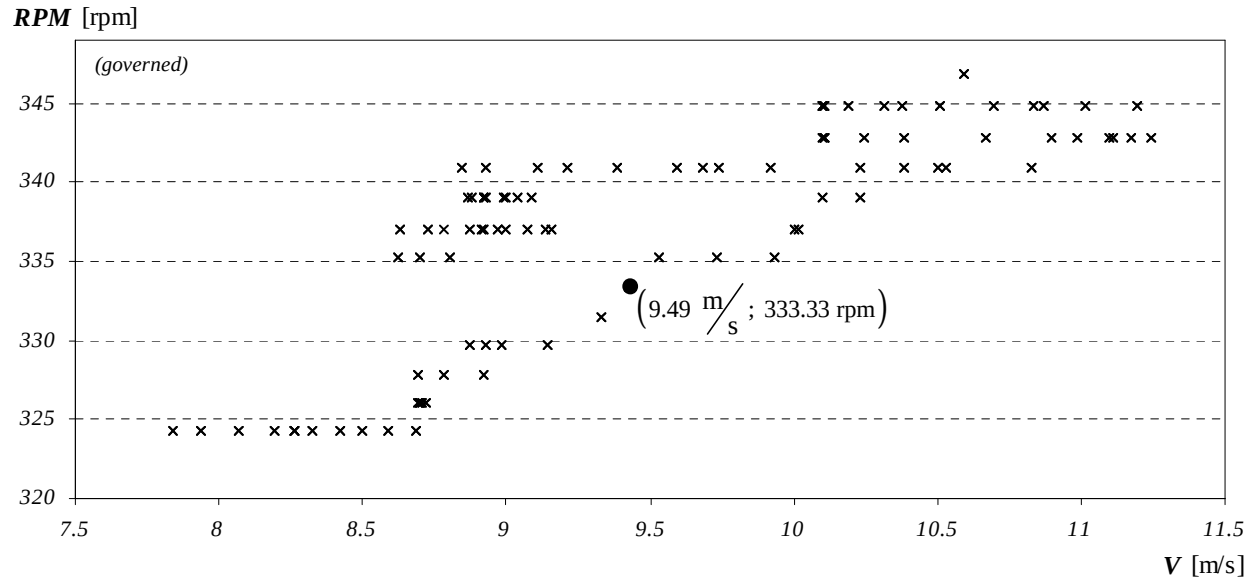

Figure 7.17 *Wind speed vs. the RPM from data sample*

Because of the inertia of the governor with the blades and variability of the wind (Figure 7.18), the spread of the data is very wide (Figure 7.19). Because of the wide spread of data the comparison of the ungoverned and governed data for the over-speed tests will be difficult.

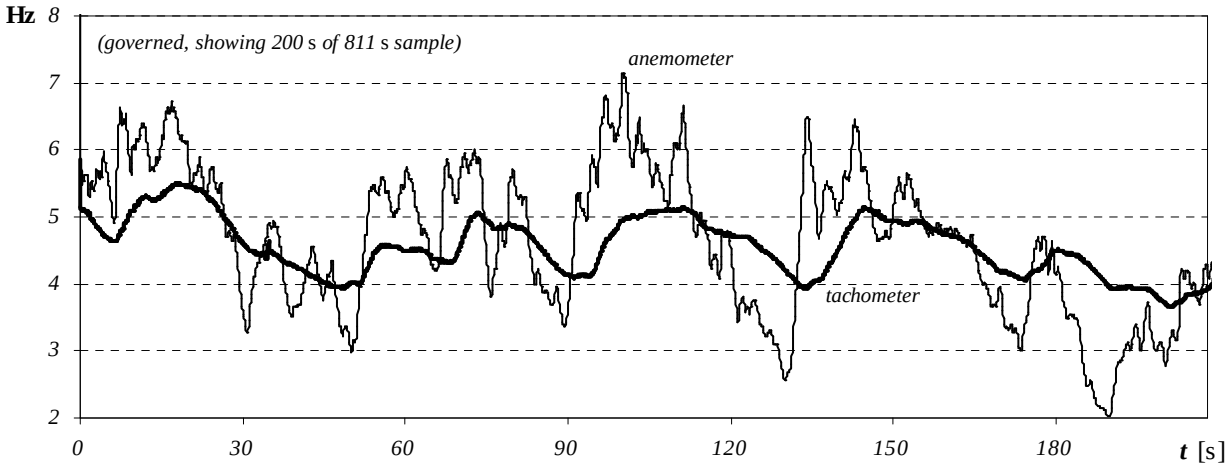

Figure 7.18 *Frequency data sample*

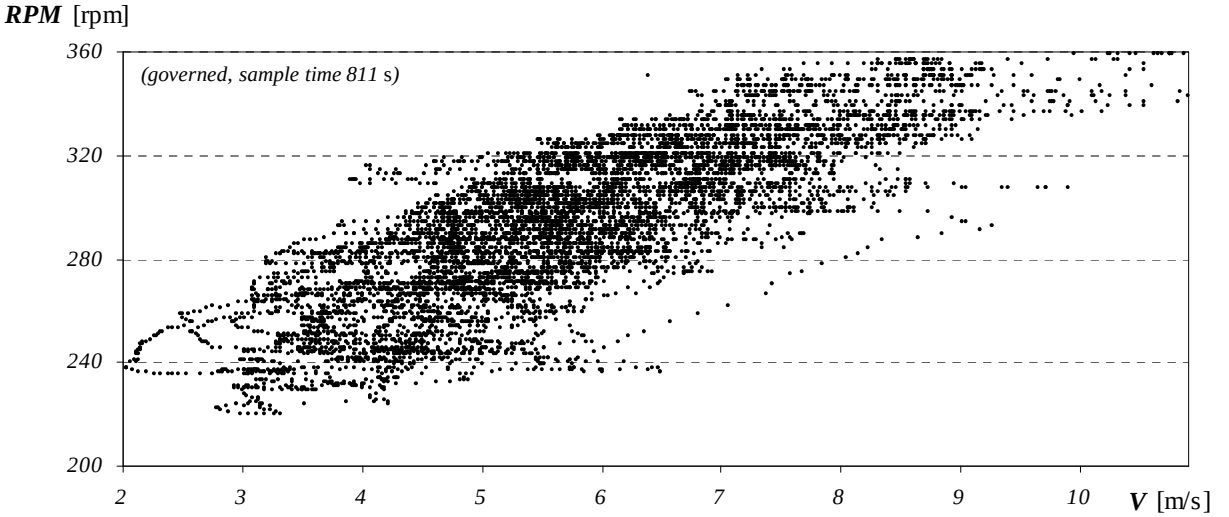

Figure 7.19 *RPM vs. wind speed data sample*

For the over-speed tests the modified prototype is configured to lower its rotational speed limit of 455.7 rpm (Figure 7.12). By removing the small spring compression spacer, the two small springs compress solid to 29 mm instead of 49.8 mm (Figure 7.20).

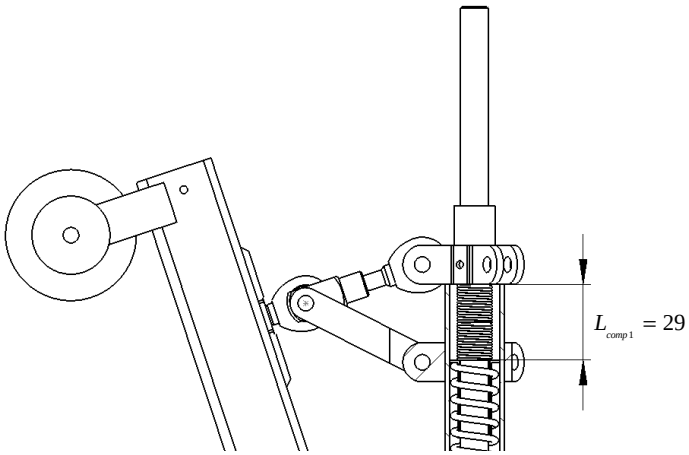

Figure 7.20 *Final test configuration of the modified prototype showing compression spacer removed*

The calculated pitch and rotational speed results are given respectively in Figure 7.21 and Figure 7.22. From Figure 7.22, the rotational speed limit is now 386.6 rpm.

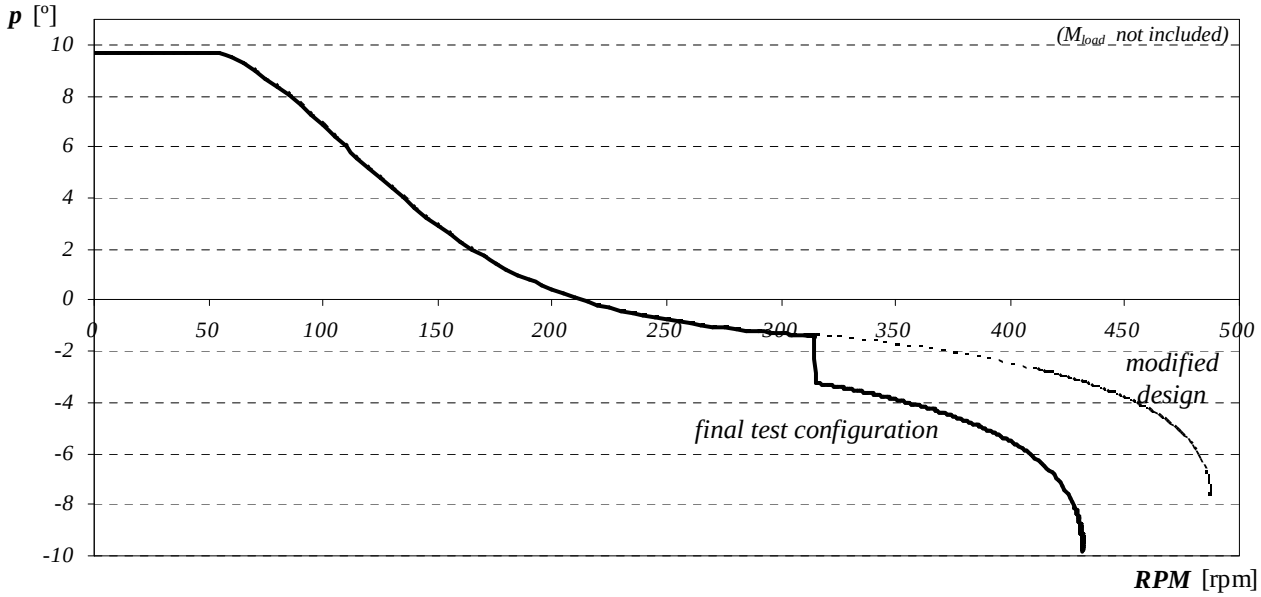

Figure 7.21 *Calculated pitch vs. RPM for the final test configuration*

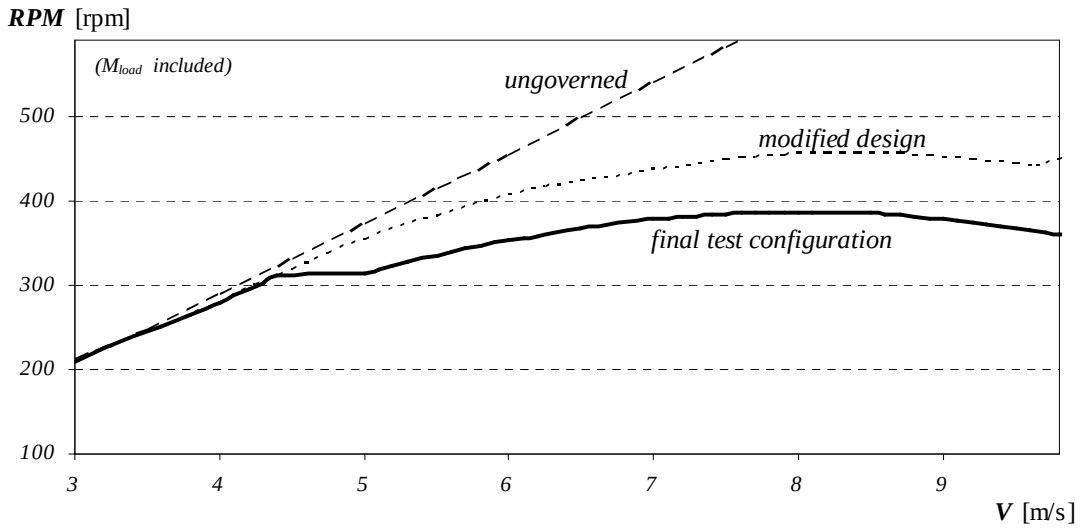

Figure 7.22 *Calculated RPM vs. wind speed for the final test configuration*

Note from Figure 7.21 that removing the compression spacer does not influence the start-up pitch of p=9.7°. Even though the normal configuration of the modified prototype will not be used in the over-speed tests, using the final test configuration will still prove whether the design can provide over-speed protection.

To do the ungoverned tests the governor's pitch must remain at p=0°. This is done by inserting a 184.8 mm spacer instead of the springs (Figure 7.23).

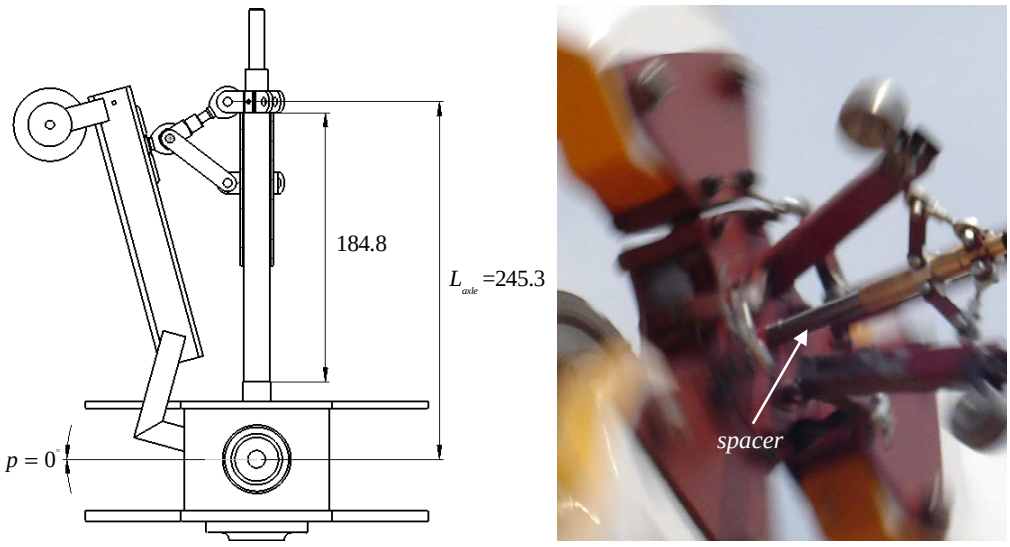

Figure 7.23 *Ungoverned configuration with the pitch fixed at p=0°*

7.3.2 Over-speed test results

The governed over-speed tests with the final test configuration are performed first because the system might get damaged during over-speeding in the ungoverned tests. The tests are performed over a few days to get high enough wind speeds. A summary of the over-speed tests are given in Table 7.3.

Table 7.3 *Over-speed test summary*

Test	Date	***Sample time*** [s]	V_{max} [m/s]
Governed over-speed	27-Sep-08	2478	4.9
	28-Sep-08	382	7.1
	29-Sep-08	1026	11.2
	1-Oct-08	1437	10.8
		Total: 5323 s	
Ungoverned over-speed	4-Oct-08	779	9.3
	7-Oct-08	794	5.7
	14-Oct-08	151	8.5
		Total: 1724 s	

Figure 7.24 shows the governor in the almost completely negative position of p=-10°.

Figure 7.24 *Modified prototype running at p=-10°*

Figure 7.25 shows the results for the governed over-speed tests. A parabolic fit going through the origin provides a good fit for the data, with the coefficient of determination $R^2 = 0.82$ (Vardeman 1994, p.107). The data is compared to the calculated results of the final test configuration in Figure 7.22. The error between the calculated and the fitted results is 20% at 10 m/s.

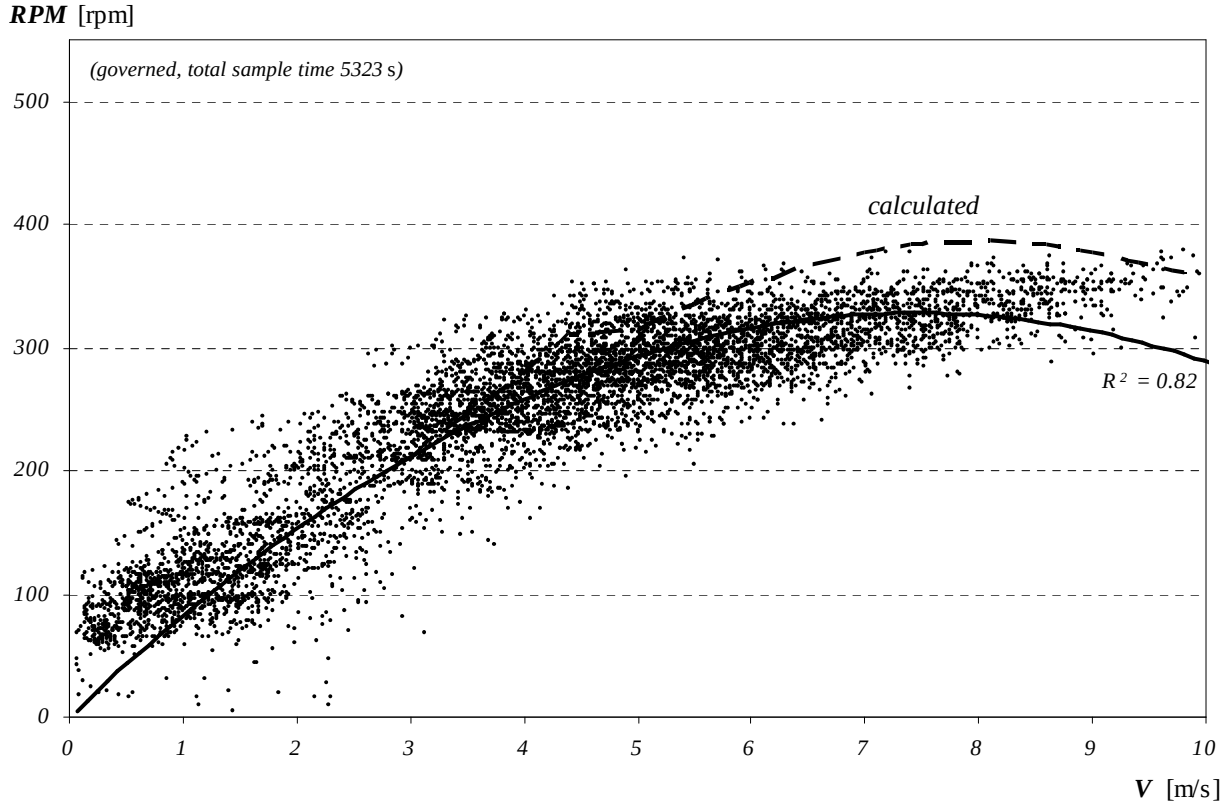

Figure 7.25 *Governed over-speed test results compared to the calculated results*

Figure 7.26 shows the results for the ungoverned over-speed tests. The spread of the data is very wide, therefore the linear fit going through the origin with $R^2 = 0.55$ is poor. The data is compared to the calculated results of the final test configuration in Figure 7.22. The largest error between the fitted and calculated results is 10% at 7 m/s.

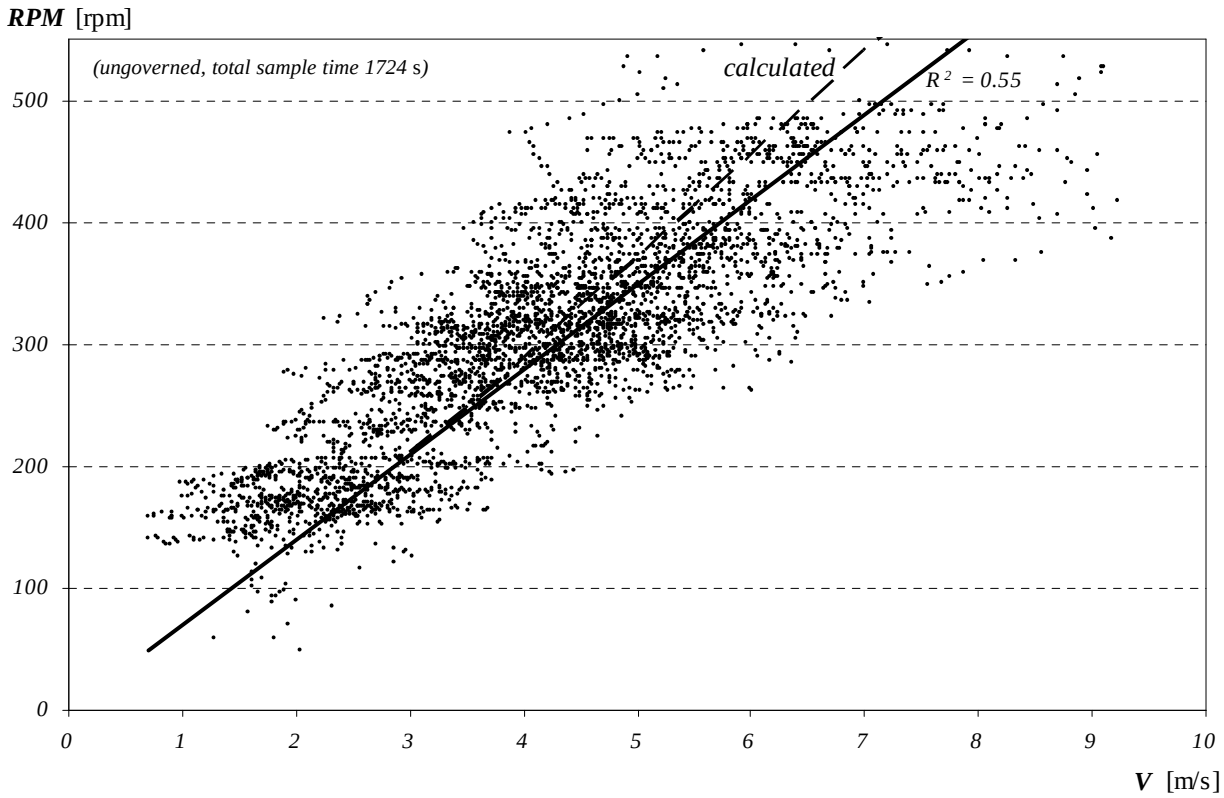

Figure 7.26 *Ungoverned over-speed test results compared to the calculated results*

From Figure 7.25 and Figure 7.26 is can be seen that the model provides good results compared to the test results, although slightly higher. The rotor blade model with the centrifugal governor model can therefore be used to provide practical results that can be used for a design.

Figure 7.27 shows the governed and ungoverned results compared to each other.

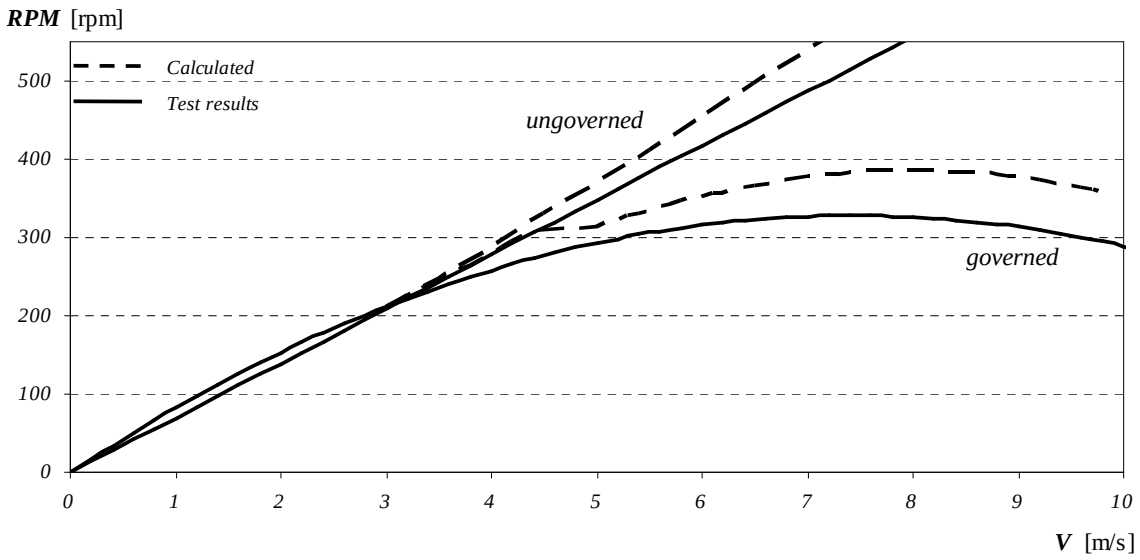

Figure 7.27 *Comparison between the governed and ungoverned over-speed results*

From Figure 7.27 it can be seen that the final test configuration of the modified prototype does limit the rotational speed. The modified prototype with the compression spacer (Figure 7.9) will also limit the rotational speed, therefore accomplishing the control objective of over-speed protection. Using a generator with the modified prototype will also limit the rotational speed, although to a slightly different level due to a different external governor moment M_{load}.

7.4 Start-up tests

7.4.1 Test setup

To test if the modified prototype can accomplish the control objective of improved start-up performance, comparative tests are done between the governed and ungoverned wind turbine system. Even though the test setup does not have a generator, the comparative tests will still prove whether the prototype can provide improved start-up performance. The following tests are done:

- Establish the system's governed and ungoverned minimum cut-in wind speed.
- Compare the governed and ungoverned cut-in wind speed to test if the system can achieve the control objective of improved start-up performance.

The start-up tests are done on the same test setup as the over-speed tests. The tests are done by letting the system start from rest in low wind conditions. The system is kept at rest with the emergency brake until the wind is still. The brake is then released and the rotor will start turning at the cut-in wind speed, which the logger will record (Figure 7.28). Because of the large inertia of the system, the wind speed must increase very gradually to provide accurate results. The test is done a few times to find the minimum cut-in wind speed. The tests are done with the governed and ungoverned system and compared to establish if the governor lowers the cut-in wind speed. The start-up torque C_Q is not measured.

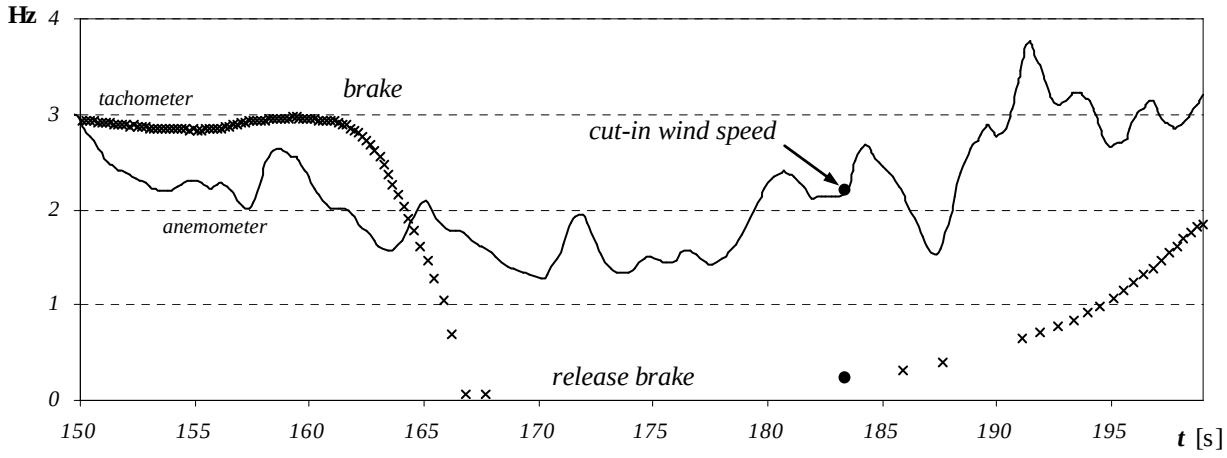

Figure 7.28 *Method for determining the cut-in wind speed*

7.4.2 Start-up test results

Figure 7.29 shows the modified prototype in the start-up position where it returns to. The distance from the tip of the governor's centre shaft to the top of the bush is 19.6 mm, which equates to a start-up pitch p=5°. It must return to a start-up pitch p=9.7°, but is still an improvement over the original design's start-up pitch of p=2.5°.

Figure 7.29 *Improved start-up position of the modified prototype*

The sorted cut-in wind speed results for the governed and ungoverned system are shown in Figure 7.30.

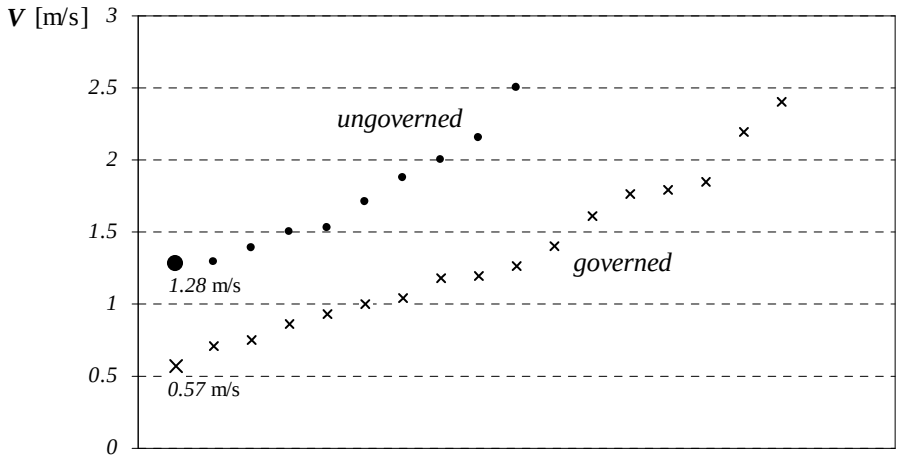

Figure 7.30 *Cut-in wind speed results*

From Figure 7.30, the minimum cut-in wind speed for the ungoverned system is V=1.28 m/s and for the governed system V=0.57 m/s. This is a clear improvement over the ungoverned system and the modified prototype lowers the cut-in wind speed.

The modified prototype therefore accomplishes the control objective of improved start-up performance. Using a generator with the modified prototype will also provide improved start-up performance.

7.5 Summary

The governor prototype was tested with and without the AE1kW wind turbine blades and the following results were found:

- The initial tests showed that the stand-alone governor prototype works as designed. The validity of the centrifugal governor model was proved.
- The problem with the governor not returning to its start-up position was corrected by modifying the design and adding an additional soft spring.
- The final tests of the modified prototype proved that it can accomplish both control objectives of improved start-up performance and over-speed protection. The validity of the rotor blade model was proved.

Chapter 8 Conclusions and recommendations

8.1 Conclusions

The conclusions of the study are as follows:

- The tests provided validation for the simulation models, which consists of the rotor blade model and a centrifugal governor model. The model can be used to analyse a wind turbine system with a centrifugal governor.
- If the effect of the external governor moment is negligible, the non-linearity of the sliding concept ensures that the rotational speed is limited to the same level irrespective of the generator load.
- The stalling or negative pitching that is used to limit the speed unfortunately causes large loads on the blades, governor and tower. This may be problematic if the concept is applied to a larger wind turbine system or used in high wind speeds.
- The final concept that was used in the design can be used on any wind turbine system, provided the rotor blades and tower are strong enough.
- The governor system can easily be modified by adjusting the masses and the lengths of the connectors and springs.

8.2 Recommendations

For future improvements and studies the following recommendations can be considered:

- The hanger and track design of L_{c1} can be improved by using linear monorail bearings.
- The start-up pitch can further be improved by using a linear bearing over the synchronization bush.
- Pitching towards feather or positive pitching can be used with the sliding concept to provide only over-speed protection. This will drastically decrease the thrust on the blades and tower.
- It may be possible to develop a governor that pitches from start-up to operation and then back towards feather for over-speed protection.

References

Bosman JJ 2003, *Design report: Design of the AE1kW wind turbine blade*, Aero Energy, Potchefstroom, South Africa.

Buhl ML Jr 2005, A New Empirical Relationship between Thrust Coefficient and Induction Factor for the Turbulent Windmill State, National Renewable Energy Laboratory, Colorado, viewed 26 September 2007, <http://www.nrel.gov/ docs/fy05osti/36834.pdf>

Burton T, Sharpe D, Jenkins N, Bossanyi E 2001, Wind Energy Handbook, J. Wiley & Sons, England.

Cheney W, Kincaid D 1999, Numerical Mathematics and Computing, Brooks/Cole Publishing Company, Pacific Grove USA.

Corbus D, Baring-Gould I, Drouilhet S, Gervorgian V, Jimenez T, Newcomb C, Flowers L 1999, 'Small Wind Turbine Testing and Applications Development', presented at Windpower '99, Burlington, Vermont, June 20–23 1999, National Renewable Energy Laboratory, Colorado, viewed 4 May 2007, <http://www.nrel.gov/docs/fy99osti/27067.pdf>

Davis Instruments, 2008, Weather Wizard III, San Francisco Bay Area, USA, viewed 24 October 2008, <http://www.davisnet.com/weather/products/weather_wiz.asp>

Dorf RC, Bishop R H 2001, Modern Control Systems, Prentice Hall, New Jersey.

Gasch R, Twele J 2005, Wind Power Plants: Fundamentals, Design, Construction and Operation, James & James, London.

Knecht K, 2004, Wind Regimes of Africa, Comparative Evaluation of Wind Data from Selected Countries, InWEnt Division, Environment, Energy and Water, Berlin, Germany, viewed 21 June 2008, <http://www.afriwea.org/download/R-WindAfrika_010404_engl.pdf>

Matweb, 2008, Material Property Data, Automation Creations Inc, Blacksburg, Virginia, viewed 26 August 2008, <http://www.matweb.com>

Moriarty PJ, Hansen AC 2005, AeroDyn Theory Manual, National Renewable Energy Laboratory, Colorado, viewed 6 November 2006, <http://www.nrel.gov/docs /fy05osti/36881.pdf>

Muljadi E, Drouilhet S, Holz R, Gevorgian V, 1995, Analysis of Wind Power for Battery Charging, National Renewable Energy Laboratory, Colorado, viewed 6 March 2007, <http://www.nrel.gov/docs/legosti/old/8170.pdf>

Muljadi E, Green J 2002, 'Cogging Torque Reduction in a Permanent Magnet Wind Turbine Generator', presented at the 21st American Society of Mechanical Engineers Wind Energy Symposium, Reno, Nevada, January 14–17 2002, National Renewable Energy Laboratory, Colorado, viewed 9 July 2007, <http://www.nrel.gov/docs/fy02osti/30768.pdf>

North-West University School of Physics, Unit for Space Physics 2006, Neutron Monitor Data, North-West University School of Physics, Potchefstroom, viewed 9 July 2008, <http://www.puk.ac.za/physics/data/>

NWUSP – see North-West University School of Physics, Unit for space physics 2006

SoMat Corporation, 2008, SoMat eDAQ-lite, Urbana, Illinois, USA, viewed, 28 October 2008, <http://www.somat.com/products/somat_edaq_lite.html>

Vardeman SB 1994, Statistics for Engineering Problem Solving, PWS Publishing Company, Boston.

Appendix A Calculation examples

A.1 Blade element-momentum theory calculation

Ungoverned wind turbine, standard atmospheric conditions, steady-state operation at 7 m/s

N	D [m]	R [m]	V_∞ [m/s]	ρ [kg/m^3]
3	3.6	1.8	7	1.225
RPM	**Ω** [rad/s]	**λ (TSR)** (3.18)	**Pitch**	
274.816	28.779	7.400	0	

RPM is solved until ΔP=0

ν [m^2/s]
0.000

x=r/R	a	a'	W [m/s] (3.1)	φ(x) [rad] (3.2)	β(x) [rad]	α(x) [rad] (3.3)	c(x) [m]	Reynolds(x)
0.15	0.311	0.166	10.261	0.489	0.352	0.138	0.256	183,331
0.2	0.312	0.093	12.308	0.402	0.285	0.117	0.272	232,942
0.25	0.354	0.063	14.493	0.317	0.223	0.095	0.285	286,923
0.3	0.386	0.045	16.804	0.259	0.182	0.077	0.292	341,041
0.35	0.403	0.034	19.199	0.219	0.158	0.062	0.296	393,879
0.4	0.416	0.026	21.642	0.190	0.141	0.049	0.297	444,789
0.45	0.423	0.020	24.119	0.168	0.128	0.041	0.293	488,893
0.5	0.425	0.016	26.620	0.152	0.116	0.035	0.283	520,771
0.55	0.426	0.013	29.139	0.138	0.106	0.032	0.270	543,190
0.6	0.429	0.011	31.668	0.127	0.096	0.030	0.257	561,646
0.65	0.431	0.009	34.208	0.117	0.088	0.029	0.244	575,805
0.7	0.429	0.008	36.756	0.109	0.081	0.028	0.231	583,796
0.75	0.427	0.007	39.311	0.102	0.075	0.027	0.217	586,353
0.8	0.431	0.006	41.867	0.095	0.068	0.027	0.203	584,894
0.85	0.441	0.005	44.423	0.088	0.061	0.027	0.190	579,355
0.9	0.461	0.004	46.978	0.080	0.055	0.026	0.176	569,255
0.95	0.509	0.004	49.520	0.069	0.048	0.021	0.163	554,477
1								

a and a' are solved until ΔdT=0 and ΔdQ=0

R_{HUB}
0.100

x=r/R	Cl(x)	Cd(x)	Cm(x)	dL(x) (3.4)	dD(x) (3.5)	F_{TIP} (3.21)	F_{HUB} (3.22)	F_{TOTAL}	c_T (3.20)
0.15	0.997	0.017	-0.036	16.456	0.285	1.000	0.870	0.870	0.857
0.2	0.892	0.014	-0.038	22.509	0.361	1.000	0.986	0.986	0.858
0.25	0.784	0.012	-0.044	28.709	0.432	1.000	1.000	1.000	0.915
0.3	0.684	0.010	-0.046	34.562	0.481	1.000	1.000	1.000	0.948
0.35	0.601	0.008	-0.049	40.154	0.539	1.000	1.000	1.000	0.962
0.4	0.538	0.007	-0.053	45.796	0.629	1.000	1.000	1.000	0.973
0.45	0.492	0.007	-0.055	51.376	0.761	1.000	1.000	1.000	0.979
0.5	0.462	0.007	-0.056	56.823	0.905	1.000	1.000	1.000	0.981
0.55	0.443	0.007	-0.056	62.263	1.043	1.000	1.000	1.000	0.982
0.6	0.429	0.007	-0.057	67.823	1.175	1.000	1.000	1.000	0.984
0.65	0.419	0.007	-0.057	73.365	1.298	0.999	1.000	0.999	0.986
0.7	0.412	0.007	-0.057	78.647	1.408	0.998	1.000	0.998	0.984
0.75	0.408	0.007	-0.057	83.765	1.511	0.995	1.000	0.995	0.983
0.8	0.407	0.007	-0.057	88.848	1.607	0.988	1.000	0.988	0.987
0.85	0.407	0.007	-0.057	93.304	1.694	0.968	1.000	0.968	0.996
0.9	0.401	0.007	-0.057	95.489	1.764	0.920	1.000	0.920	1.014
0.95	0.373	0.007	-0.057	91.166	1.803	0.792	1.000	0.792	1.066
1									

x=r/R	dT(x) (3.6)	$dT(x)_{mom}$	ΔdT (3.23)	dQ(x) (3.8)	$dQ(x)_{mom}$	ΔdQ (3.24)	dT(r).dr (3.12)	dQ(r).dr (3.13)
0.15	14.660	14.660	0.000	2.020	2.020	0.000	1.598	0.182
0.2	20.855	20.855	0.000	3.052	3.052	0.000	2.172	0.275
0.25	27.411	27.411	0.000	3.846	3.846	0.000	2.743	0.346
0.3	33.534	33.534	0.000	4.526	4.526	0.000	3.278	0.407
0.35	39.309	39.309	0.000	5.175	5.175	0.000	3.798	0.466
0.4	45.090	45.090	0.000	5.784	5.784	0.000	4.314	0.521
0.45	50.778	50.778	0.000	6.358	6.358	0.000	4.819	0.572
0.5	56.308	56.308	0.000	6.921	6.921	0.000	5.315	0.623
0.55	61.812	61.812	0.000	7.471	7.471	0.000	5.816	0.672
0.6	67.428	67.428	0.000	7.989	7.989	0.000	6.320	0.719
0.65	73.017	73.016	0.000	8.494	8.494	0.000	6.811	0.764
0.7	78.334	78.334	0.000	9.012	9.012	0.000	7.282	0.811
0.75	83.482	83.482	0.000	9.500	9.500	0.000	7.744	0.855
0.8	88.598	88.598	0.000	9.863	9.863	0.000	8.176	0.888
0.85	93.091	93.090	0.000	9.990	9.990	0.000	8.479	0.899
0.9	95.322	95.322	0.000	9.583	9.583	0.000	8.388	0.862
0.95	91.071	91.071	0.000	7.733	7.733	0.000	4.098	0.696
1								

T_{ALL} [N] (3.12)	Q_{ALL} [Nm] (3.13)	P [kW] (3.14)	P_{gen}
273.448	**31.675**	**0.912**	0.912
C_T (3.16)	C_Q (3.17)	C_P (3.15)	ΔP (3.19)
0.895	**0.058**	**0.426**	**0.000**

A.2 Two-spring centrifugal governor calculation

Two spring centrifual governor at 50 rpm

RPM	Ω [rad/s]		L_{UNDEF1} [m]	L_{COMP1}	k_1 [N/m]
50.000	5.236		0.038	0.000	200
m [kg]	L_M [m]	θ_M	L_{UNDEF2} [m]	L_{COMP2}	k_2 [N/m]
1.5	0.15	0	0.15	0.000	1300
r_{OFF}	r_{OFF2}				
0.000	0.000				
L_{C1} [m]	L_{C2} [m]				
0.15	0.15				
L_{TOP}	L_{BOT}				
0	0				

$\theta_{C1.GUESS}$ [rad]
0.613

θ_{C1} is solved until $\Delta M=0$

		$\theta_{C1.MIN}$ [rad] (3.36)
		0.003
Z (3.37)		$\theta_{C1.MIN2}$ (3.38)
0.000	1.571	0
Z (3.39)		$\theta_{C1.MAX}$ [rad]
0.188	0.677	0.677

θ_{C1} [rad]	θ_{C1} [deg]
0.613	35.133

	θ_{C2} [rad] (3.30)	
	0.613170784	
	$L_{SPRINGS}$ [m] (3.31)	
	0.17264033	
	L_{S1} [m] (3.33),(3.34)	L_{S2} [m] (3.33),(3.34)
	0.025	0.148
	F_{S1} [N] (3.32)	F_{S2} [N] (3.32)
	2.662	2.662

F_{CENT} [N] (3.28)	F_{SPRING} [N] (3.32)	
5.045	5.325	
M_{CENT} [Nm] (3.27)	M_{SPRING} [Nm] (3.29)	**ΔM** [Nm] (3.26)
1.306	1.306	0.000

θ_{OFF} [deg]	**p** [deg] (3.35)
28.805	**6.328**

A.3 Sliding centrifugal governor calculation

Sliding centrifual governor at 400 rpm

RPM	Ω [rad/s]		L_{UNDEF1} [m]	L_{COMP1}	k_1 [N/m]
400.000	41.888		0	0	0
m [kg]	L_M [m]	θ_M	L_{UNDEF2} [m]	L_{COMP2}	k_2 [N/m]
1	0.25	0	0.2	0.050	4500
r_{OFF}	r_{OFF2}				
0	0				
L_{C2} [m]	L_{C1} [m]	$L_{C1\perp MIN}$	$L_{C1\perp MAX}$ [m]	$L_{C1\perp}$ [m] (5.1)	
0.04	0.175	0	0.25	0.175	
L_{TOP}	L_{BOT}				
0	0				

θ_{C1} is solved until ΔM=0

$\theta_{C1.GUESS}$ [rad]
1.347

		$\theta_{C1.MIN}$ [rad] (3.36)
		1.341
Z (3.37)		$\theta_{C1.MIN2}$ (3.38)
0.050	#NUM!	0
Z (3.39)		$\theta_{C1.MAX}$ [rad]
0.200	1.402	1.402

θ_{C1} [rad]	θ_{C1} [deg]
1.347	77.157

	θ_{C2} [rad] (3.30)	
	0.224	
	$L_{SPRINGS}$ [m] (3.31)	
	0.180	
	L_{S1} [m] (3.33),(3.34)	L_{S2} [m] (3.33),(3.34)
	0.000	0.180
	F_{S1} [N] (3.32)	F_{S2} [N] (3.32)
	0.000	90.256

F_{CENT} [N] (3.28)	F_{SPRING} [N] (3.32)	
97.508	90.256	
M_{CENT} [Nm] (3.27)	M_{SPRING} [Nm] (3.29)	Δ**M** [Nm] (3.26)
71.301	71.301	0.000

θ_{OFF} [deg]	**p** [deg] (3.35)
78.463	**-1.307**

A.4 External governor moment calculation

Combined concept wind turbine, standard atmospheric conditions, steady-state operation at 7 m/s

N	D [m]	R [m]	V_∞ [m/s]	ρ [kg/m^3]
3	3.6	1.8	7	**1.225**
RPM	**Ω** [rad/s]	**λ (TSR)** (3.18)	**Pitch**	
264.525	27.701	7.123	-0.834	

x=r/R	W [m/s] (3.1)	c(x) [m]	C_M(x)	$dM_{0.25}$(x) (3.43)	$dM_{0.25}$(r).dr (3.43)
0.15	10.033	0.256	-0.028	0.114	0.015
0.2	11.968	0.272	-0.035	0.229	0.028
0.25	14.042	0.285	-0.039	0.383	0.045
0.3	16.238	0.292	-0.044	0.610	0.066
0.35	18.532	0.296	-0.047	0.867	0.093
0.4	20.876	0.297	-0.051	1.192	0.122
0.45	23.254	0.293	-0.054	1.529	0.149
0.5	25.656	0.283	-0.055	1.788	0.169
0.55	28.075	0.270	-0.056	1.974	0.185
0.6	30.505	0.257	-0.056	2.127	0.197
0.65	32.946	0.244	-0.057	2.246	0.205
0.7	35.397	0.231	-0.057	2.314	0.209
0.75	37.853	0.217	-0.057	2.337	0.210
0.8	40.312	0.203	-0.057	2.327	0.207
0.85	42.773	0.190	-0.057	2.281	0.202
0.9	45.233	0.176	-0.056	2.199	0.193
0.95	47.683	0.163	-0.056	2.086	0.094
1					
					$M_{0.25}$ [N.m] (3.44)
					2.389

x=r/R	dT(x) (3.6)	dT(r).dr (3.40)	dU(x) (3.7)	dU(r).dr (3.42)
0.15	14.929	1.643	7.714	0.745
0.2	21.575	2.238	8.837	0.795
0.25	28.161	2.818	8.837	0.782
0.3	34.456	3.371	8.544	0.760
0.35	40.460	3.915	8.340	0.742
0.4	46.538	4.462	8.149	0.725
0.45	52.617	5.004	7.956	0.708
0.5	58.581	5.540	7.783	0.693
0.55	64.520	6.080	7.624	0.679
0.6	70.591	6.625	7.458	0.664
0.65	76.642	7.157	7.304	0.652
0.7	82.407	7.669	7.185	0.641
0.75	88.017	8.176	7.067	0.628
0.8	93.668	8.661	6.891	0.607
0.85	98.804	9.028	6.602	0.569
0.9	101.824	9.019	6.039	0.483
0.95	98.595	4.437	4.696	0.211
1				
		T [N] (3.40)		U [N] (3.42)
		95.843		11.085

a [m]	b [m]	$M_{T,U}$ [N.m] (3.46)
0.055	0.021	**5.504**

m_{Blade} [kg]	c [m]	d [m]
5.416	0.01891	0.000
	c_{TRANS} [m]	d_{TRANS} [m]
	0.018908	-2.752E-04
		M_C [N.m] (3.46)
		-0.022

c and d are transformed because of the non-zero pitch

M_{load} [N.m] (3.48)
-3.093

A.5 Pitching shaft stress calculation

Stress calculation at point r_b=0.1, out-of-plane forces
Potchefstroom atmospheric conditions, steady-state operation at 9 m/s

N	R_{OFFSET} [m]	D [m]	R [m]	V_∞ [m/s]	ρ [kg/m^3]
3	0.1	3.8	1.9	9	1.000
RPM	**Ω** [rad/s]	**λ (TSR)** (3.18)	**Pitch**		
500.000	52.360	11.054	-5.500		

r_c [m]
0.1224
x_c [m]
0.064

x_{new} [6.1]	x	$\beta(x)_{new}$ [rad]	$c(x)_{new}$ [m]	dT(x) (3.6)	dT(r).dr (3.40)	dF(x) (3.40)	dF(r).dr (3.41)
0.195	0.15	0.239	0.403	20.314	2.324	3.303	0.507
0.242	0.2	0.258	0.345	28.610	3.245	7.370	1.015
0.289	0.25	0.274	0.274	39.705	4.411	14.000	1.795
0.337	0.3	0.287	0.212	53.150	5.776	23.790	2.894
0.384	0.35	0.293	0.174	68.444	7.253	37.138	4.316
0.432	0.4	0.297	0.151	84.252	8.808	53.719	6.073
0.479	0.45	0.296	0.135	101.181	10.478	74.125	8.215
0.526	0.5	0.290	0.122	119.403	12.284	98.818	10.795
0.574	0.55	0.277	0.111	139.211	14.260	128.436	13.882
0.621	0.6	0.263	0.100	160.992	16.424	163.826	17.547
0.668	0.65	0.250	0.091	184.774	18.717	205.579	21.769
0.716	0.7	0.235	0.083	209.278	21.068	252.724	26.499
0.763	0.75	0.221	0.077	234.263	24.401	305.151	33.046
0.811	0.8	0.206	0.070	279.451	29.284	390.561	42.448
0.858	0.85	0.192	0.062	337.044	34.543	503.072	53.319
0.905	0.9	0.178	0.055	390.173	39.337	619.439	64.427
0.953	0.95	0.164	0.048	437.966	20.803	736.922	35.004
	1						
					T [N] (3.40)		**F** [N.m] (3.41)
					273.415		343.551

r_a [m]	r_b [m]	r_c [m]
0.036	0.100	0.1224

R_a [N]	R_b [N]
-5463.672	5737.087

E [GPa]
210
D [m]
0.025
A [m^2]
4.909E-04
I [m^4]
1.917E-08

m_{Blade} [kg]	R_{CENT}	F_{CENT} [kN] (3.45)
5.416	0.737	10.943
m_{Plates} [kg]	$R_{CENT.PLATES}$	$F_{CENT.PLATES}$
4.100	0.177	1989.548
		$F_{CENT.TOTAL}$ [kN]
		12.933

The mass of the plates that hold the blade is also included in the calculation of the centrifugal force.

σ_{CENT} [MPa]
26.346

r_b [m]	M_{BEND} [N.m]	σ_M [Mpa]
0.100	**349.675**	227.953

σ_{Comp} [Mpa]	$\sigma_{Tension}$ [Mpa]	σ_{Yield} [MPa]	SF
-201.6	**254.3**	370.0	**1.5**

Appendix B Blade Centre of Gravity determination

To determine the AE1 KW blade's centre of gravity, it is freely suspended from a point, with a string also suspended from the point. The string will intersect the blade's centre of gravity. By suspending the blade from two or more different positions and superimposing the photos, the intersection of the strings will indicate the centre of gravity.

Figure B.1 *Method used to determine the blade centre of gravity*

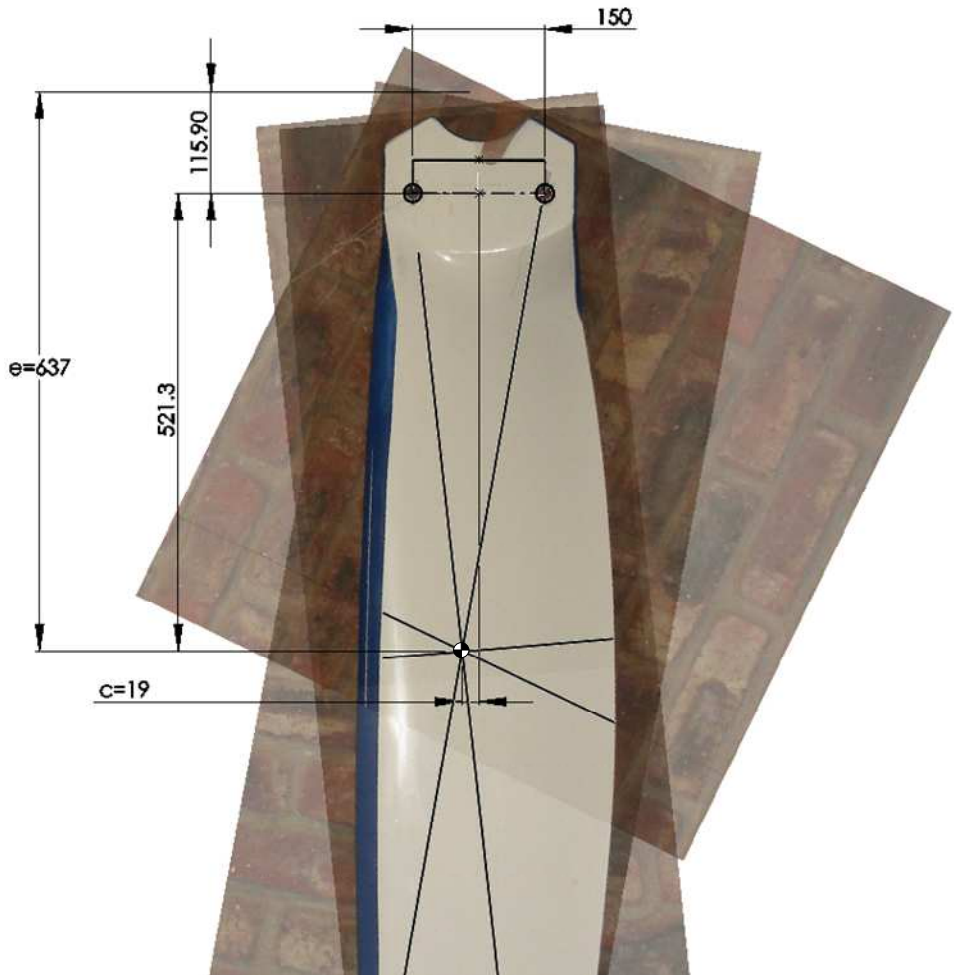

Figure B.2 *AE1kW blade centre of gravity*

Appendix C Detail design drawings

The detail design drawings of the prototype, modified prototype and its final test configuration are given in the following drawings.

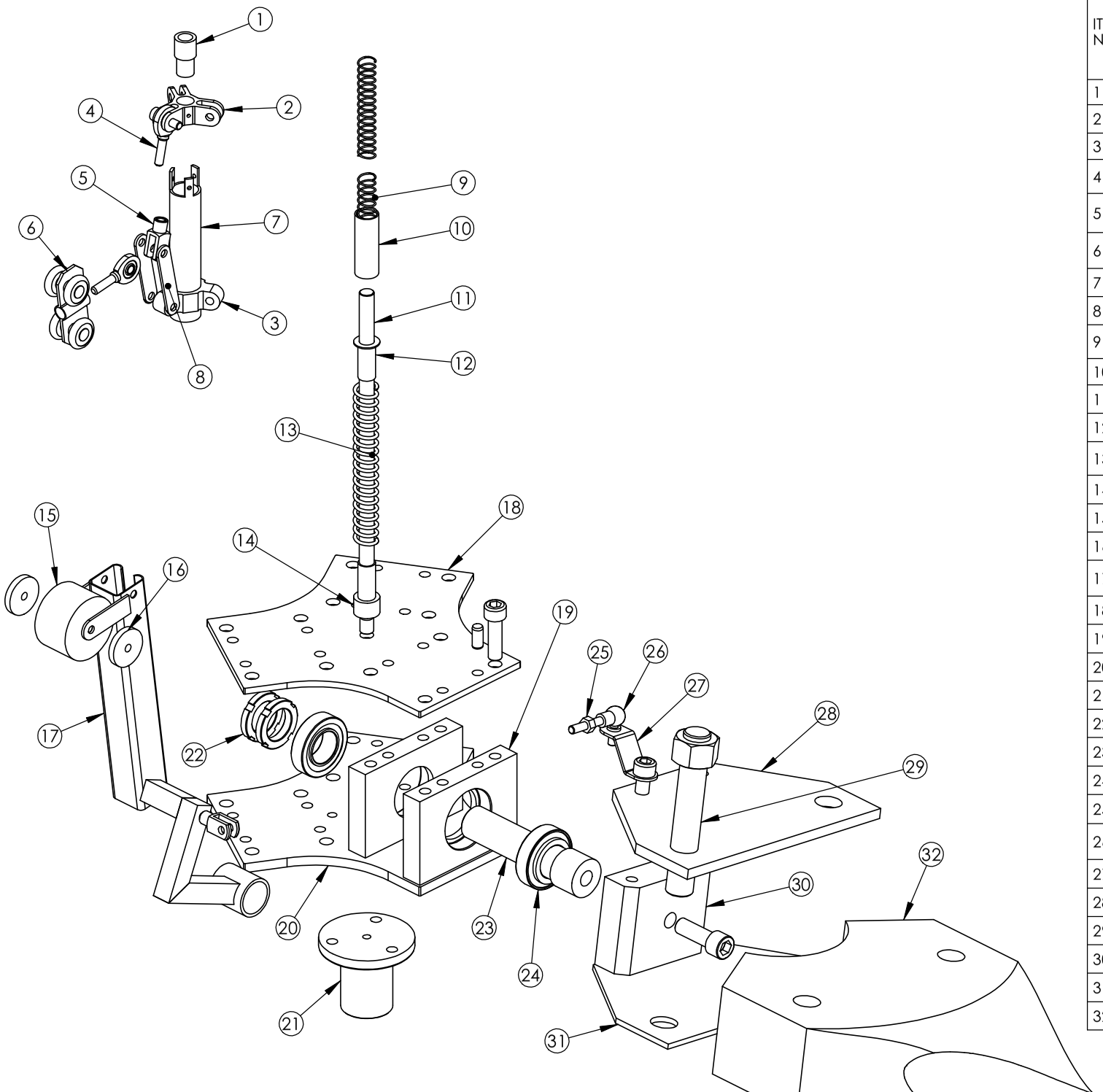

ITEM NO.	DESCRIPTION	Uncom Set angle/QTY.	MATERIAL
1	FRONT CONNECTOR BUSH	1	BRASS
2	FRONT CONNECTOR	1	EN8
3	SYNC CONNECTOR	1	ALUMINIUM
4	ROD END	6	INA GAR6-UK
5	CLEVIS	6	WURTH M6X12
6	ROLLER	3	HILLALDAM 100
7	SYNC BUSH	1	BRASS
8	SYNC LINK	6	MILD STEEL
9	SOFT SPRING	2	MUSIC WIRE 1MM
10	SOFT SPRING COMPRESSION SPACER	1	EN8
11	SPRING SHAFT	1	EN8
12	HARD SPRING BUSH	1	BRASS
13	HARD SPRING	1	MUSIC WIRE 2.5MM
14	HARD SPRING SPACER	1	EN8
15	MASS	3	MILD STEEL
16	MASS SMALL	6	MILD STEEL
17	TRACK	3	HILLALDAM 100
18	FRONT PLATE	1	MILD STEEL
19	BEARING HOLDER	6	MILD STEEL
20	BACK PLATE	1	MILD STEEL
21	FLANGE	1	EN8
22	LOCK NUT M25 X 1.5	6	MILD STEEL
23	PITCHING SHAFT	3	EN8
24	TAPERED BEARING	6	SKF 32005X
25	SETTING NUT	3	M6
26	BALL JOINT	3	WURTH M6X12
27	ADJUSTMENT PLATE	3	MILD STEEL
28	BLADE TOP PLATE	3	MILD STEEL
29	BLADE BOLT	1	EN8
30	BLADE CONNECTOR	1	MILD STEEL
31	BLADE BOTTOM PLATE	3	MILD STEEL
32	AE1KW BLADE	3	

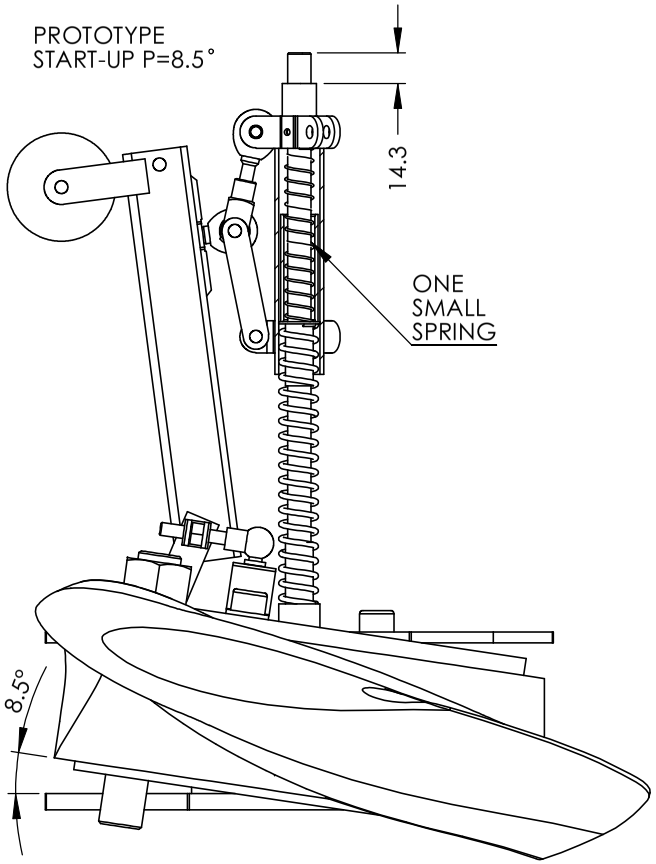

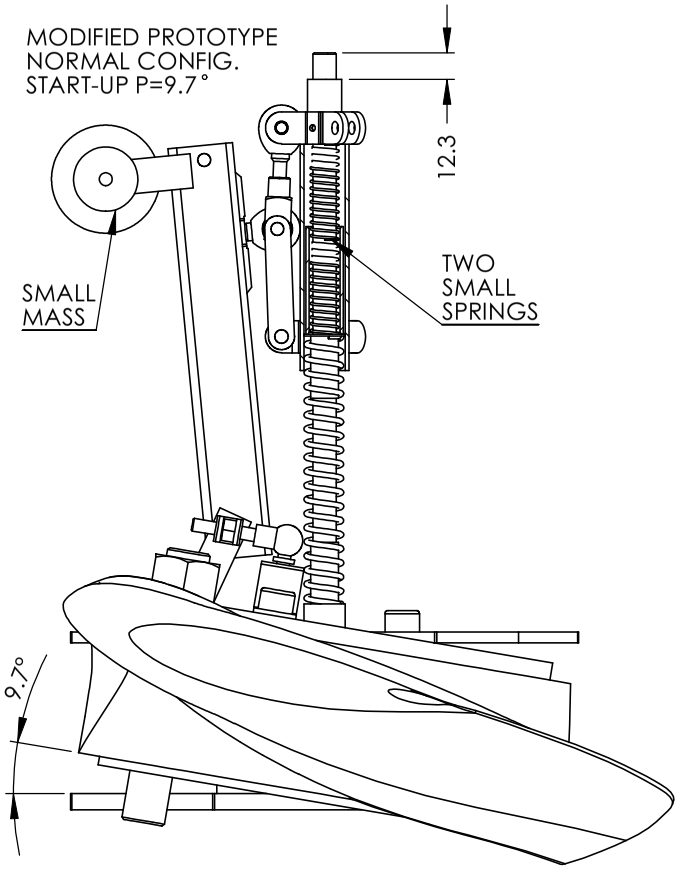

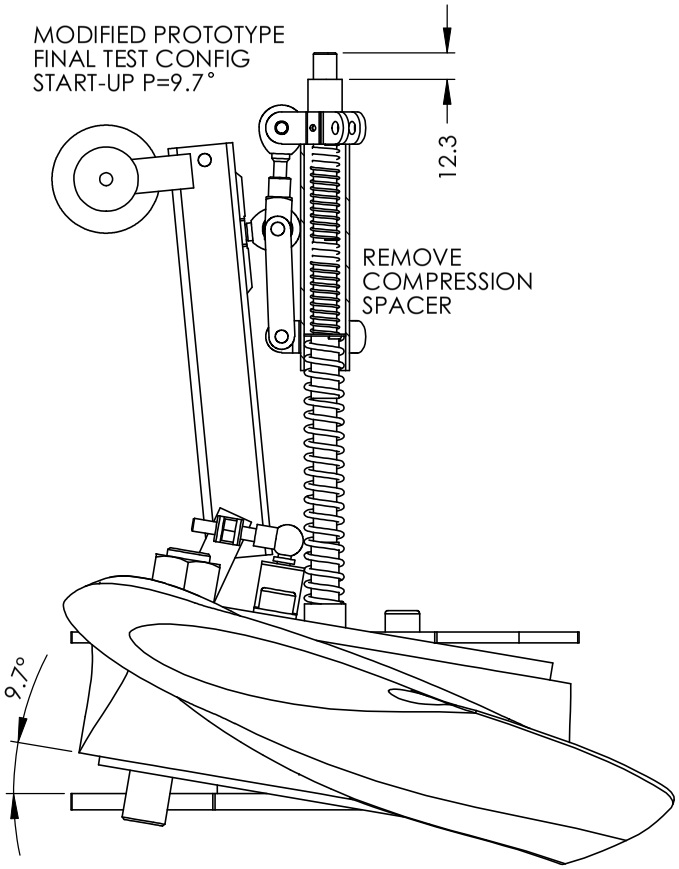

(32) AE1KW BLADE
QUANTITY: 3

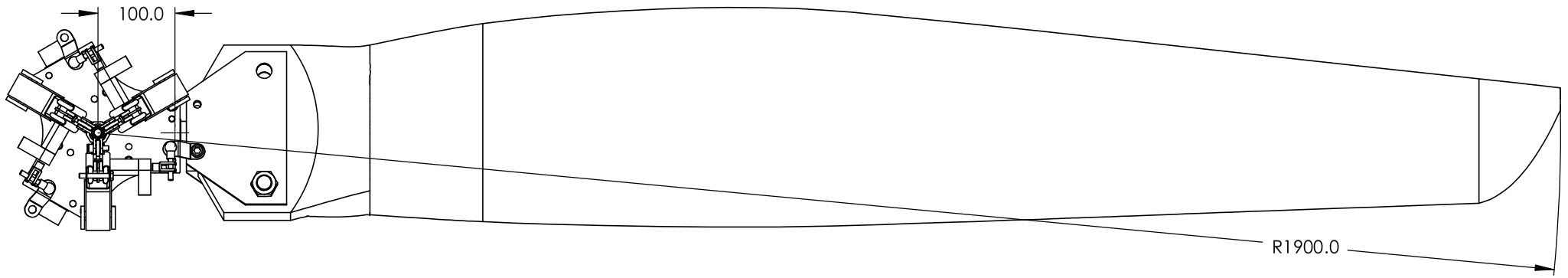

(19) BEARING HOLDER
QUANTITY: 6
MATERIAL: MILD STEEL

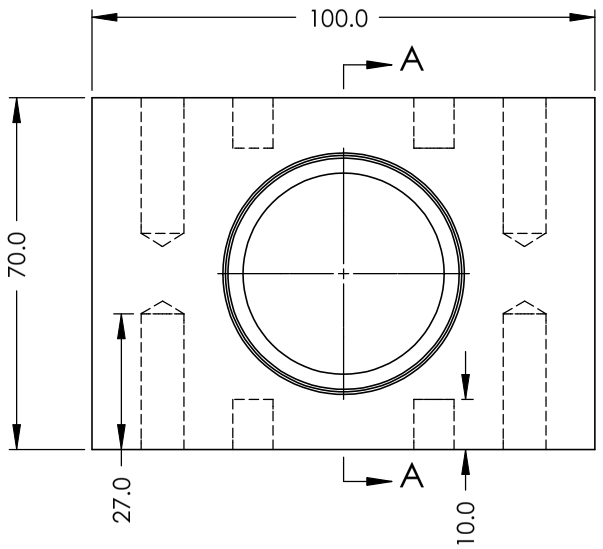

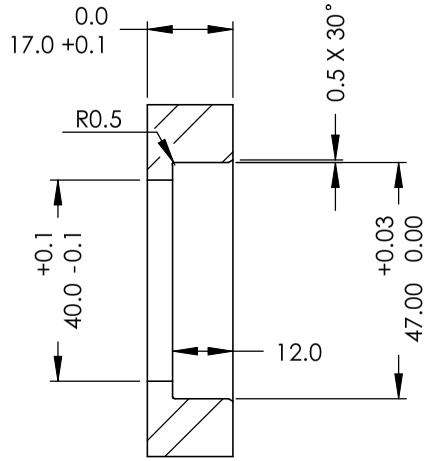

SECTION A-A

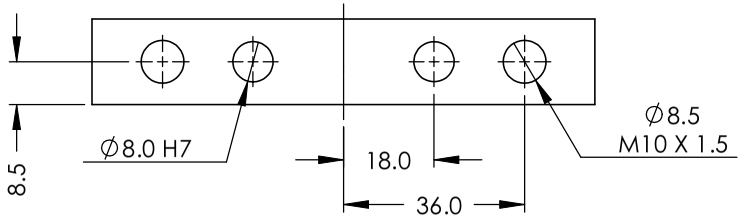

(21) FLANGE
QUANTITY: 1
MATERIAL: EN8

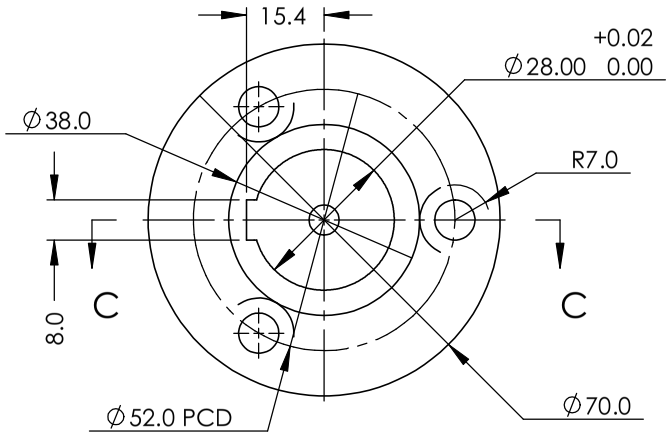

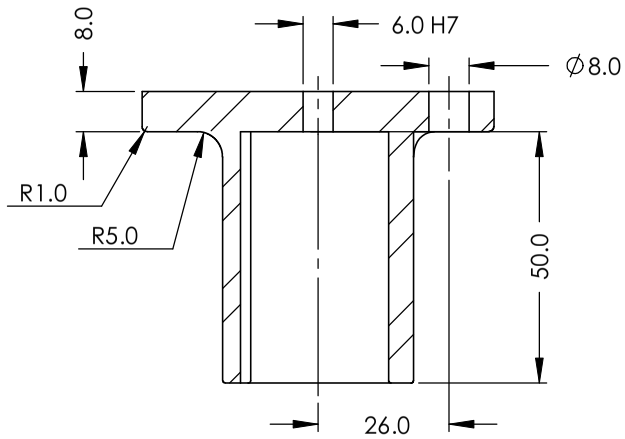

SECTION C-C

(23) PITCHING SHAFT
QUANTITY: 3
MATERIAL: EN8

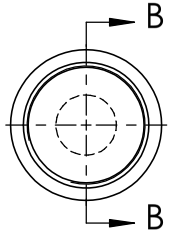

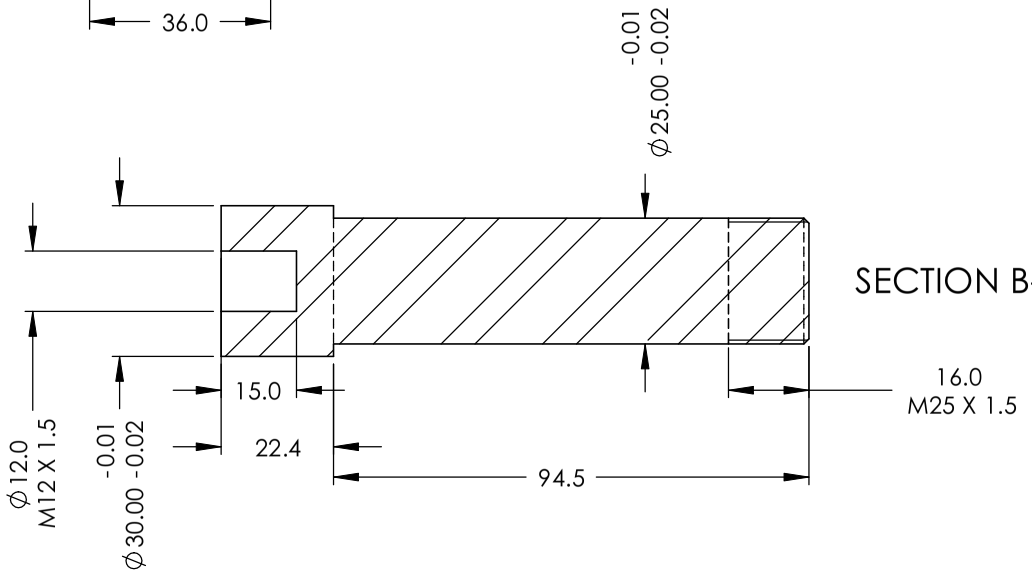

SECTION B-B

⑱ FRONT PLATE
QUANTITY: 1
MATERIAL: MILD STEEL
THICKNESS: 5MM

⑳ BACK PLATE
QUANTITY: 1
MATERIAL: MILD STEEL
THICKNESS: 7.5MM

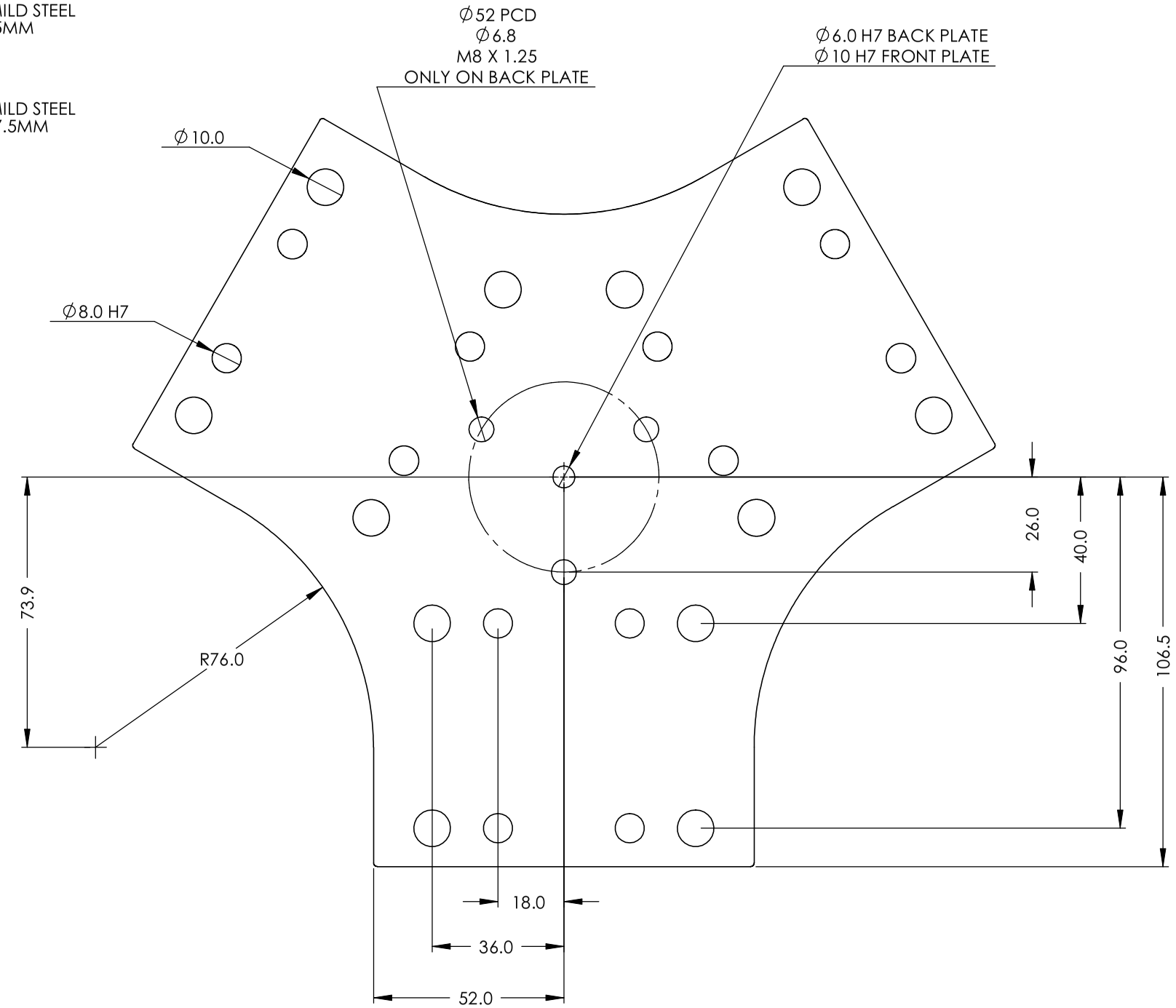

⑪ SPRING SHAFT
QUANTITY: 1
MATERIAL: EN8

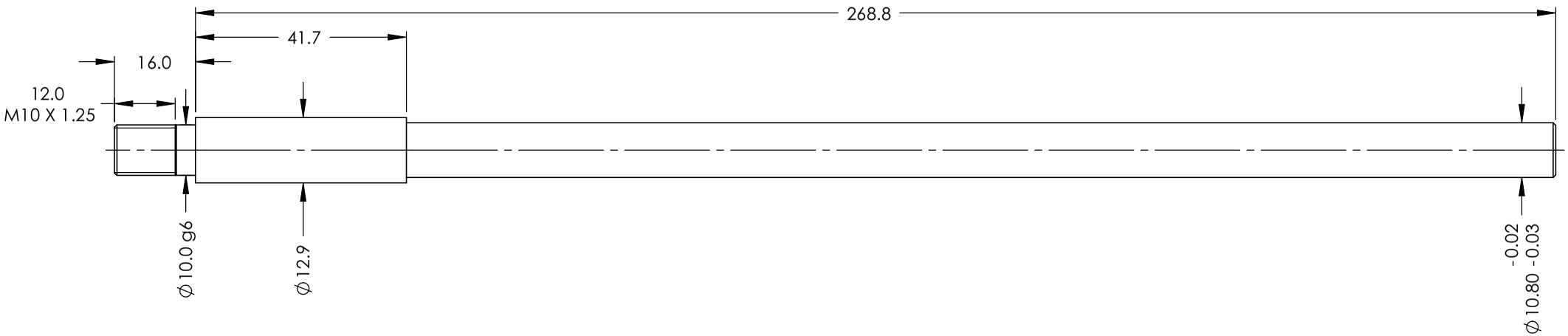

⑭ HARD SPRING SPACER
QUANTITY: 1
MATERIAL: EN8

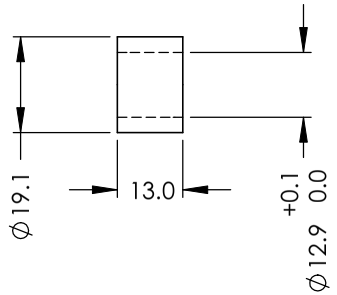

⑫ HARD SPRING BUSH
QUANTITY: 1
MATERIAL: BRASS

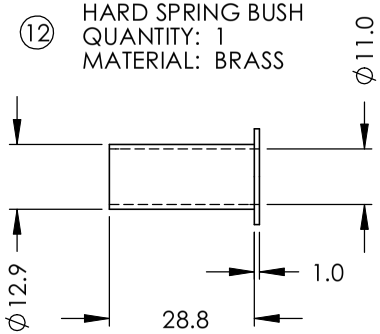

⑩ SOFT SPRING COMPRESSION SPACER
QUANTITY: 1
MATERIAL: EN8

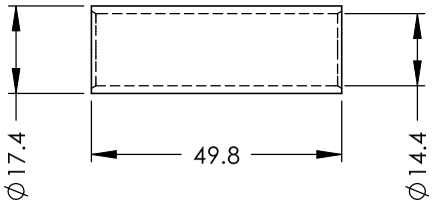

⑬ HARD SPRING
QUANTITY: 1
MATERIAL: MUSIC WIRE 2.5MM
SPRING RATE: 5.25 N/MM

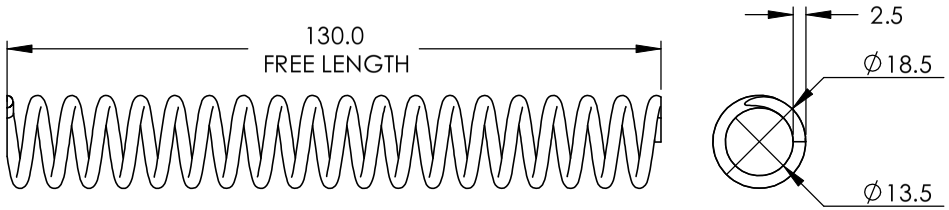

⑨ SOFT SPRING
QUANTITY: 2
MATERIAL: MUSIC WIRE 1MM
SPRING RATE: 0.41 N/MM

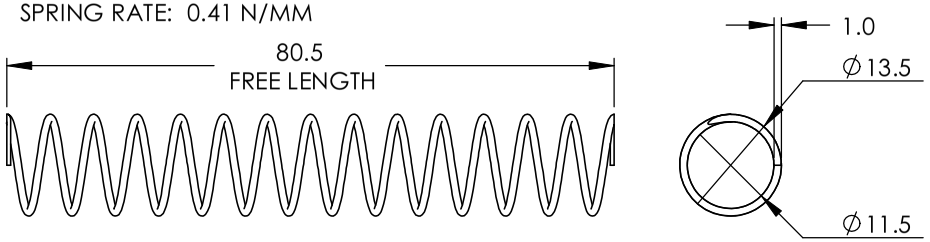

② FRONT CONNECTOR
QUANTITY: 1
MATERIAL: EN8

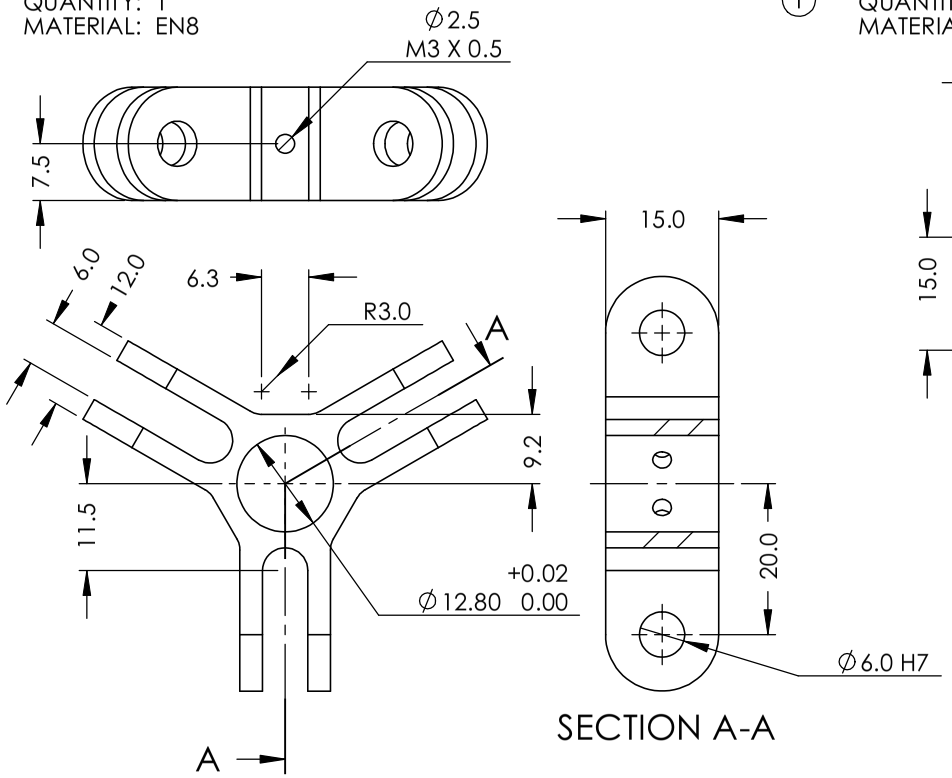

SECTION A-A

① FRONT CONNECTOR BUSH
QUANTITY: 1
MATERIAL: BRASS

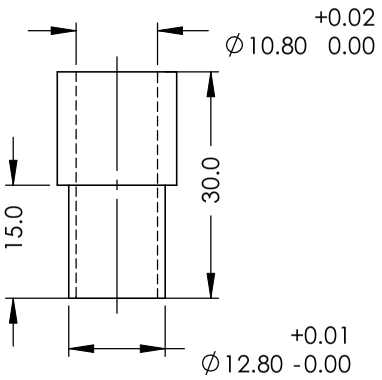

⑦ SYNC BUSH
QUANTITY: 1
MATERIAL: BRASS

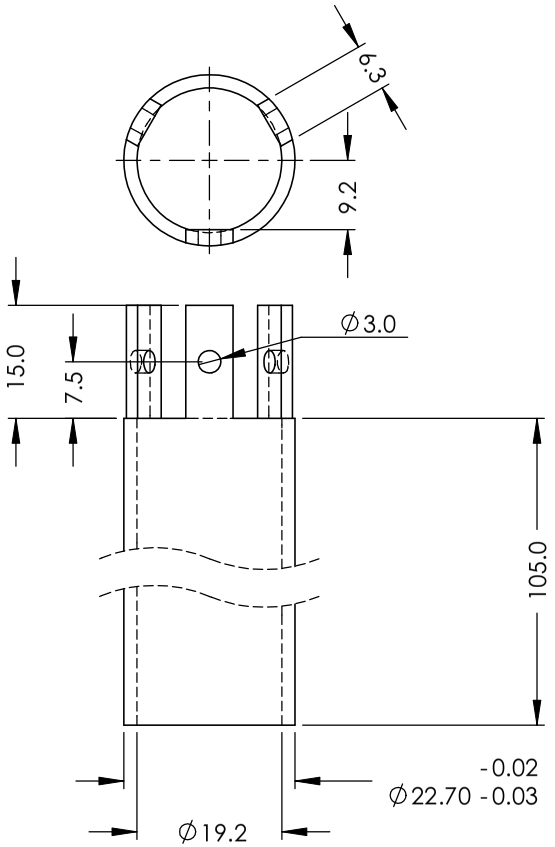

③ SYNC CONNECTOR
QUANTITY: 1
MATERIAL: ALUMINIUM

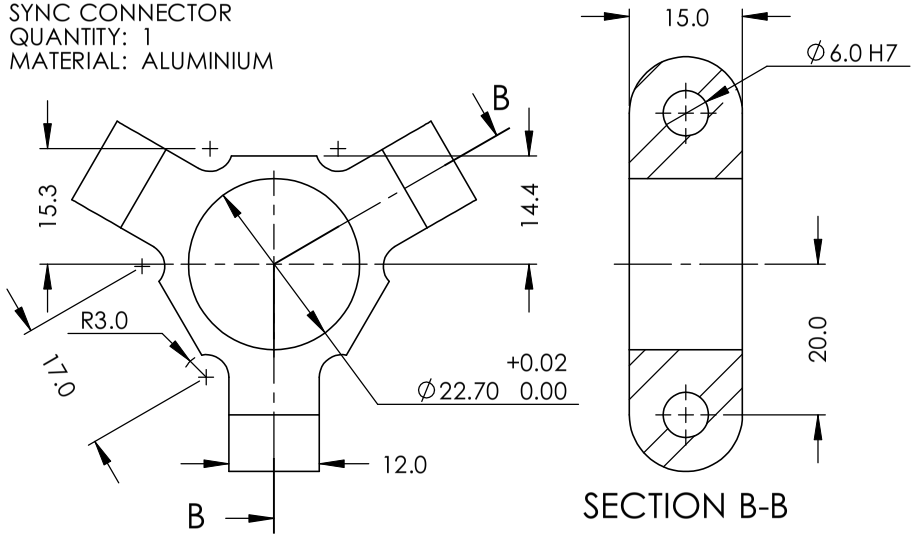

SECTION B-B

⑧ SYNC LINK
QUANTITY: 6
MATERIAL: MILD STEEL

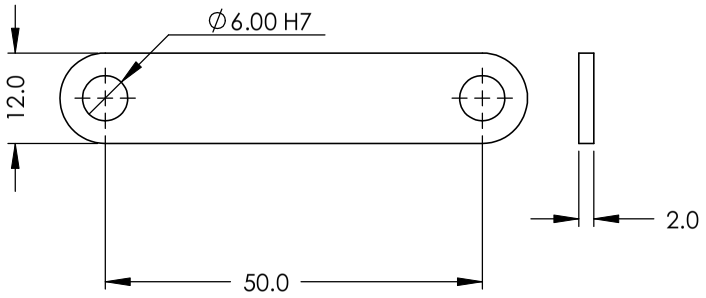

(30) BLADE CONNECTOR
QUANTITY: 3
MATERIAL: MILD STEEL

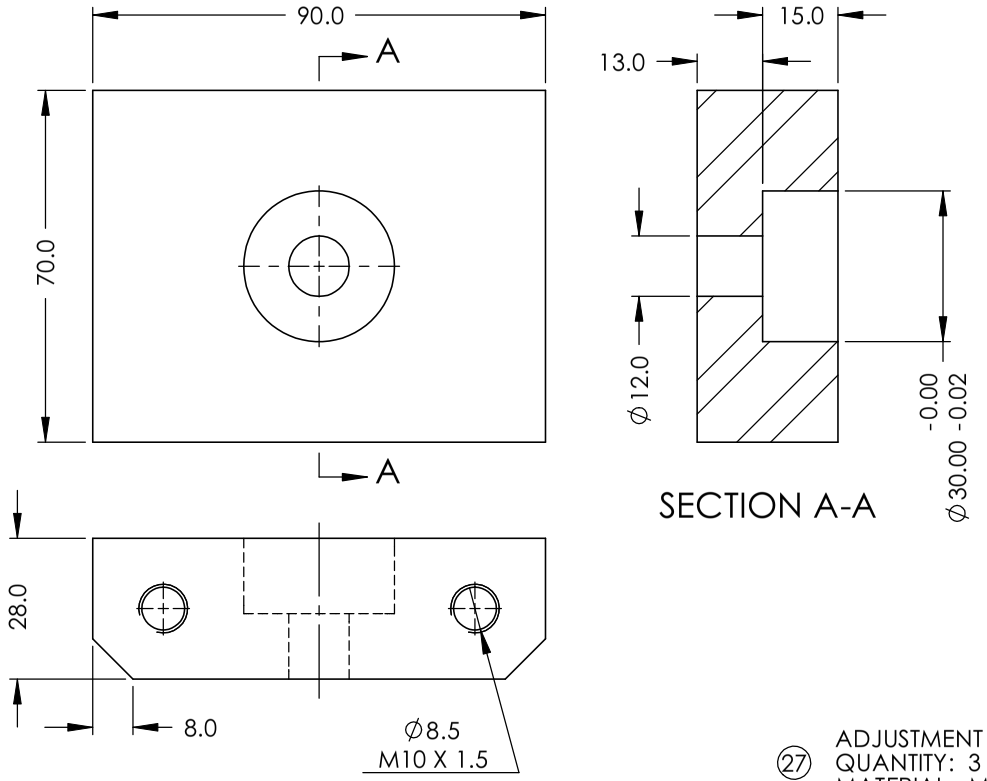

(28) BLADE TOP PLATE
QUANTITY: 3
MATERIAL: MILD STEEL

(31) BLADE BOTTOM PLATE
QUANTITY: 3
MATERIAL: MILD STEEL

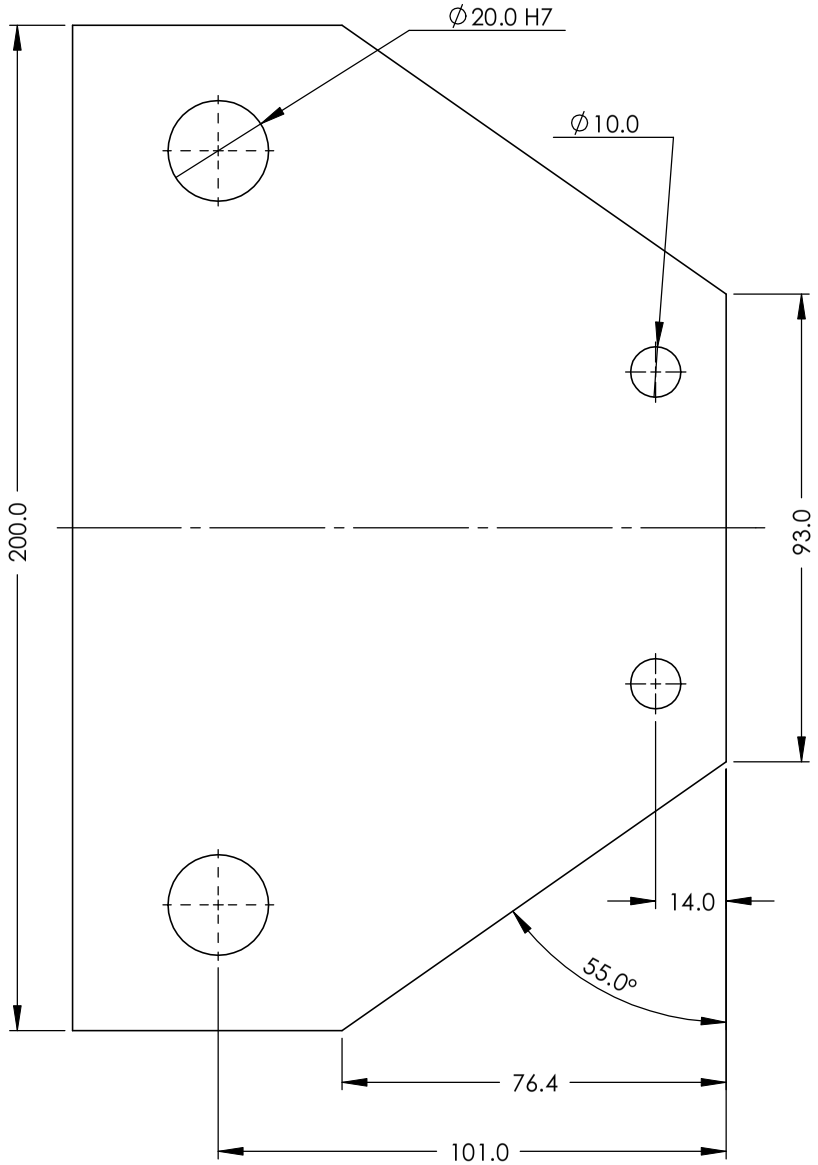

(29) BLADE BOLT
QUANTITY: 6
MATERIAL: EN8

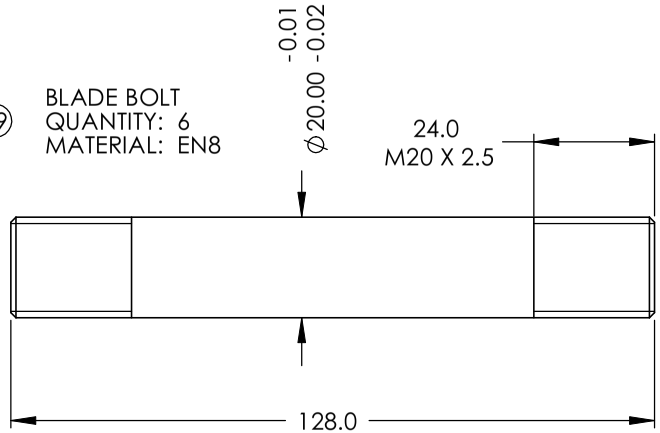

(27) ADJUSTMENT PLATE
QUANTITY: 3
MATERIAL: MILD STEEL

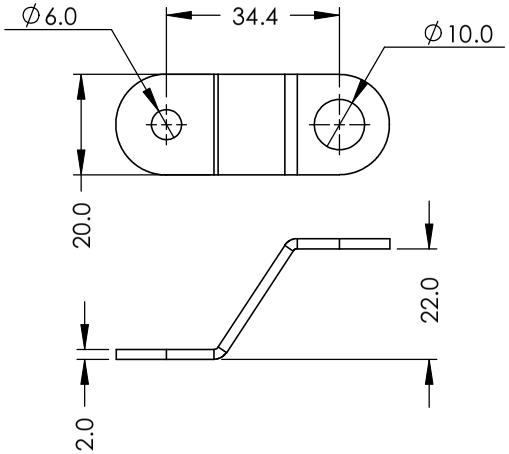

⑰ TRACK
QUANTITY: 3
MATERIAL: HILLALDAM 100

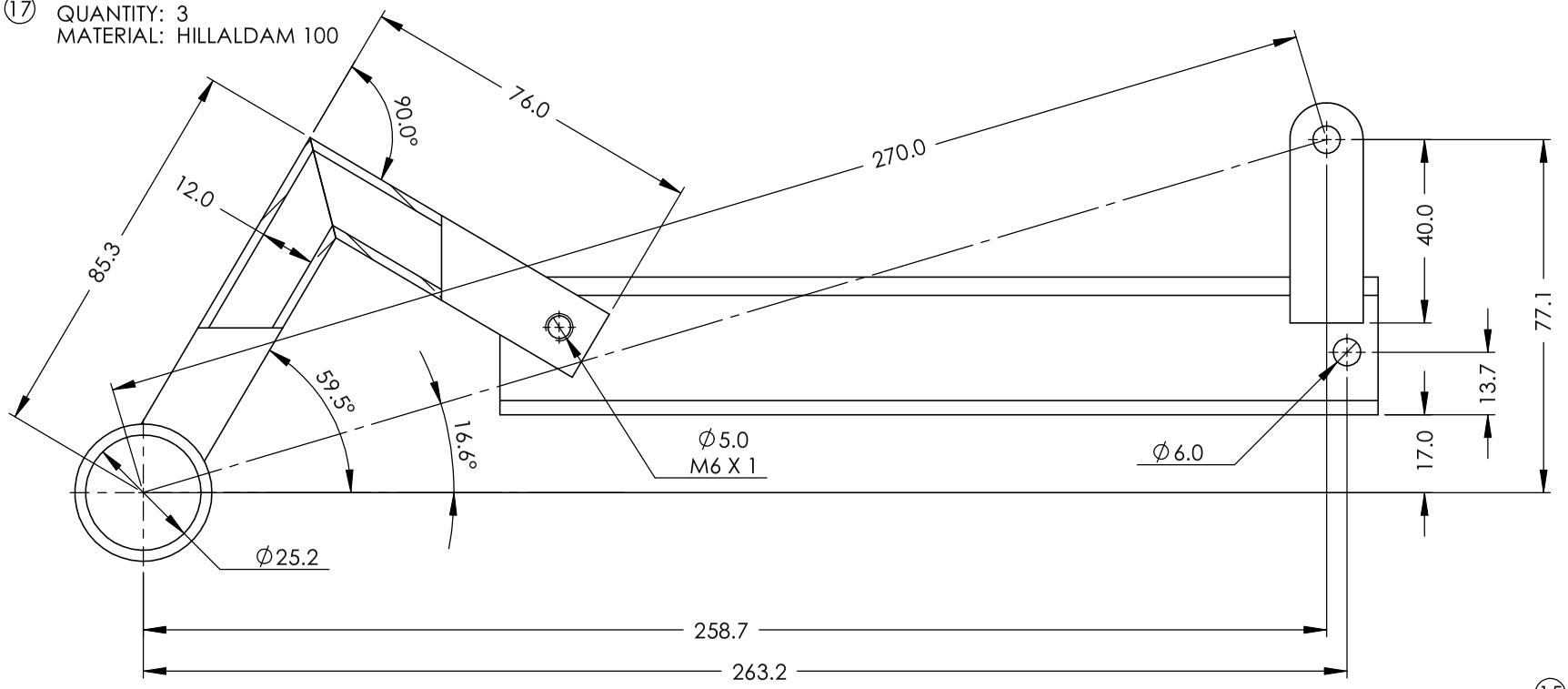

⑯ MASS SMALL
QUANTITY: 6
MATERIAL: MILD STEEL

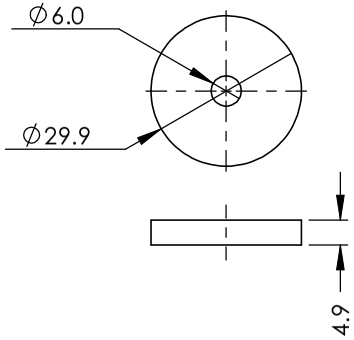

⑮ MASS
QUANTITY: 3
MATERIAL: MILD STEEL